

A Detailed Parameterization of the Atmospheric Boundary Layer

By

Peter J. Wetzel

Department of Atmospheric Science
Colorado State University
Fort Collins, Colorado



**Department of
Atmospheric Science**

Paper No. 302

A DETAILED PARAMETERIZATION OF THE ATMOSPHERIC BOUNDARY LAYER

by

Peter J. Wetzel

Research Supported by the

National Center for Atmospheric Research
NOAA, NASA,
The U.S. Nuclear Regulatory Commission
and the
National Science Foundation
Under Grants
NCAR-24-73, 04-5-022-8,
NSG 1023 Supp #1 and NSG 5105,
NRC-04-75-197, and GA 31588 and
ATM 77-09770 respectively.

Department of Atmospheric Science
Colorado State University
Fort Collins, Colorado

December, 1978

Atmospheric Science Paper No. 302

ABSTRACT OF THESIS
A DETAILED PARAMETERIZATION
OF THE ATMOSPHERIC BOUNDARY LAYER

A one-dimensional parameterized model of the planetary boundary layer (PBL) is developed and tested. The model predicts layer averaged values of wind, temperature and moisture under both stable and unstable conditions by assuming standard profile shapes (i.e. the "jump-model" profile for unstable conditions and linear profiles for stable conditions). A predictive equation is developed for the unstable PBL height z_i , and a new diagnostic equation is used for the stable z_i . Transition between stable and unstable regimes is accomplished by the model without difficulty. The model incorporates a detailed surface energy budget--shown to be of vital importance to an accurate quantitative description of the PBL. The surface is assumed to be a layer of finite mass within which the mean "interface layer" temperature is predicted. New parameterizations for evaporation and soil heat flux are constructed and shown to work well under a wide range of conditions.

The model is tested against data from O'Neill, Nebraska and from the Wangara experiment, and it is compared with other models of the PBL. Results show that the model simulates the observations well, and that it is equal or superior to the other models examined. Sensitivity tests and exploratory tests of the model were performed. In these it is shown that the PBL is very sensitive to changes in parameters such as the mass of the layer at the surface, the difference

between the characteristic heights for moisture (z_q) and momentum (z_o), the amount of dew present at dawn, and the soil moisture content. During testing of the O'Neill general observation period 5 case it was found that the PBL could not be simulated accurately without accounting for some rather strong moisture advection. A search for moisture sources revealed no recent rains upstream, however an extensive area of irrigated cropland was found to exist. As a result tests were run which simulated a "patchy" irrigated surface containing 20% saturated soil and 80% dry soil. This test simulates the observations accurately and shows that such land use has a remarkably large effect on the unstable boundary layer, even $2\frac{1}{2}$ hours downstream from the nearest irrigation. Such tests are useful in studying man's inadvertent modification of the weather through land use patterns.

Peter J. Wetzel
Department of Atmospheric Sciences
Colorado State University
Fort Collins, Colorado 80523
November, 1978

ACKNOWLEDGEMENTS

I would like to thank Dr. Bill Cotton for his guidance and numerous discussions during the course of this research. Dr. Peter Sinclair also has my gratitude for his support and guidance. Drafts of this paper were reviewed by Drs. Donald Lenschow and James Deardorff who offered numerous, very helpful suggestions. Thanks go also to Ms. Karen Greiner, Mrs. Kathy Pursley and especially to Ms. Polly Cletcher for typing the manuscript, and to Mrs. Lucy McCall for drafting the figures.

This research was sponsored by the following project grants: National Center for Atmospheric Research grant NCAR-24-73, NOAA grant 04-5-022-8, NASA research grants number NSG 1023 Supp. #1 and NSG 5105, grant number NRC-04-75-197 from the U.S. Nuclear Regulatory Commission, and National Science Foundation grants GA 31588 and ATM 77-09770.

TABLE OF CONTENTS

<u>Chapter</u>	<u>Page</u>
ABSTRACT	ii
ACKNOWLEDGEMENTS	iv
TABLE OF CONTENTS	v
LIST OF TABLES	vii
LIST OF FIGURES	viii
I. INTRODUCTION	1
II. PREVIOUS WORK	5
III. MODEL FORMULATION	11
A. The interface layer temperature	14
1. The radiation balance	18
2. Sensible heat flux	23
3. Evaporation from the interface layer	24
4. Heat flow into the ground	34
B. The surface layer	37
C. Outer layer assumptions	49
1. The height of the boundary layer, z_i	51
The unstable case	52
The stable PBL height	65
The transition periods	69
2. Temperature, wind, and moisture	72
The unstable surface layer	76
The unstable mixed layer	78
Transition periods	81
The stable PBL	82
The source and sink terms	84
3. The cloud-topped PBL	85
D. The free atmosphere	86
E. The radiation calculations	88
F. Applicability to non-homogeneous terrain	89
G. Initialization and numerical solution	91
H. Application to a parent model	94
IV. TESTING THE MODEL	98
A. Comparison with observations and with other models.	98
1. Wangara, day 33	99

TABLE OF CONTENTS CONTINUED

<u>Chapter</u>	<u>Page</u>
2. O'Neill, Nebraska; Period 2	118
3. O'Neill, Nebraska; Period 5	130
4. Wangara, day 16	154
B. Further considerations and experiments	
on model sensitivity.	156
1. The wind structure	156
2. Thermodynamic influences	162
Further numerical experiments	162
Qualitative considerations	169
V. CONCLUSIONS	172
VI. SUGGESTIONS FOR FUTURE RESEARCH	175
BIBLIOGRAPHY.	177
APPENDIX	191

LIST OF TABLES

<u>Table</u>	<u>Page</u>	
1	Values of ψ used in eqs. (24), (25) and (26). Values of ψ_{\max} only are subject to corrections given in table 2	42
2	Correction values to be added to the values of ψ_{\max} given above. This table is used only when $0 > L > -50$ meters	43
3	Comparison of z_1 predictive eqs. (35) and (36-38). Data is adapted ¹ from Deardorff's (1974a) numerical simulation of Day 33 of the Wangara experiment	55
4	Temporally averaged soil moisture and evaporation rate for the period 1030-1130 on the second day of general observation period 5	137
5	Factors affecting PBL temperature structure and behavior	170

LIST OF FIGURES

<u>Figure</u>		<u>Page</u>
1	Modelled PBL structure showing representative assumed profiles of virtual potential temperature and wind	13
2	Some observed and theoretical estimates of the relationship between evaporation rate and available soil moisture content, both plotted on normalized scales	27
3	Idealized representation of the evaporation process in a unit block of soil as implied by: a) eq. (14) b) eq. (15), and c) a realistic situation where both processes occur. Shaded areas are saturated	30
4	Schematic representation showing the redefinition of z_i when real heat flux profiles are adapted to the jump model	56
5	Schematic of some interactions between parent model and two forms of application of the PBL model.	95
6	Surface energy budget--Wangara 33.	100
7	Virtual potential temperature profiles--Wangara 33	103
8	Ground level temperature--Wangara 33	107
9	4 meter wind--Wangara 33	109
10	Wind profiles--Wangara 33	111
11	Moisture profiles--Wangara 33.	113
12	Boundary layer height--Wangara 33	117
13	Surface energy budget--O'Neill general observation period 2	119
14	Virtual potential temperature profiles--O'Neill general observation period 2	121
15	Ground level temperature--O'Neill general observation period 2	126

LIST OF FIGURES CONTINUED

<u>Figure</u>		<u>Page</u>
16	4 meter wind--O'Neill general observation period 2	127
17	Boundary layer height--O'Neill general obser- vation period 2	129
18	Surface energy budget--O'Neill general observation period 5	133
19	Virtual potential temperature profiles--O'Neill general observation period 5	138
20	Ground level temperature--O'Neill general obser- vation period 5	147
21	4-meter wind--O'Neill general observation period 5	149
22	Moisture profiles--O'Neill general observation period 5 (second day).	151
23	Boundary layer height--O'Neill general obser- vation period 5.	153
24	Surface energy budget and cloud cover--Wangara 16. . .	155
25	Virtual potential temperature profiles-- Wangara 16	157
26	Ground level temperature--Wangara 16	159
27	Boundary layer and cloud base height-- Wangara 16	160
28	Boundary layer height--Wangara 33. Sensitivity tests for dew, z_0 and biomass.	163
29	Interface layer temperature--Wangara 33. Sensitivity tests for dew, z_0 and biomass	165

LIST OF FIGURES CONTINUED

<u>Figure</u>		<u>Page</u>
30	Interface layer temperautre--Wangara 33. Sensitivity tests for characteristic heights z_{θ} and z_q	166
31	Latent heat flux--Wangara 33. Sensitivity tests for characteristic heights z_{θ} and z_q	167

I. INTRODUCTION

Mesoscale disturbances in the atmosphere interact with both the large scale atmospheric flow and with the smaller scale motions which dominate the layer of air near the earth's surface. In a numerical model of a mesoscale system, the largest part of the computer space-time obviously must be devoted to the mesoscale flow itself, but accurate input from the larger and smaller scales is also necessary for an accurate simulation of a real situation. There has been much interest recently in the development of good but simple representations of the longer and shorter scales of motion as the study of the mesoscale has burgeoned. This thesis presents a parameterization of the small scale (the motions within the planetary boundary layer) which is detailed and accurate but relatively simple and quick. It is intended for use in those meso- and large-scale models where the quantitative result is important.

Representation of the small scale is especially desirable for mesoscale motions over inhomogeneous surfaces. There the larger scale takes on secondary importance. If a region under study contains mountains, or a land-water boundary, or adjoining urban and rural areas, a characteristic mesoscale pattern is observable within almost all types of large scale flow. The pattern results from heating and frictional differences which occur across the heterogeneous terrain. For example, Dirks (1969) identified a mountain-plains circulation in the lee of the Colorado Rockies and simulated it numerically. Later Wetzel (1973), examining a large body of observational data, confirmed the existence of this diurnal circulation and

showed that it had an effect on the formation, growth, and motion of convective systems in the area. He also showed that this topographically induced flow could be identified on two thirds of all summer days in the area. As another example of the dominance of surface effects on mesoscale flow, Hsu (1969), studying the sea breeze of the Texas Gulf coast, found that the sea breeze effect is virtually always present and discernable from other-scale influences. It is in these kinds of topographically dominated situations where it is most important to depict the earth's surface and the boundary layer precisely.

The model developed in this study is designed to provide accurate lower boundary conditions for mesoscale models, and should be particularly useful for the simulation of topographically induced flows. Some of the notable or distinctive features of this model are:

- 1). Vertically averaged values of wind, virtual potential temperature, and mixing ratio are used. Two atmospheric values for each are predicted--one for the surface layer and one for the mixed layer.
- 2). Both the daytime (unstable) and night time (stable) boundary layers are modelled and there is a smooth transition between the two.
- 3). The modelled surface layer of variable depth contains freely varying vertical profiles of heat and momentum flux.
- 4). The use of eddy diffusivity (exchange coefficients) is avoided, so that gradients in the boundary layer can be of either sign or zero.

- 5). An accurate prognostic equation for surface temperature has been developed which includes parameterized ground heat flux and evaporation, and which embraces a detailed radiation balance.
- 6). The model formulation lends itself to use of Ekman layer resistance law formulation if and when sufficient observational data have been collected to set reliable values of the empirical constants.
- 7). A new simple prognostic equation for the height of the unstable boundary layer is presented, which is more general and appears to be more accurate than existing formulations.
- 8). Condensation is permitted at the top of the boundary layer. The height of cloud base is calculated when a cloud exists, and its existence is crudely accounted for in the radiation calculations.
- 9). The shortwave incoming radiation calculation includes consideration of the slope vector of the surface.
- 10). The model is numerically simple with no apparent theoretical maximum time step; and it is reasonably fast.
- 11). Under a wide range of conditions, the model has compared favorably with observations as well as with the results of many other models.

The long range goals for the development of this model are first to enable the mesoscale modeller to closely describe the development of mesoscale systems, particularly severe convective storms, squall lines, etc., which are at least in part controlled by topographic

effects, and secondly, to eventually realize operational forecasts of the location and time of such storms.

II. PREVIOUS WORK

Although the study of the atmospheric boundary layer stems from the work of Ekman and others early in the century, it has only been in the last decade that the study of the diabatic boundary layer has come into its own. In addition, very recent work has given some minimal consideration to the baroclinic boundary layer. The intensified study of the atmospheric boundary layer coincides with growing interest in mesoscale systems, their evolution, and their interaction with the large scale.

An important determinant of the diabatic boundary layer behavior is the surface energy budget. A vast quantity of literature discusses this equation and its individual components. Munn (1966) gives a comprehensive review of the subject, and a recent publication (Monteith, 1975) covers the vegetated interface in great detail.

Study of the atmospheric surface layer dates back to Prandtl (1932) who discussed the limiting cases of neutral and free convection wind profiles. The modern treatment of the diabatic surface layer originated in an outstanding paper by Obukhov (1946) which was not generally known to the scientific community until the publication of a later paper (Monin and Obukhov, 1954). In the original paper Obukhov first derived the functional form of the diabatic wind profile which came to be known as the KEYPS formula. It was later derived independently by several authors (Kazansky and Monin, 1956; Ellison, 1957; Yamamoto, 1959; Panofsky, 1961; Sellers, 1962). More recently an empirical formulation, the so-called Businer-Dyer profiles (Businger et al., 1971; Dyer and Hicks,

1970; Dyer, 1974), has come into general acceptance and rather wide use. There is still, however, some discussion of the proper form for profiles under very stable conditions (Webb, 1970; Hicks, 1976). Also numerous other profiles throughout the stability range have been proposed (see for example Pruitt et al., 1973).

Above the surface layer, a great deal of discussion has centered upon the unstable boundary layer structure and behavior. Particularly in the last five years, the unstable, well mixed layer capped by an inversion has received a great deal of attention, while the stable boundary layer has remained only poorly understood. In a pioneering paper, Ball (1960) set forth the basic structure of the unstable boundary layer. He presented a simple model which has come to be known as the "jump" model, in which the capping inversion layer is assumed to be infinitesimally thin. The jump model was later developed in detail by Tennekes (1973), Betts (1973), and Carson (1973). Deardorff (1973) found the jump model useful in explaining the observed stress profiles in the unstable boundary layer. Discussion continues as to the proper way to express the rate of entrainment of heat and mass through the capping inversion (Zilitinkevich, 1975; Tennekes, 1975). Stull (1973; 1976a,b,c) defines a vertical velocity of the inversion due to entrainment, w_e , and he attempts to evaluate w_e on the basis of detailed physical arguments. Zeman and Tennekes (1977) have developed an elegant inversion model based on the turbulent kinetic energy equation. Finally the jump model has been extended to stratus-topped boundary layers by Lilly (1968), who was expanding on the work of Ball (1960),

and by Deardorff (1976) who removed many of the objections to Lilly's work.

In miscellaneous other discussions of the theory of boundary layer behavior, Hoxit (1973, 1974) and Wyngaard et al. (1974) discuss the effect of baroclinicity on the boundary layer. Mahrt and Lenschow (1976) have modelled the unstable boundary layer with provision for the effects of baroclinicity on the generation of turbulent kinetic energy. Kraus and Turner (1967) applied the theory of Ball (1960) to the ocean's seasonal thermocline. Businger and Arya (1974) have developed a steady state model for the stable boundary layer by assuming an exponential decrease of stress with height. Clarke (1970) mentions that the very stable boundary layer is the least amenable to currently accepted similarity theory. He also finds that u_* / f is a better scaling factor for wind profiles in the unstable boundary layer than is z_1 , the height of the inversion. Also discussing the problem of scaling, Zilitinkevich (1972) proposes the possibility that the scaling factors for wind speed and stress are not the same in the unstable boundary layer.

Another much discussed aspect of planetary boundary layer (PBL) theory which, when resolved, will be of great help in parameterizing boundary layer processes, is the so-called unified FBL theory, or the geostrophic drag and heat transfer laws. This theory attempts to relate the large scale or free atmosphere values of wind and temperature directly to the fluxes of momentum and heat at the earth's surface. There is still much disagreement about proper scaling, the value of empirical coefficients, etc. The concept was originated by Kazansky and Monin (1960) and was expanded upon in

several early papers (Zilitinkevich and Chalikov, 1968; Gill, 1968; Csanady, 1967, 1972; Hess, 1973; Brown, 1974). Discussion of the height scaling for wind is far from resolved, with the Australians (Clarke and Hess, 1973) claiming u_* / f to be a better scale while several American and Soviet groups (e.g. Zilitinkevich and Deardorff, 1974; Arya, 1975) maintain that z_i is the better scale. There have been a number of analyses of observational data in which the values of the similarity functions A, B, and C are determined. A, B, and C are functions which arise from matching the surface layer and outer layer profile equations for the wind components tangential and normal to the surface wind, and for the potential temperature respectively. They are generally assumed to be some function of a nondimensional scale height, the nature of which is in dispute. Unfortunately, values differ and some cannot even be compared because of differing methods of scaling and nondimensionalizing the relations. Some of the notable analyses are given by Zilitinkevich and Chalikov (1968), Deacon (1973), Clarke and Hess (1974), Melgarejo and Deardorff (1974), Arya and Wyngaard (1975), and Zilitinkevich (1975). The study by Clarke and Hess also estimates the dependence of the values of A and B on baroclinicity. Recently Yamada (1976) has suggested the use of a mean PBL geostrophic wind rather than a free atmospheric value to calculate the velocity defect profiles. The reduced scatter in plots of A, B, and C vs. stability indicate that there may be some advantage to this approach.

Techniques for modelling and parameterizing the boundary layer have developed in conjunction with the broadening base of theory. A number of one dimensional grid point models of the boundary layer

have been developed to study micrometeorological problems. One of the earliest is by Estoque (1963) whose model was later revised by Krishna (1968). The Estoque model has also been used by McElroy (1973) to study the urban heat island. Another model, originally applied to the ocean surface, by Pandolfo (1969, 1971) has been applied to the urban heat island by Atwater (1972). Sasamori (1970) developed a boundary layer model with emphasis on the processes of heat and moisture flow within the soil.

Many other one dimensional boundary layer grid point models have been developed and tested in conjunction with mesoscale and large scale three dimensional models (Gadd and Keers, 1970; Delsol et al., 1971; Hadeen and Friend, 1972; Orlanski et al., 1974; Busch et al., 1976). The boundary layer parameterization in Pielke (1973) using the eddy diffusivity profiles suggested by O'Brien (1970), has produced good results. This parameterization has been improved with better surface layer parameterization (Mahrer and Pielke, 1975), and a surface energy budget (Gannon, 1976). Recently Benoit (1976) has developed an excellent treatment of the PBL which includes a treatment of cumulus and stratocumulus clouds and explicit treatment of the surface energy budget. His parameterization was applied to a global circulation model.

In other studies, Clarke (1970), Deardorff (1972b), and Arya (1977) have proposed methods of parameterizing the boundary layer in large scale models with coarse vertical resolution. Lavoie (1972), with a single layer prognostic model, simulated the Great Lakes snow squalls, which are strongly forced by boundary layer

characteristics. As is done in the present study, he predicted the temporal trend for variables which are averaged vertically through the boundary layer. Also using vertically averaged variables, Schubert (1976) integrated the cloud-topped jump model of Lilly (1968) through a diurnal period, and Albrecht (1977) developed a model of tropical oceanic trade wind boundary- and cumulus-layers under suppressed conditions. The studies of Lavoie, Schubert, and Albrecht consider only the unstable boundary layer.

Finally a number of high-order closure boundary layer models of various levels of detail have been developed. Deardorff (1972a, 1974b) developed a very detailed three dimensional model with fine resolution with which he explored the structure of turbulence in the unstable boundary layer. A much simpler but accurate model of the unstable boundary layer was developed by Wyngaard and Coté (1974). Other discussions of higher order turbulence closure techniques are presented by Donaldson (1973), Lumley and Khajeh-Nouri (1974), and Mellor and Yamada (1974). The latter paper showed that a considerable simplification of the full set of Reynolds equations can still yield quite accurate results. A recent paper by Manton and Cotton (1977) applies the higher order equation set to the more general problem of turbulence in and around a deep cumulus cloud. The current "state-of-the-art" in application of the Reynolds stress equations to the unstable boundary layer is presented in a remarkable paper by Zeman and Lumley (1976) in which it was shown to be advantageous to treat the triple correlation terms much more explicitly and to parameterize fourth order terms.

III. MODEL FORMULATION

There are, in the literature, two basic kinds of formulation used to model the boundary layer. The more common type is the grid point model in which the vertical gradients of quantities like wind and temperature are evaluated from a number of grid points stacked vertically within the boundary layer. The other type of model, of which this work is an example, shall be called the layer-averaged model in which some kind of assumption is made about the shape of the vertical profiles of wind, temperature, etc. With the exception of the high-order closure grid point models where turbulence is treated more explicitly, it is not obvious that the grid point treatment of the PBL will produce more accurate results. In a first order grid point model, the basic prognostic equation for an arbitrary variable X is

$$\frac{dX}{dt} = \frac{\partial}{\partial z} (K(z) \frac{\partial X}{\partial z}) + Q,$$

where K is the turbulent eddy diffusivity for X, and Q represents all other sources and sinks of X. The crux of the problem becomes prescribing the value of K. This may be done, for example, by assuming a functional form of the K profile such as that proposed by O'Brien (1970). The difficulty with this method arises when $\partial/\partial z$ changes sign within the boundary layer, as is the case with θ in the unstable PBL. In this case the true value of K becomes infinite at some point within the boundary layer, and elsewhere can be of either sign. The grid point model typically assumes a

continuous positive K , and thus forces $\partial X/\partial z$ to maintain the same sign throughout the PBL.

On the other hand, the layer-averaged model is formulated with an equation in the more direct form

$$\frac{dX}{dt} = \frac{\partial}{\partial z} (\overline{-w'X'}) + Q, \quad (1)$$

where one directly models the mean vertical eddy flux of X . In this form a vertical grid is not needed within the PBL (see below) if an assumption is made about the vertical profile of $\overline{w'X'}$. Also, since $\overline{w'X'}$ is a much better behaved quantity than K , we should introduce less error by assuming a $\overline{w'X'}$ profile than is introduced by assuming a K profile. The development of this method will be discussed in detail later in this chapter.

The basic domain for our model is a vertical column through the atmosphere. Horizontal variations are assumed to be gradual enough that the net lateral transport of all quantities is small compared to the vertical turbulent transport. The implications of the assumption of horizontal homogeneity are discussed in Section F. below. The domain is divided into six layers, the lowest of which is the soil (see Figure 1). Notice that in this model a vertical grid is used to describe the atmosphere above the boundary layer. This is found to be the most convenient way to describe the lapse rates of potential temperature, wind, etc. above the boundary layer, which may vary with height. The grid is also useful in that it allows one to maintain exact conservation of all quantities during the processes of entrainment and detrainment through the PBL top.

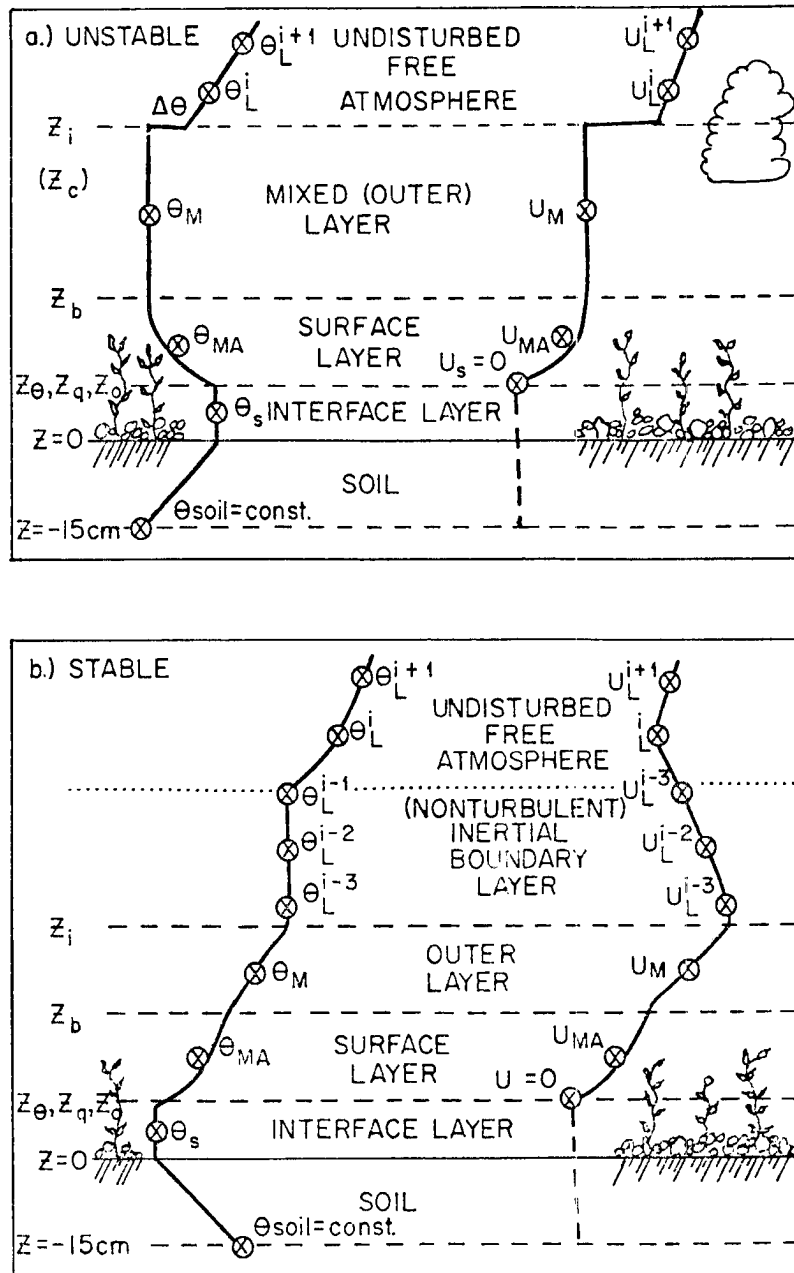


Figure 1. Modelled PBL structure showing representative assumed profiles of virtual potential temperature and wind speed.

Dummy grid points are maintained below z_i for the cases when the height of the boundary layer top decreases.

The equations and assumptions applying to each layer in Figure 1 will be discussed in this chapter, beginning with the soil and interface layers which are treated in the next section. The following section covers the surface layer, and discusses the calculation of the turbulent fluxes of heat and momentum at the surface layer top z_b and at z_o . We derive the prognostic equation for the height of the boundary layer, z_i , in the subsequent section; and we consider other aspects of the inversion and the well-mixed layer. Other sections deal with the calculations made at each of the grid points in the free atmosphere, the radiation calculation, the applicability to non-uniform topography, computational aspects of the model, and application to a three dimensional numerical prediction model.

A. The interface layer temperature

The energy budget of the earth's surface is probably the most neglected aspect of boundary layer modelling. Most models in the literature discuss the entire subject in a single brief paragraph. Some simply specify the surface temperature. During the course of the work presented here, it has become apparent that the surface energy budget, and its various components, are without doubt the most important determinants of the nature and behavior of the diabatic atmospheric boundary layer (see section IV.B). As such, precise formulation of these energy components is imperative. A good deal of effort was expended to achieve accurate values of

surface temperatures and energy fluxes under a wide range of conditions, and the resultant equations are discussed below.

We have chosen to represent the earth's surface as a layer of finite thickness within which the temperature is uniform. This approach is supported by the following reasoning. The earth-atmosphere interface of almost every naturally occurring land surface is a gradual transition zone between packed earth and unobstructed air. This being obvious, it is puzzling why the idealized, flat, infinitesimally thin interface is assumed in many surface calculations. In order to more closely represent reality, we will define an "interface layer" which extends from $z = 0$, where the soil is sufficiently compact to be capable of molecular conduction of significant amounts of heat, up to some height near the foliage canopy top where the air is adequately free to transport substantial amounts of heat by convection. In the present model where a single temperature describes the interface, it is convenient to assume uniform temperature through this interface layer. There is some justification for this assumption since the layer is virtually always either the warmest or the coldest region of any in the vicinity, thus the temperature gradient must change sign and must become zero somewhere in the layer. Also, because of radiative interaction between "roughness elements", the mean temperature gradient within the interface layer is usually much less than the temperature gradients above and below. There must be, therefore, a comparatively uniform temperature through the interface layer.

As a consequence of the above, we will use a single temperature as the boundary condition to calculate both the convective heat transfer to the atmosphere and the conduction of heat into the soil. In a number of other studies, (see for example Deardorff, 1974; Gannon, 1977; Pielke and Mahrer, 1975) the calculated surface temperature based on an infinitesimal interface is too high to yield accurate convective heat transfer values, and an empirical relation between $T(0)$ and $T(z_0)$ is imposed. The difference between the two can be several degrees. Our use of an average interface temperature and more realistic assumptions about the interface obviates the need for such a relationship.

The interface layer of finite thickness is not only physically realistic, it also lends itself to a simple form of surface energy budget equation which is prognostic in surface temperature. To obtain the equation we combine the first and second laws of thermodynamics into the general statement:

$$TdS = \sum dq_{\text{rev.}} = de + dW + dW'_{\text{max}}, \quad (2)$$

where dS is the change of entropy of a system, $\sum dq_{\text{rev}}$ is the reversible equivalent energy entering or leaving the system in all forms, de is the change in the internal energy of the system, dW is the pressure work done by, or upon the system, and dW'_{max} is the maximum (reversible) work other than pressure work which the system performs. All terms are assigned dimensions of specific (per unit mass) energy. The work terms in Eq. (2) may be neglected when compared to the change in internal energy of the finite interface layer for several reasons. Air motion is restricted by

the solid matter in the interface layer, the total mass of air in the layer is very small, and the thermodynamic properties, including temperature as discussed above, are quite uniform through the layer. If the heat source term is divided into its most important components and the work terms are dropped, Eq. (2) becomes

$$de = dQ_S - dQ_L - dQ_E - dQ_H - dQ_G \quad (3)$$

where the five terms on the right represent net short wave, net long wave, latent energy, sensible heat, and soil heat flow respectively. If these quantities are rewritten in terms of heat flux per unit area, H_x (for example in $\text{ergs cm}^{-2} \text{sec}^{-1}$), we have

$$dQ_x = \frac{H_x dt}{m} \quad (4)$$

where dt is the time increment to be considered and m is the mass per unit area of the interface layer. Neglecting magnetic, atomic, and other meteorologically unimportant forms of energy, the change in internal energy of the layer may be written

$$de = c_s dT_s \quad (5)$$

where c_s is the layer-averaged specific heat capacity of all material in the interface layer. Substituting (5) and (4) into (3) we reach the prognostic form of the interface temperature equation:

$$mc_s \frac{dT_s}{dt} = H_S - H_L - H_E - H_H - H_G. \quad (6)$$

The value of (mc_s) varies with surface cover. Generally highest values will occur on forested surfaces and in the "concrete canyons" of urban centers. The lowest values will be found over bare soils and solid rock surfaces. We will define a quantity, which will be called "biomass", as the water equivalent mass of material in the interface layer--that is, the amount of mass that would be present if the specific heat capacity of the material was $1 \text{ cal gm}^{-1} \text{ }^\circ\text{C}^{-1}$. The significance of the biomass is that it is a cover of loose material and plant matter which is not well linked to the soil. It is therefore a poor conductor of heat to the soil, and functions as a buffer region, accumulating heat during warm periods and releasing it when the surroundings are cold. One would expect surfaces with high biomass to have somewhat less extreme variations of mean interface layer temperature--and this is in fact observed when forested areas are compared to adjacent grassland. Rutter (1975) quotes observed biomass values, as defined here, ranging from around 0.6 cm water equivalent for agricultural crops, 0.9 for grassland, and between 3 and 5 cm for mature forests. The effect of varying biomass in the model developed here has been tested, and the results will be presented later in this paper. However we will now discuss the form taken by each component on the right side of eq. (6).

1. The radiation balance

Radiation, as the basic driving force of the diabatic boundary layer, is the most important component of the surface energy budget. We will discuss the longwave energy balance first. The net longwave radiation is divided into incoming and outgoing values. The incoming longwave energy flux (H_L) is determined as a part of a complete

radiative cooling rate calculation which will be discussed later in this chapter. It will suffice to say here that the value calculated includes the contribution from both water vapor and carbon dioxide. The upward radiation emitted from the interface layer is given by

$$H_L \uparrow = \epsilon \sigma T_s^4,$$

where σ is the Stefan-Boltzman constant. Many studies assume a value of 1 for ϵ , the surface emissivity, on the grounds that the difference between observed upward, and calculated blackbody radiation is small. When the upward radiation is measured from an atmospheric platform, the observed value is actually a combination of emitted and reflected radiation (see Yamamoto and Kondo, 1959). Therefore we have

$$H_L' \uparrow = \epsilon \sigma T_s^4 + (1-\epsilon)H_L \downarrow \approx \sigma T_s^4,$$

where $H_L' \uparrow$ is the apparent radiation emitted by the surface. $H_L' \uparrow$ happens to be close to the black body surface radiation since $H_L \downarrow$ is usually comparable to $H_L \uparrow$. However, when calculating net longwave radiation on the assumption that $\epsilon = 1$, the error is more significant. The measured net longwave radiation close to the surface is identical to that actually experienced by the surface,

$$H_L = \epsilon(\sigma T_s^4 - H_L \downarrow), \quad (7)$$

but different from the value calculated in other studies (Estoque,

1963; Sasamori, 1970),

$$H_L' = \sigma T_s^4 - H_L \downarrow. \quad (8)$$

Since the longwave emissivity of most natural surfaces is around 0.9 to 0.95 (Sellers, 1965; Ross, 1975), the net radiation calculated by (8) will always be five to ten percent too large. The inclusion of ϵ as a simple constant eliminates much of this error without perceptibly complicating the calculation, so Eq. (7) is used to determine the net longwave radiative flux for this study.

The shortwave radiation absorbed by the interface layer depends primarily on the geometry of the surface with respect to the sun, however the intervening atmosphere depletes some of the incoming energy before it reaches the surface. The attenuation of the solar beam by the atmosphere is calculated based on an equation given by Allen (1963). We have changed the empirical constant and added a linear dependence on surface pressure so that the parameterization will apply at all elevations. The equation then becomes

$$I_s = I_o \left[1.0 - 0.23 \left(\frac{P_s}{1000} \right) \sqrt{\csc h} \right], \quad I_s \geq 0, \quad (9)$$

where I_s is the effective solar constant at the earth's surface, I_o is the solar constant, P_s is surface pressure in millibars, and h is the elevation angle of the sun. The constant 0.23 indicates the amount of radiation which is intercepted by a path length of one atmosphere. It was determined based on the following set

of assumptions:

- 1). The atmosphere is clear and aerosol free.
- 2). 7% of the solar constant is reflected back to space by the atmosphere.
- 3). 3% of the solar constant is absorbed by Ozone above the troposphere.
- 4). 0.6% of the solar constant is absorbed by oxygen, mostly in the upper troposphere.
- 5). 0.4 % of the solar constant is absorbed by CO₂, mostly in the upper troposphere.
- 6). Approximately 12% of the solar constant is absorbed, mostly in the lower troposphere, by water vapor. This value assumes a precipitable water of 2 cm (Yamamoto, 1962).

We should note here that, although the absorption of short wave radiation by CO₂, O₂, and O₃ is not important to the boundary layer radiative energy balance, the absorption by water vapor may be significant. The daytime warming due to H₂O absorption in the lower atmosphere is around 1°C per day. This warming has been parameterized and is discussed in the section on radiation cooling rate.

The amount of solar radiation actually absorbed by the surface is then calculated from

$$H_s = \begin{cases} c(1-a) \times I_s \times \sin (h+h') & \\ 0 \text{ if } h \leq 0 \text{ or if } (h+h') \leq 0 & \end{cases} \quad (10)$$

$$h = \sin^{-1} \left[\sin \phi \sin \delta - \cos \phi \cos \delta \cos \left(\frac{2\pi t}{24} \right) \right]$$

$$\delta = -23.5 \cos \left[\frac{2\pi}{365} (d + 9) \right]$$

$$h' = \tan^{-1} \left[- \left| \frac{dh_s}{ds} \right| \cos \left(\frac{\overrightarrow{dh_s}}{ds} - az \right) \right]$$

$$az = \sin^{-1} \left[- \frac{\cos \delta \sin \left(\frac{2\pi t}{24} \right)}{\cos h} \right],$$

where the symbols have the following meanings:

c is an attenuation factor due to cloud cover which can range from 1 for clear skies to 0 for a totally opaque cloud

a is the albedo of the surface which may be constant or a function of elevation angle (see below)

h' is the slope angle of the surface in the direction of the sun

ϕ is the latitude

δ is the declination of the sun

t is the local solar time in hours

d is the day number counting from 1 January

$\frac{dh_s}{ds}$ is the vector of the true slope of the earth's surface pointing uphill with magnitude $\left| \frac{dh_s}{ds} \right|$ and direction $\frac{\overrightarrow{dh_s}}{ds}$ measured

clockwise from north

az is the azimuth angle of the sun measured clockwise from north

For many types of surface cover, the albedo is a function of elevation angle (Lettau and Davidson, 1957; Budyko, 1956). When the O'Neill data were simulated, the following expression for albedo was used:

$$a = \begin{cases} \bar{a}_o + \frac{\bar{a} - \bar{a}_o}{45} h & h \text{ (in degrees)} < 45 \\ \bar{a} & h \geq 45 \end{cases}$$

$$\bar{a}_o = \begin{cases} 0.215 & \text{for gen. obs. period 2} \\ 0.54 & \text{for gen. obs. period 5,} \end{cases}$$

Values of \bar{a} and all other initial conditions are given in the appendix.

2. Sensible heat flux

The flux of virtual sensible heat at the interface layer is given by the following expression:

$$H_H = \bar{\rho} c_p \overline{w' \theta'_{vs}} \quad (11)$$

where $\bar{\rho}$ is a grid square average surface air density, c_p is the specific heat capacity of air, and $\overline{w' \theta'_{vs}}$ is the grid average eddy flux of virtual potential temperature calculated at the surface (with prior knowledge of the surface mixing ratio, q_s). The Businger-Dyer surface layer formulations are used to calculate the eddy flux of virtual potential temperature at the top of the surface layer. This formulation requires knowledge of θ_v at the top of the surface layer and at the surface, where the θ_v is calculated from the temperature, pressure, and mixing ratio as follows:

$$\theta_v = \left(\frac{1 + 1.609q}{1 + q} \right) \left(\frac{1000}{P} \right)^{R/c_p}$$

where R is the gas constant for dry air. The value of $\overline{w'\theta'}$ is obtained by extrapolating downward from the top of the surface layer. The details of this calculation are presented in Section B of this chapter.

3. Evaporation from the interface layer

The latent heat flux is the most difficult component of the energy budget to measure accurately, and therefore it is the most difficult to model. There have been innumerable formulations for evaporation presented in the literature. We will distill some of the reasoning behind these various models, and point out the common ground which many of them share. Then, with this qualitative analysis as background, we will discuss the formulation chosen for use here.

Basically, most evaporation equations are of the form

$$E = F \frac{\delta q}{\delta z} \quad (12)$$

where E is evaporation rate, F is some function which, however obliquely, depicts the turbulent exchange process above the interface, and q is some measure of the moisture content of the air and/or soil. Thus F represents the atmospheric processes controlling evaporation, and the moisture gradient upon which F acts depends in part on the soil properties, which are treated in the $\delta q/\delta z$ term.

One can visualize two limiting cases for evaporation. First, when the interface is sufficiently wet, the local relative humidity approaches 100%, and the evaporation rate is solely dependent on surface temperature and atmospheric processes. On the other hand, when the atmosphere is very turbulent, either due to high winds or

strong instability, and when the soil is rather dry, the evaporation rate is completely controlled by the processes of moisture flow through the soil. In many models, including the one we will apply here, the processes within the atmosphere and soil can be further separated by choosing an integrated form of equation (12):

$$E = F' (q_a - q_s) \quad (13)$$

We choose q_a to be an atmospheric value of moisture, calculated or measured at least several meters above the surface, and we define q_s as the measure of atmospheric moisture within the interface layer. The value of q_a is then controlled by turbulent mixing in the atmosphere, but, since turbulence is unimportant in the interface layer, q_s is determined simply by the rate of moisture extraction from the soil (or by the temperature of the interface layer when the soil is saturated or when condensation is occurring). It becomes apparent that the problem of determining the latent heat flux at the earth's surface may be conveniently divided into two separate problems:

- 1) determine q_s from the soil properties and the interface layer temperature, and,
- 2) knowing q_a and q_s , determine the evaporation rate by evaluating F' . We will first address ourselves to the calculation of q_s .

The moisture content of the air in the interface layer is dependent upon many factors, such as the content of liquid water in the soil and its variation with depth, the diffusivity of the soil to both liquid and gaseous water, the capillary attraction of the soil to liquid water, and the moisture extracting ability and stomatal resistance to transpiration of any plants. Unfortunately, a complete

physical treatment of the problem becomes prohibitively complex for our purpose, particularly where there is vegetative cover (see Rutter, 1975). In an attempt to simplify the problem we will look at observations of the relationship between q_s and the single most important factor which controls it--the liquid water content of the soil. Assuming that any vegetation in the interface layer transpires sufficient moisture, then when the soil is saturated q_s in the interface layer becomes identical to q_{sat} , the saturation value determined by T_s , and the evaporation rate E becomes E_{pot} , the potential or maximum rate. Also, when the soil moisture content is zero, q_s takes on the ambient atmospheric value q_a , and E becomes 0. However, the shape of the q_s (or E/E_{pot}) vs. soil moisture curve between these two extreme cases is the subject of much discussion.

The literature offers many observations and suggestions for this relationship. Usually a plot is presented comparing E/E_{pot} with W/W_s where W is available soil moisture content integrated through some sufficiently great depth, and W_s is the saturation, maximum, or field capacity value of W . Since E has a direct, linear relationship to q_s through eq. (13), this is a convenient method of presentation to use here. Figure 2 shows a number of proposed curves which are applicable under different conditions. It is clear that the shape of the curve is highly variable, and that it varies with soil type, plant cover, and evaporation rate. No single curve can adequately describe the relationship for all conditions. However, for the purposes of an atmospheric model, where limited computer space does not permit storage of soil and plant cover types, a single average curve, such as that proposed by Budyko (1948, 1956) and

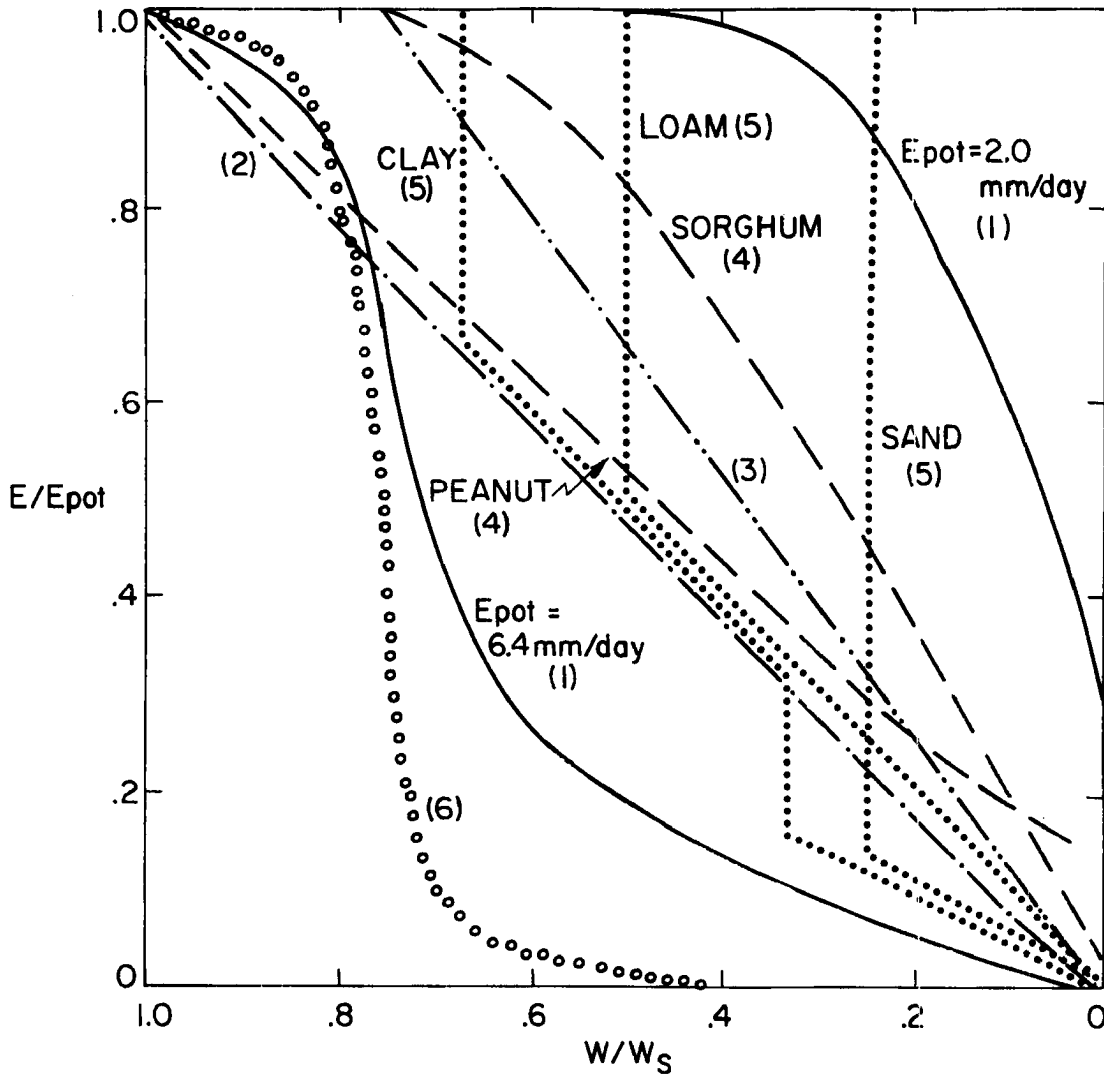


Figure 2. Some observed and theoretical estimates of the relationship between evaporation rate and available soil moisture content, both plotted on normalized scales. 1) Denmead and Shaw (1962) over corn -- colo silty clay loam -- with varying E_{pot} , 2) Thornthwaite and Mather (1955); and Baier (1969), who found ten years of data over grass in mathilda loam to fit this curve best, 3) Budyko (1956) and Manabe (1969) assumed this curve to apply under all conditions, 4) Slatyer (1956) compared plants with different root configurations in Australia. 5) Idealized curves for forested surfaces of varying soil type during the growing season as modelled by Zahner (1967). 6) An example for bare soil as formulated by Phillip (1957) and modelled by Sasamori (1970).

Manabe (1969), or that proposed by Baier (1969), is the best one can do. Furthermore, there has never been a comprehensive treatment proposed which systematically accounts for variation of soil, plant cover, and evaporation rate, since the observations to date have been insufficient.

The proposed average curves in Figure 2 assume a linear relationship between soil water content and evaporation (or q_s) for natural vegetated surfaces. There are two possible linear equations which occur frequently in the literature:

$$q = q_a + \frac{W}{W_s} (q_{sat} - q_a), \quad q_s \leq q_{sat} \quad (14)$$

and

$$q_s = q_{sat} \frac{W}{W_s}, \quad q_s \geq q_a, \text{ but } q_s = q_{sat} \text{ when } \quad (15)$$

$$q_{sat} < q_a.$$

Eq. (14) relates the moisture difference between the interface layer and the free air to the soil water content, while (15) completely neglects the effect of the free air mixing ratio. Thus when W approaches zero, q_s approaches q_a in (14), and approaches zero in (15). Both equations require $q_s \rightarrow q_{sat}$ as $W/W_s \rightarrow 1$. Except for the two limiting cases of saturated soil and $q_a = 0$, (14) always produces a larger value of q_s than (15), and thus should produce a larger evaporation rate. These two formulae have been tested and compared by Nappo (1975), and as expected eq. (14) was found to produce higher evaporation rates than eq. (15). Nappo concluded that eq. (14) is preferable for simulating rural environments.

In a number of experiments by this author, it was found that eq. (14) is more accurate when potential evaporation rates are low, while eq. (15) produces better results for high potential evaporation rates. When eq. (14) was applied to the hot, dry soil conditions of O'Neill, Nebraska in August, the predicted evaporation rate around midday was two to three times larger than both the rate observed and the rate calculated by (15). The better performance of the more conservative evaporation rates predicted by eq. (15) under such conditions is explained by the extreme drying of the upper few centimeters of soil, and by the increased stomatal resistance to transpiration under hot, dry conditions (Rutter, 1975). On the other hand, when the air is cool, such as in the morning at O'Neill, or during the winter (e.g. The Wangara experiment in Australia), eq. (15) was found to predict no evaporation at all because the calculated value of q_s was less than the ambient atmospheric mixing ratio, q_a . Eq. (14) yielded quite reasonable evaporation rates under these conditions.

On the basis of these results, it appears necessary to find a satisfactory combination of the two formulae which will correctly predict evaporation over a wide range of conditions. The two equations available may be interpreted as describing two different mechanisms for evaporation. Eq. (14) represents a semi-potential evaporation process. That is, it may be visualized that each unit of surface area is divided into two sections--a totally saturated section covering $100(W/W_g)\%$ of the unit, and a totally dry area covering the remainder of the unit. The saturated portion does not offer any resistance to evaporation; and no evaporation occurs from

the dry portion. However, thermal properties remain uniform across the unit. On the other hand, eq. (15) may be considered a total-resistance evaporation process. Here the water vapor must penetrate a resistance inversely proportional to W/W_s before it is released.

Figure 3 shows a schematic representation of the two cases in a unit block of soil at the earth's surface. The dry parts of the block offer a uniform resistance to vertical moisture flow per unit distance; and the moist parts are assumed saturated and offer no resistance. When the entire block is saturated with water it is assumed that $W=W_s$. The third case, which represents a more realistic situation in which both mechanisms come into play, should be easily represented in terms of a combination of (14) and (15). To this end

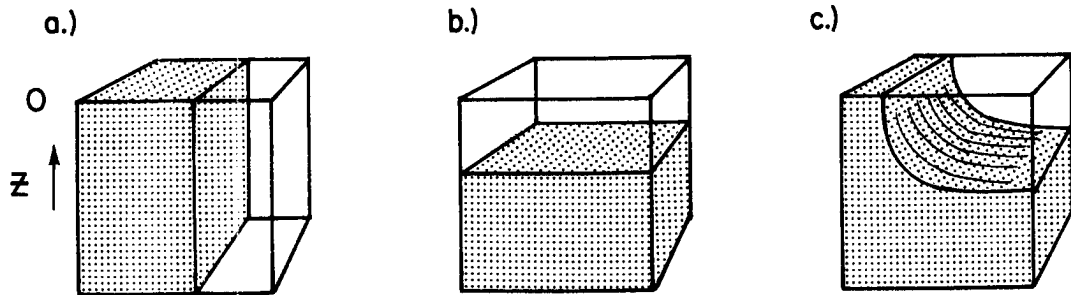


Figure 3. Idealized representation of the evaporation process in a unit block of soil as implied by: a) eq. (14), b) eq. (15), and (c) a realistic situation where both processes occur. Shaded areas are saturated.

we define a pair of effective soil moisture values such that $E(W) = E_p(W_p) = E_R(W_R)$, where E and W are the actual values of evaporation rate and soil moisture content respectively, and W_p and W_R are the effective soil moisture required to permit equations (14) and (15) respectively to yield the true evaporation rate. Thus we have

$$q_s = q_a + \frac{W_p}{W_s}(q_{sat} - q_a) \quad (16)$$

$$= \frac{W_R}{W_s} q_{sat} \quad (17)$$

In order to close the system we require an additional equation which we obtain by applying the concepts of potential and resistance to their electrical analog. The familiar concept that potential equals current times resistance may be applied by noting that the magnitude of the potential for evaporation is related to the effective available moisture for the semi-potential process, W_p . Also, the source of resistance to evaporation is the effective depth of dry soil through which moisture must flow to reach the surface. In the ideal total-resistance case this depth is large when W_R is small, and vice versa, so the resistance may be represented by the inverse of the effective available moisture W_R . Finally, the manifestation of the current, which ultimately results in the evaporation, is the amount of soil moisture which has crossed the resistance barrier to become atmospheric vapor at the surface (q_s). In non-dimensional form we may write

$$\frac{W_p W_R}{W^2} = A \frac{q_s}{q_{sat}}, \quad (18)$$

where, for convenience, the soil moisture values have been scaled by their true value, W , and the surface mixing ratio has been scaled by its saturation value. The value of the constant of proportionality, A , must be determined experimentally. Eliminating W_R and W_p from equations (16), (17) and (18), we find

$$q_s = q_a + A \frac{W^2}{W_s^2} (q_{\text{sat}} - q_a). \quad (19)$$

The constant A has been assigned a value of 0.5. With this value, (19) coincides with (15) at moderately high evaporation rates, and approaches (14) when the evaporation becomes weak.

The value of W_s is set at 10 cm, although the calculation over a period of less than 24 hours is quite insensitive to the choice of this value compared to the value of the ratio W/W_s . The slow decrease of W with time is calculated from the rate of evaporation. Allowance is made for the accumulation of dew when the latent heat flux is downward. This occurs, of course, when the interface layer saturation mixing ratio is less than the mixing ratio of the air in the surface layer above. When dew is present it is assumed that the mixing ratio of the air at the interface is saturated. Under conditions of evaporation all dew is allowed to be depleted before evaporation of soil moisture begins.

Having calculated q_s by the procedure described above, we must now determine E from our knowledge of the atmospheric moisture gradient and the turbulent exchange acting on that gradient. We have a choice of a number of formulae, such as the aerodynamic method in which a

drag coefficient for moisture is applied, and in which the evaporation rate depends on the wind velocity directly (Deardorff, 1978; Manabe, 1969). Or we may choose from a variety of surface layer profile functions which empirically relate the evaporation rate directly to the turbulent process and which account for changes in atmospheric stability. A number of these surface layer functions have been tested by Pierson and Jackman (1975). They found the Businger-Dyer (B-D) surface layer formulation to be less accurate in describing their observational data than some other equations given in the literature. However, Pierson and Jackman noted that their test of the B-D equations was not comparable to their other tests, since they did not regress the needed empirical parameters to their data, as was done for the other profile functions they tested. Instead they simply used values of the parameters quoted in the literature. Furthermore Pierson and Jackman used an unnecessarily circuitous relationship given by Brutsaert (1965) in determining evaporation for all their tests. Brutsaert's formula relates evaporation to the profile function for the wind through the parameter $\eta = K_W/K_M$ and K_M are the eddy diffusion coefficients for water vapor and momentum respectively. He assumes ipso facto that the profile function for moisture itself is unknown. Finally, the data used by Pierson and Jackman all come from a thoroughly irrigated field of grass, under strong unstable conditions, in a region where the natural soil surface is very dry (the Davis, California lysimeter site). Thus the data strictly apply to a very narrow range of conditions, i.e. an oasis in the summertime where evaporation is always occurring at nearly the potential rate.

In a number of numerical experiments by this author, it was found that the B-D profile formula for water vapor used directly gives results very close to the formulae found superior by Pierson and Jackman (1975), and that it may be more accurate under a broader range of conditions. The B-D form tested is much simpler mathematically, and it has the further advantage of being consistent with the B-D surface layer profiles for wind and temperature which are generally accepted today, and are used in this model. Therefore we have chosen to use the B-D form to calculate evaporation.

Using the E-D form, recognizing that the profile functions for heat and water vapor are nearly the same (Dyer, 1967), and extrapolating the calculated moisture flux value to the surface in a manner which will be described in section B. of this chapter, we determine the heat flux of evaporation as follows:

$$H_E = \bar{\rho} L^* \overline{w'q'_s} \quad (20)$$

Here L^* is the latent heat of condensation, and $\overline{w'q'_s}$ is the surface value of the eddy flux of moisture.

4. Heat flow into the ground.

The transfer of heat within the soil may be calculated exactly from the equation

$$\frac{\partial T}{\partial t} = \frac{\partial}{\partial z} \left(\frac{k}{\rho c} \frac{\partial T}{\partial z} \right) \quad (21)$$

where k is the conductivity of the soil, ρ is the soil density, and c is the specific heat capacity. In general, k , ρ and c vary with depth in the soil and with the moisture content of the soil. Numerical

solution of eq. (21) requires knowledge of the temperature (and soil properties) at a number of levels within the soil (Carslaw and Jaeger, 1959), and imposes a restriction on the time step of the model. In keeping with the objective of this model to represent reality in a numerically simple form, we seek a parameterization based on eq. (21) which does not require storage of numerous levels of soil temperature, and which is computationally efficient. Toward this goal a number of numerical tests were performed in which eq. (21) was evaluated through as many as 51 levels for a diurnal cycle. The calculated heat flow was compared with observational data and with the results of the steady state heat flow equation

$$H_G = -k \frac{dT}{dz}, \quad (22)$$

in finite difference form with $\Delta Z = 15$ cm and $T_{15 \text{ cm}}$ kept constant. As a result of these experiments, it was found that eq. (22) could be modified in a way to simulate the "true" solution for a typical diurnal cycle. This was done by specifying a variable effective 15 cm depth soil temperature and multiplying the right side of eq. (22) by a constant. Specifically, the formulation used is:

$$H_G = 1.75 k \frac{(T_s - T_{\text{soil}})}{15 \text{ cm}} \quad (23)$$

where

$$T_{\text{soil}} = \begin{cases} T_{15 \text{ cm}}^{-16.5} \sin \left[2\pi \left(\frac{t-7}{14} \right) \right] \sin \left[\pi \left(\frac{t-7}{14} \right) \right] \dots \\ \dots \text{for } 0700 < t(\text{in hours}) < 2100 \\ T_{15 \text{ cm}} & \text{for all other } t. \end{cases}$$

This representation of the soil temperature at 15 cm. is clearly not meant to represent reality at that level. Rather, it is a construct which permits an accurate representation of the soil temperature gradient near the surface -- the required quantity for eq. (22). However it is convenient to retain eqs. (23) in this awkward form, and to store the 15 cm. soil temperature as a constant, because it permits an actual observable value to be used as input and unchanging reference point for our parameterization. A depth of 15 cm. is as close to the surface as one can safely make the assumption that the diurnal wave has been damped completely (Munn, 1966), so that a single constant value may be used as input for the model.

This parameterization becomes less adequate when non-diurnal heating of the earth's surface is important. For example, when the surface temperature is modified by abrupt changes in cloud cover, or by a frontal passage, the steady state assumption is grossly violated.

An exactly analogous soil heat flow parameterization developed by Blackadar (1976), has been discussed by Deardorff (1978). It was found to be the most accurate yet devised which does not require knowledge of the soil temperature profile or of the past history of the soil surface temperature. The method, called by Deardorff the "force-restore" method, includes two terms. The force term modifies the soil surface temperature by assuming that an effective mass per unit area of soil is uniformly heated by the residual of the surface energy budget. Thus, the force term is expressed exactly by eq. (6) above, except that the biomass coefficient mc_s is replaced by a coefficient which assumes a sinusoidal surface temperature cycle with

period $\tau = 24$ hours. The coefficient may be written $(\frac{1}{2}\sqrt{\pi}) \sqrt{\rho c k \tau}$, and its magnitude is typically similar to a typical value of mc_s . The second term of this formulation, as discussed by Deardorff, is called the restore term because it acts to return the soil surface temperature to a fixed equilibrium deep-soil temperature. This term is identical to eq. (23) except that the coefficient $1.75 k/\Delta z$ is replaced with a coefficient of the same magnitude: $(\pi \rho c k / \tau)^{\frac{1}{2}}$.

B. The Surface Layer

The surface layer is defined as the region of the atmosphere in which the length scale of turbulent motions is primarily controlled by mechanical generation of turbulence at the surface. The depth of this layer can range from less than a meter to more than a kilometer although it is typically between 10 and 100 meters. There is strong support for the contention that the depth is proportional to the absolute value of the Obukhov length, L . This is true for unstable stratification (Lilly, 1968; Tennekes, 1970; Deardorff, 1972a; Wyngaard et al., 1974; Kaimal, et al., 1976) as well as for stable conditions (Webb, 1970; Businger and Arya, 1974).

The surface layer has often been called the "constant-flux" layer, and it has been so treated in many models of the boundary layer (e.g. Estoque, 1963; Pielke and Mahrer, 1975; Sasamori, 1970). The origin of the concept that the surface layer is a layer through which the fluxes of heat and momentum do not vary significantly with height dates back to the beginning of study of the surface layer itself. Calder (1939) presented a theoretical proof of the constant flux hypothesis although some of the assumptions he made are questionable. Observations in the atmospheric surface layer also have lent support

to this hypothesis, because, across the few tens of meters of the surface layer, the variation of the heat and momentum fluxes is only a few percent of the total value - often within the measurement error of the instrumentation. In reality, however, the rate of variation with height of fluxes within the surface layer may often be greater than anywhere else in the PBL (Deardorff, 1972b). This is apparent from eq. (1) since the diurnal extremes of temperature are greater in the surface layer than they are in the outer layer. We will treat the surface layer as a variable-flux layer, and calculate a flux at its top and bottom.

The fluxes at the top of the surface layer are calculated from the Businger-Dyer (B-D) profile functions (Businger et al., 1971) as integrated by Paulson (1970). They are

$$-\overline{w'\theta'_v} = \frac{\kappa u_{*b}}{0.74} (\theta_{vb} - \theta_{vs}) / \left(\ln \frac{z}{z_0} + \psi_H \right) \quad (24)$$

$$-\overline{w'q'_b} = \frac{\kappa u_{*b}}{0.74} (q_b - q_s) / \left(\ln \frac{z}{z_0} + \psi_H \right) \quad (25)$$

$$u_{*b} = \kappa \sqrt{u_b^2 + v_b^2} / \left(\ln \frac{z}{z_0} + \psi_U \right) \quad (26)$$

where $u_* = \sqrt{u'w'}$, θ_v indicates virtual potential temperature, and the subscripts s and b denote values at height z_0 and at the top of the surface layer ($z = z_b$) respectively. The value of κ , the Von Karman constant, is set at 0.35, and ψ_H and ψ_U are the stability-dependent integrated profile functions for heat and momentum. The disposition of these functions will be discussed below. Paulson compared the B-D profile functions to several others including the

KEYPS formula and found the B-D empirical form to most closely fit data from Kerang, Australia. Businger et al. (1971) found the same form also closely fit their data from a Kansas wheatfield.

The integration of the B-D formulae was performed by Paulson under two assumptions which should be examined. First he integrated from height $z = 0$ to some height z , whereas the surface layer formulations do not apply between $z=0$ and $z=z_0$. The exact lower bound for integration should be z_0 . Nickerson and Smiley (1975) integrated the B-D profiles in this exact manner, and produced a more involved expression; but their analysis shows that, with the exception of very unstable conditions with large z_0 , the error in using Paulson's integration is negligible. The Nickerson-Smiley integration is used here in the sensitive determination of the surface fluxes. Otherwise the Paulson form is used with a simple correction factor applied when conditions warrant (see below). The second aspect of Paulson's integration is that it is derived under the constant-flux assumption, i.e. $\overline{w'\theta'}$ _{vb} and u_{*b} are held constant during the vertical integration. However, because the B-D functions are rooted in actual observational data, any effect resulting from variation of fluxes with height is necessarily captured in the empirical functions Ψ -- at least to the extent that the actual data fit the proposed curves.

In developing the B-D profile functions, it was assumed that the functions Ψ depend only on the non-dimensional height $\frac{z}{L}$, where the scaling length L is the Obukhov length -- a stability parameter given by

$$L = \frac{u_{*b}^3}{\kappa(g/\theta_{vb}) (-\overline{w'\theta'_{vb}})} \quad (27)$$

Paulson's integrated expressions for $\Psi\left(\frac{z}{L}\right)$ are rather complicated and require iteration or the inversion of a rather protracted equation to determine the fluxes of heat and momentum at a constant fixed height z . However, in keeping with our goal of maintaining simplicity where possible, we find that storing a table of Ψ values indexed to various ranges of L presents very little loss of accuracy. The surface layer top, z_b , is restricted to be no higher than 50 meters, and when $|L|$ is smaller than 50 meters, z_b is assigned the value $|L|$ since it is not clear that the B-D functions apply above $z = |L|$ (Dyer and Hicks, 1970). Under these restrictions, the largest values of Ψ occur when $|L| \leq 50$ meters:

$$\Psi_{H_{\max}} = \begin{cases} -1.466 & L \leq 0 \\ +6.35 & L > 0 \end{cases}$$

$$\Psi_{U_{\max}} = \begin{cases} -1.084 & L \leq 0 \\ +4.7 & L > 0, \quad |L| \leq 50 \text{ meters.} \end{cases}$$

As $|L|$ approaches infinity Ψ approaches zero. Thus tables of 15 values of Ψ were considered adequate to determine the fluxes to within a few percent. When $|L| > 50$ meters the table value used may be in error by a maximum of ± 0.4 for stable conditions and ± 0.05 during unstable conditions. Since the logarithmic term in (24), (25) and (26) is virtually always between 3 and 10 when $z = z_b = 50$ meters, the maximum possible error in the denominator of (24), (25) and (26) (and thus in the calculated flux value) is about 5%. This is within the uncertainty limits of flux measurement and of the B-D profile functions themselves.

When $z_b = |L| \leq 50$ meters the value of ψ equals ψ_{\max} and there is no error except for that caused by Paulson's lower bound of integration. This condition often prevails for most of the daylight hours and many nights. Only during the hours around sunrise and sunset and on some cloudy days will $|L|$ remain greater than 50 meters.

For $0 > \frac{L}{z_o} \geq -50$ Paulson's integration produces significant error and a correction factor must be applied to the value of ψ . Again a table of values is employed, ranging from near zero when $\frac{L}{z_o} = -50$ to approximately +1 when $\frac{L}{z_o} \sim -1$. For the case where $|L| > 50$ meters this correction is not applied for two reasons. First when $z_b \neq |L|$ the correction becomes a function of $\frac{z_b}{L}$ as well as of $\frac{L}{z_o}$ and a two dimensional table would be required. Secondly the correction is not needed unless z_o exceeds 100 cm., which is a rather unusually large value, even over forested terrain.

In summary, the table values of ψ used in this model and the table of correction terms are presented in tables 1 and 2. Using these tables the maximum possible deviation from the Nickerson-Smiley surface layer formulation is about 5% and the average deviation will be much less.

The use of a variable height for the upper bound of the surface layer presents problems of mass continuity which will be confronted in the next section. In order to maintain the integrity of the outer layer, the height of the PBL top (z_i) is required to remain at or above 60 meters. Similarly a lower limit on the surface layer thickness is established: $z_b \geq z_o + 50$ cm. This maintains at least a

Table 1 Values of ψ used in equations (24), (25) and (26).
 Values of ψ_{\max} only are subject to corrections given
 in Table 2. Note: $\psi_U \text{ stable} = 0.74 \psi_H \text{ stable}$.

$ L $ (meters)	unstable ψ_H	stable ψ_H	unstable ψ_U
(ψ_{\max}) < 50	-1.466	6.35	-1.084
50 - 59.99	-1.4	5.8	-1.04
60 - 69.99	-1.3	4.9	-0.96
70 - 79.99	-1.2	4.23	-0.89
80 - 89.99	-1.124	3.74	-0.84
90 - 99.99	-1.06	3.34	-0.79
100 - 149.99	-0.905	2.54	-0.68
150 - 199.99	-0.74	1.81	-0.56
200 - 249.99	-0.62	1.41	-0.47
250 - 299.99	-0.54	1.16	-0.42
300 - 399.99	-0.46	0.91	-0.35
400 - 499.99	-0.38	0.71	-0.29
500 - 999.99	-0.25	0.42	-0.20
1000 - 1499.99	-0.16	0.25	-0.13
≥ 1500	-0.1	0.16	-0.08

Table 2 Correction values to be added to the values of ψ_{\max} given above. This table is used only when $0 > L > -50$ meters.

$-\frac{L}{z_0}$	ψ_H correction	ψ_U correction
2	1.2	0.89
2 - 2.99	0.9	0.68
3 - 3.99	0.74	0.56
4 - 4.99	0.62	0.47
5 - 5.99	0.54	0.42
6 - 6.99	0.48	0.37
7 - 7.99	0.43	0.33
8 - 8.99	0.39	0.31
9 - 9.99	0.36	0.28
10 - 14.99	0.29	0.23
15 - 19.99	0.22	0.17
20 - 24.99	0.18	0.14
25 - 29.99	0.15	0.12
30 - 34.99	0.13	0.10
35 - 39.99	0.11	0.09
40 - 44.99	0.10	0.08
45 - 49.99	0.09	0.07
≥ 50	0	0

minimal amount of mass in the surface layer for numerical stability of the surface layer variables. This restriction is only needed under very rare cases of extreme stratification.

Fluxes at the interface. In order to determine the fluxes at the bottom of the surface layer the wind, temperature and moisture profiles are extrapolated from z_b downward to near the surface using the Nickerson-Smiley (N-S) integrated profile functions. The lowest point to which these profile shapes apply (which we will label z_h) on a real surface is somewhere in the vicinity of the highest protruding solid objects. Generally, for most surfaces this height is of the order $z_h \approx 10z_o$ (e.g. Garratt, 1978) although this value can vary depending on the vertical variation of the density of the vegetation and on the horizontal spacing of plants or obstacles. Given the fluxes and mean values of θ_v , u , and q at z_b , the N-S equations lead to the mean value at z_h for unstable stratification through the following process. The N-S integrated profile equations are

$$\frac{\kappa u}{u_*} = \ln \left[\frac{(\xi_o - 1)(\xi_o + 1)}{(\xi + 1)(\xi_o - 1)} \right] + 2 \left[\tan^{-1} \xi - \tan^{-1} \xi_o \right] = f(z, z_o)$$

$$\xi = \left(1 - 15 \frac{z}{L} \right)^{1/4} \quad (28)$$

$$\frac{\kappa}{0.74} \frac{(\theta_v - \theta_{vs}) u_*}{(-w' \theta' / v)} = \ln \left[\frac{(\eta - 1)(\eta_o + 1)}{(\eta + 1)(\eta_o - 1)} \right] = g(z, z_o)$$

$$\eta = \left(1 - 9 \frac{z}{L} \right)^{1/2} \quad (29)$$

If we set $z=z_h$ in the above equations and then divide each equation by the corresponding equation for $z=z_b$, we have, after manipulation

$$u_h = \frac{f(z_h, z_o)}{f(z_b, z_o)} u_b \quad (30)$$

$$\theta_{vh} = \theta_{vs} + \frac{g(z_h - z_o)}{g(z_b - z_o)} (\theta_{vb} - \theta_{vs}) \quad (31)$$

Note that the exact N-S equations are required here because of the proximity to z_o , where the error in Paulson's integrations becomes significant.

Now in order to find the fluxes leaving the plant canopy, we must define representative values of temperature, wind, and mixing ratio in the canopy, and we must specify a characteristic height of the plant canopy as the source of the characteristic value. To do so each variable must be treated separately. For momentum, the proper characteristic height is the experimentally determined roughness length z_o . This is the height at which the ideal wind profile goes to zero -- our desired representative value in the plant canopy. The problem is less straightforward in the case of the temperature and moisture values. The representative temperature we seek is some value near the top of the layer in which most of the solar radiation is absorbed. Its characteristic height must be great enough so that this temperature may be transmitted to the free atmosphere by convection as though it were unobstructed by solid objects. Similarly the representative mixing ratio value must come from the upper portion of the layer of vegetation in which most of the evapotranspiration is

taking place. Clearly we are dealing with a complex problem of parameterizing four interacting quantities: the representative temperature and mixing ratio, and their characteristic heights. Even under fixed external conditions the four parameters may vary depending on the profile of vegetation density. Furthermore the effective vegetation density profile for evapotranspiration will not generally be the same as the effective vegetation density profile for radiation exchange; and both profiles may vary with the time of day. To simplify the problem for this model we use a simple parameterization to specify a representative temperature and mixing ratio for all types of surfaces based on just one parameter--the total biomass of the interface layer for temperature, the soil moisture content for mixing ratio. Then the characteristic heights at which these values should apply are estimated based on the available information about the vegetation at each site.

The temperature to be used is the mean interface layer temperature given by eq. (6), and the representative mixing ratio is the surface value q_s described by eq. (19). In order to reach some rational estimate of the height at which these values should apply we refer to the simpler case of the momentum flux. As the momentum flux is parameterized, all momentum is represented as transferring downward, without obstruction, to z_0 where there is an infinite resistance in an infinitesimal layer. Under these assumptions the wind velocity profile is described by the appropriate surface layer profile function right down to z_0 . In fact, for small z ($z \ll |L|$) the profile is very accurately described by the logarithmic (or neutral) profile. Therefore, in our model, we assume a logarithmic wind profile between

$z_h (=10z_o)$ and z_o , and determine the friction velocity at z_h using the equation

$$u_{*s} = \frac{\kappa u_h}{\ln \frac{z_h}{z_o}} = 0.152u_h \quad (32)$$

where u_h is the wind velocity at height $z_h=10z_o$. If, in exact analogy to the momentum case, one were to assume that the source of heat and moisture is an infinitesimal layer at z_o , we could immediately write equations similar to (32). However, as discussed earlier, the infinitesimal layer is a poor assumption on which to predict surface temperature. Therefore, unlike the momentum case where we can be sure of a parameterization that sets $u=0$ at z_o , we cannot so easily define a temperature at z_o for such an ideal case. The observed level of maximum temperature within vegetation is generally at some height greater than z_o (Geiger, 1959). Thus the layer-averaged interface temperature is calculated, and its characteristic height must be estimated. We assume, since the interface layer temperature is the average temperature of all solid matter above $z=0$, that the characteristic height should be near the average top of the solid obstacles-- i.e., the height where any protruding elements are a minimal obstruction to convection. Thus the characteristic height is chosen so that, as with the momentum, the temperature and moisture profiles above this height are described by the appropriate surface layer profile function.

Let us call the characteristic height for temperature z_θ , and that for moisture z_q . If we integrate the B-D profile function from z_θ or z_q to z_h , we get an equation of the form of (29) or (24). In both cases, when $z_h \ll L$ the equations reduce to logarithmic profiles and we may therefore write

$$\overline{w'\theta'}_{vs} = \frac{\kappa u_* s (\theta_{vh} - \theta_{vs})}{0.74 \ln z_h/z_o} \quad (33)$$

$$\overline{w'q'}_s = \frac{\kappa u_* s (q_h - q_s)}{0.74 \ln z_h/z_q} \quad (34)$$

It should be noted that the two heights z_θ and z_q may be unequal. The effects of varying the values of z_θ and z_q have been tested and results are presented in chapter IV. For the cases of rather sparse vegetation at O'Neill and the Wangara experiment, satisfactory results were obtained setting the two heights equal at the following values:

$$\begin{aligned} z_\theta = z_q &= 1.14z_o && \text{for O'Neill} \\ z_\theta = z_q &= 2.0z_o && \text{for Wangara.} \end{aligned}$$

Based on several studies Garratt (1978) has concluded that an analogous characteristic height for temperature z_T has the magnitude $z_T = z_o/7$, however that height corresponds to a measured horizontal average surface temperature rather than a vertically averaged interface layer value as is used here. Finally we should state that the sensible heat flux at the surface, as determined by $\overline{w'\theta'}_{vs}$, is calculated separately from,

and is based upon surface layer temperatures already modified by the radiative flux divergence calculation. So the value of $\overline{w'\theta'_s}$ which is calculated by our model is complementary to whatever method is used to determine the radiative heating of the surface and boundary layers.

Because we have determined the fluxes of heat and momentum at both the upper and lower boundaries of the surface layer, it is possible to predict a mean temperature, moisture, and wind for the layer using an equation such as eq. (1). Mathematically such a calculation is independent of the temperature and wind structure in the PBL above z_b . However, because of the free exchange of mass between the surface layer and layers above, any calculation of the surface layer mean temperature and wind must be closely linked with the values above, or unreasonable profiles of these quantities would quickly develop. We will therefore defer the discussion of the surface layer temperature and wind to the next section where the entire PBL temperature and wind structure is discussed.

C. Outer layer assumptions.

The outer layer or mixed layer extends from the top of the surface layer upward to the level where the direct influence of the surface vanishes. More specifically, the upper limit of the outer layer coincides with the top of the PBL at height z_i for the purposes of this model. This height is defined as the level at which surface-forced thermal and mechanical turbulence disappears. There is a vast difference in the behavior and depth of the outer layer between day and night, and it is therefore convenient to use separate parameterizations for each regime.

The use of the word parameterization here refers to the assumptions which are made about the shape of the temperature and wind profiles. A single mean outer layer value of θ_v , u , and v is calculated based on the assumed profile shapes. During unstable stratification, the transition layer variables are assumed to be well mixed, having constant values with height. An infinitesimally thin inversion, or zero order discontinuity of all variables is assumed at z_i -- this is the source of the name "jump" model (Ball, 1960; Tennekes, 1973; etc.). The corollary to the assumption that the unstable outer layer is well mixed requires the eddy flux profiles to vary linearly with height (with the exception of the momentum flux profiles under conditions of geostrophic shear). This is supported by observations and by model results (Lenschow, 1970; Rowland, 1973; Deardorff, 1972a, 1973; Cattle and Weston, 1975). When the stratification is stable there is some question as to the proper shape of the profiles of transition layer variables. Businger and Arya (1974) present an argument which suggests that the profiles should be essentially linear above $|L|$. On the other hand, Webb (1970) finds that the profiles above height $|L|$ become roughly logarithmic. We have chosen to assume that the variables may be represented by linear profiles, with a first order discontinuity rather than a "jump" at z_i . This assumption seems to satisfactorily fit the data (eg. the Wangara and O'Neill data - see figures 7 e,f; 14 h; 19 e,f,g,h,i,p below). The only corollary statement that can be made about the flux profiles under this assumption is that they vary smoothly with height and are single valued everywhere in the outer layer. Wyngaard (1975), in some higher order numerical experiments, found the flux profiles to vary approximately linearly with

height; however, since our model calculates only layer-averaged values of the variables, it is not necessary to specify the flux profiles. It is only required to know the flux values at the top and bottom of each layer. For the stable outer layer the fluxes at the bottom (at z_b) are given by (24), (25) and (26), and the fluxes at the top of the layer (z_i) are set to zero by definition. The formulation of, and the consequences of these assumptions are discussed in detail below.

Previous parameterized PBL models of the type used here (Lavoie, 1972; Schubert, 1976) have treated only the unstable or neutral boundary layers. Considerable effort was expended in this study to parameterize the less well-understood stable case, and to effect a transition between unstable and stable regimes which is consistent with observations. Also, new methods of calculating the stable and unstable PBL height, z_i , were developed and incorporated into the model. These are discussed in the subsection below. In following subsections we cover the temperature and wind calculations for the surface and transition layers, and the treatment of clouds within the transition layer.

1. The height of the boundary layer, z_i .

In the diabatic atmosphere, the height of the PBL is controlled to a large extent by thermal forcing. During the daytime, heat is added at the surface and is transported upward in the form of buoyant thermal turbulent eddies. These eddies move freely until they encounter a sufficiently stable layer of air at z_i . The continued bombardment of the stable layer by the thermals steadily erodes or entrains the stable air so that, in the absence of subsidence, z_i will

rise as long as there is an upward heat flux at the surface. At night heat is removed from the earth's surface, and the cold layer is extended upward by mechanical turbulence. The height to which the nocturnal inversion extends (z_i) depends on the wind speed as well as the cooling rate at the surface. We will first discuss the unstable boundary layer height, then the less well-understood stable boundary layer height will be covered, and finally we will consider the periods of transition around sunrise and sunset.

The Unstable case. The boundary layer height in an unstable atmosphere is a time dependent phenomenon in that it requires a prognostic equation to describe its behavior. This is not necessarily the case for the neutral and stable PBL, which are to be discussed later. The unstable boundary layer is capped by a strong inversion or temperature "jump" which, for the purposes of this model, is assumed to be contained within an infinitesimally thin layer. In the absence of clouds the average lapse rate below the inversion is dry adiabatic. The height of the inversion, z_i , is controlled by changes of the potential temperature in the dry adiabatic mixed layer, by the lapse rate in the stable air above z_i , and by changes in the inversion strength, or temperature jump $\Delta\theta_v$.

An early prognostic equation for z_i is given by Deardorff (1972):

$$\frac{\partial z_i}{\partial t} = w_i - \vec{V}_{z_i} \cdot \vec{\nabla} z_i + \frac{\partial \theta_{vm}}{\partial t} / \Gamma_L, \quad (36)$$

This simply states that z_i responds to the changes in PBL temperature and inversion strength in a manner proportional to the lapse rate of the air through which the inversion must rise. Now, the second term in the parentheses, the change of mixed layer temperature, θ_{vm} , is controlled by the layer-average PBL heat flux divergence which is calculated separately (see below); but the strength of the inversion, $\Delta\theta_v$, is dependent on the activity at the inversion itself. The value of $\Delta\theta_v$ is determined by a balance between the rate of rise of z_i and the rate of entrainment of stable air from above. In equation form we have

$$\Delta\theta_v = (-\overline{w'\theta'_{vi}}) / \frac{\partial z_i}{\partial t}. \quad (37)$$

For a given rate of rise of the inversion, the downward transfer of heat will be greater if the temperature jump is larger. On the other hand, for a given entrainment heat flux, a rapidly rising inversion requires less temperature jump than a slowly rising z_i . In order to close the system of eqs. (36) and (37), Tennekes used the widely quoted assumption that the entrainment rate is a fixed percentage of the surface heat flux--specifically,

$$\overline{w'\theta'_{vi}} = -0.2 \overline{w'\theta'_{vs}}. \quad (38)$$

This assumption is inadequate for use in the present model, and a more general statement has been obtained, which will be discussed shortly. However eq. (38) is satisfactory for situations where z_i changes only slowly, as is the case in the example which follows.

In order to test the validity of eq. (36) and to compare it with the earlier form, eq. (35), we employ the results of a sophisticated numerical model due to Deardorff (1974a). Table 1 in that paper tests eq. (35) and presents most of the numerical values of the variables needed to test the system of eqs. (36), (37) and (38). A modified version of this table appears here as Table 3. The changes from the original table are twofold. First, the table has been expanded so that it includes morning values (which were reported by Deardorff (1974a) but not included in his table), and so that it includes an additional two columns of data necessary to test eqs. (36), (37) and (38). The second modification to the table is more fundamental in nature. The reported values of $\overline{w'\theta'}_{vi}$ and $\Delta\theta_v$ have been modified as a result of redefining z_i -- a procedure which is discussed below.

It is necessary to carefully define the boundary layer top when comparing a jump model with "real" horizontally averaged data. The definition of z_i used by Deardorff (1974a), which applies to his horizontally averaged numerical results, is that it is the level where the sensible heat flux, $\overline{w'\theta'}_v$ is a minimum (see Figure 4). The jump model assumes that the heat flux decreases linearly to a minimum value at z_i , above which it is zero. If z_i is arbitrarily assigned the same value for the real data and the jump model, the total negative area within the $\overline{w'\theta'}_v$ curves will not necessarily be the same for both cases, as is shown in Figure 4. In order to keep the boundary layer represented by the jump model comparable to the data it simulates, z_i must be redefined, and the values of $\Delta\theta_v$ and $\overline{w'\theta'}_{vi}$ must

Table 3. Comparison of z_i predictive eqs. (35) and (36-38). Data is adapted from Deardorff's (1974a) numerical simulation of Day 33 of the Wangara Experiment. $d\theta_L/dz = 7.5^\circ\text{C km}^{-1}$.

Time	\bar{z}_i (m) (real)	z_i (m) (jump model)	(real & model) $\frac{dz_i}{dt}$ (cm sec ⁻¹)	$\frac{-w'\theta'v_i}{\text{cm sec}^{-1} \text{ } ^\circ\text{C}}$	$\frac{w'\theta'v_i}{\text{cm sec}^{-1} \text{ } ^\circ\text{C}}$	$\Delta\theta_v$ ($^\circ\text{C}$)	$\frac{d(\Delta\theta_v)}{dt}$ ($^\circ\text{C hr}^{-1}$)	equation (38) $\frac{-w'\theta'v_i}{w'\theta'v_i}$ vs	equation (37) $\frac{dz_i}{dt} \frac{\Delta\theta_v}{-w'\theta'v_i}$	equation (35) $\frac{dz_i}{dt} \cdot \frac{d\theta_{vL}}{dz} \frac{1.2\bar{w}'\theta'v_i}{\text{vs}} / z_i$	equation (36) $\frac{dz_i}{dt} \cdot \frac{d\theta_{vL}}{dz} \frac{1.2\bar{w}'\theta'v_i}{\text{vs}} + \frac{d(\Delta\theta_v)}{z_i dt}$
1000	280	290	—	1.3	14.5	0.5	—	0.09	—	—	—
1030	—	—	—	0.0	—	0.0	—	0.00	—	—	—
1100	840	900	6.0	4.0	17.8	0.8	0.80	0.22	1.20	1.90	0.98
1200	1050	1100	4.7	5.1	20.6	1.2	0.25	0.25	1.11	1.57	1.20
1300	1190	1230	3.2	3.8	20.2	1.3	0.15	0.19	1.09	1.22	1.01
1400	1305	1340	3.0	4.0	20.5	1.5	0.15	0.20	1.12	1.23	1.00
1500	1415	1440	2.5	4.0	21.5	1.6	0.00	0.19	1.00	1.05	1.05
1600	1480	1490	1.4	2.1	15.0	1.5	-0.05	0.14	1.00	0.87	0.98
EXPECTED VALUE								~0.2	1.0	1.0 ?	1.0

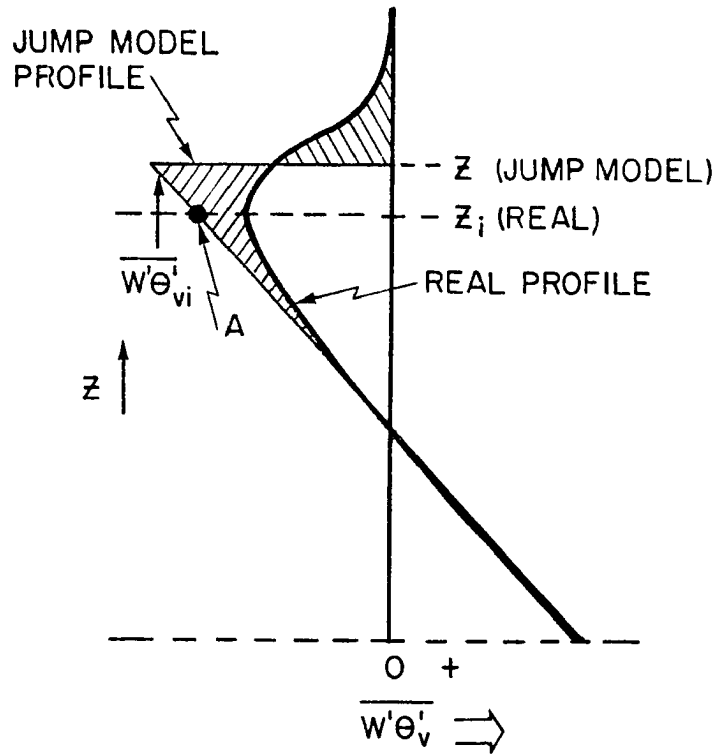


Figure 4. Schematic representation showing the redefinition of z_i when real heat flux profiles are adapted to the jump model.

be consistent with the redefined value. The appropriate redefinition is one in which the area of negative heat flux for both situations is kept the same. This assures that the total flow of heat downward into the PBL is the same for model and reality. It is also the equivalent of requiring the buoyant production of turbulent kinetic energy to be the same in both cases. Because the kinetic energy considerations are quite important to the entrainment process at z_i , a brief digression to discuss the kinetic energy balance is useful here before returning to table 3.

A simplified form of the turbulent kinetic energy equation which we will apply to the region near z_i is given by Zilitinkevich (1975):

$$\frac{\partial \overline{KE}}{\partial t} = \frac{g}{\theta_{vs}} \overline{w'\theta'_v} - \frac{\partial}{\partial z} (\overline{w'KE'}) - \epsilon_{KE} \quad (39)$$

where \overline{KE} is the local value of turbulent kinetic energy, and ϵ_{KE} is the rate of eddy dissipation of \overline{KE} . The first two terms on the right are the buoyant production and vertical transport terms respectively. In the vertical transport term the effects of pressure fluctuations have been ignored. Furthermore, the assumption has been made that buoyant production is sufficiently large to overshadow the mechanical generation of \overline{KE} , and the latter has been neglected. This is a good assumption for the bulk of the unstable mixed layer (Tennekes, 1970), however near z_i the buoyant term is small, and the complicated effects of wind shear near the inversion become important. In the vicinity of z_i some kinetic energy is destroyed by the local negative

buoyancy. Unless all this energy is replaced by transport from below, the process of entrainment must generate turbulent KE as the PBL rises to maintain a balance. The two sources of KE near z_i which are not accounted for in (39) are the mechanical generation and the transport of pressure fluctuations. Recently a more complete and meticulously detailed analysis of the turbulent kinetic energy budget as it applies to the capping inversion has been presented by Zeman and Tennekes (1977). Their analysis leads to a comprehensive equation describing the behavior of the inversion height z_i and the entrainment rate. This paper is recommended for a more complete discussion of the subject.

However, from the incomplete eq. (39), we can see that in order for the jump model to represent the true KE balance near z_i , eq. (39), when integrated vertically through the layer of negative heat flux, must be the same for both the jump model and the true conditions. Thus the jump model must have a carefully defined z_i which is not necessarily the same as the "true" horizontally averaged value. Finally, returning to Table 3, it is necessary to redefine the values of $\overline{w'\theta'_{vi}}$ and $\Delta\theta_v$ in conjunction with the redefinition of z_i , since Deardorff's (1974a) original values were estimated from a jump model in which z_i was not redefined (point A on Figure 4).

Using the carefully redefined values of z_i , $\overline{w'\theta'_{vi}}$, and $\Delta\theta_v$, determined from the data presented in Deardorff's paper (1974a), Table 3 was constructed, and the effectiveness of eqs. (35-38) for this case was analyzed. The last four columns show the calculated and expected values of the ratio of the right and left side of each

equation. Note that $\frac{\partial \theta}{\partial t} \overline{vM}$ has been replaced by the nearly equivalent expression $1.2 \frac{\overline{w'\theta'_{vs}}}{z_i}$ which results from applying eqs. (28) and (38) to the jump model. The calculated ratio $\frac{-\overline{w'\theta'_{vi}}}{\overline{w'\theta'_{vs}}}$ appears to be consistent with the expected value except during the earliest time periods. Between 1000 and 1100 on this day, the boundary layer was rising rapidly through a nearly dry adiabatic layer which had remained above the nocturnal inversion from the convection of the previous day. It is under such conditions that eq. (38) breaks down, and a more general formulation must be used (see below). The $\Delta\theta_v$ relationship (eq. (37)) appears to be fairly consistent with the data although the calculated values average nearly ten percent too large. The test of eq. (35) appears to show a systematic decrease in values of the ratio as the day progresses while at the same time $\Delta\theta$ is steadily getting larger. In fact, it appears that on this day, the observed growth of $\Delta\theta_v$ completely accounts for the systematic error in (35). When $\frac{d(\Delta\theta_v)}{dt}$ is accounted for (eq. 36)), the prediction of $\frac{dz_i}{dt}$ is quite good as shown in the last column of Table 3.

Considering the example of Table 3, as well as the simplicity and physical soundness of eq. (36), we have chosen to use this relationship along with eq. (37), to predict z_i . To close the system a suitable equation for $\overline{w'\theta'_{vi}}$ must be derived to replace eq. (38). Returning to eq. (39), and following the reasoning of Zilitinkevich (1975), the non-stationary kinetic energy equation leads to the desired result. Again, near z_i the dissipation-term is small and can be ignored. The kinetic energy itself is proportional to σ_w^2 , the variance of the vertical velocity fluctuations; and the flux

divergence term is retained and considered to be proportional to σ_w^3/z_i (Tennekes, 1973). As mentioned above, the $\frac{\partial(\overline{KE})}{\partial t}$ term is dependent on the entrainment rate in some unspecified manner which can be represented in a bulk sense by the fractional change of boundary layer thickness. Therefore we have, following Zilitin-kevich (1975),

$$\frac{\partial(\overline{KE})}{\partial t} \sim KE \frac{1}{z_i} \frac{\partial z_i}{\partial t} \sim \frac{\sigma_w^2}{z_i} \frac{\partial z_i}{\partial t} = \frac{\sigma_w^2}{z_i} \frac{(-w'\theta'_{vi})}{\Delta\theta_v} .$$

The last step above comes from applying eq. (37), and helps to illustrate the relationship of this term to the entrainment rate.

Using the above substitutions, eq. (39) becomes

$$c_1 \frac{\partial \sigma_w^2}{z_i} \frac{\partial z_i}{\partial t} = - \frac{g}{\theta_{vs}} (-w'\theta'_{vi}) + c_2 \frac{\sigma_w^3}{z_i} . \quad (40)$$

The constants c_1 and c_2 were estimated roughly by Tennekes (1975) to be 3.1 and 8.8 respectively, although these values may range higher or lower by as much as a factor of 3. At this point it is convenient to assume, for free convection, that the velocity variance σ_w^2 is proportional to the square of the convective velocity scale w_* which is defined by

$$w_* \equiv \left(\frac{g}{\theta_{vs}} \overline{w'\theta'_{vi}} z_i \right)^{\frac{1}{3}} . \quad (41)$$

Strictly speaking this definition originates with the stationary kinetic energy budget--setting the left side of eq. (39) equal to

zero. However, without regard to its origin, the parameter w_* is a useful quantity because it appears to be well related to σ_w in the observational data (Willis and Deardorff, 1974) under non-stationary laboratory conditions. Specifically, the "constant" of proportionality between σ_w^2 and w_*^2 appears to be a function of the non-dimensional height z/z_i in the laboratory data, and it may also be a function of the lapse rate of the stable air above z_i , however the data available are well enough clustered at any given height that it seems acceptable to postulate the relationship $\sigma_w^2 \approx c_3 w_*^2$. The constant of proportionality is not important in the present analysis although near z_i it appears to be somewhere in the range 0.1-0.3. Eq. (40) now may be rewritten

$$b \frac{w_*^2}{z_i^2} \frac{\partial z_i}{\partial t} = - \frac{g}{\theta_{vs}} - \overline{(w'\theta'_{vi})} + a \frac{w_*^3}{z_i^3}$$

where a and b are constants to be determined. Substituting eq. (41) into the above and rearranging, the final relationship becomes

$$\overline{w'\theta'_{vi}} = -\overline{w'\theta'_{vs}} \left(a - b \frac{\frac{\partial z_i}{\partial t}}{w_*} \right) . \quad (42)$$

In order to determine the values of the constants a and b, the following observations are noted. When z_i is rising through an adiabatic layer the entrainment, $\overline{w'\theta'_{vi}}$, vanishes so the term in parentheses must be zero. Furthermore, the numerical experiments by Deardorff (1974a) reveal that, when rising through an adiabatic layer, the rate of rise of z_i is given by

$$\frac{\partial z_i}{\partial t} = 0.2 w_* \quad (43)$$

Finally, if eq. (38) is assumed to be accurate in the steady state situation for which it was derived ($\frac{\partial z_i}{\partial t} \sim 0$), the constants a and b can be uniquely defined. By imposing eq. (43) in the limiting case of no entrainment, and eq. (38) in the limit of no change in z_i , it is found that

$$a = 0.2$$

$$b = 1.0 .$$

We now have a closed system of equations capable of determining the height of the unstable PBL for any value of the lapse rate in the free air above z_i . In practice a semi-implicit method is employed to solve this system. The following considerations lead to the ultimate equation set for calculating z_i in the model:

1. Eq. (41) is used to obtain w_* from the values

$$z_i(t) \text{ and } \overline{w'\theta'_{vs}}(t+\Delta t).$$

2. We combine eqs. (42) and (37) to get $\overline{w'\theta'_{vi}}$

from the equation

$$\overline{w'\theta'_{vi}} = -0.2 \overline{w'\theta'_{vs}}(t+\Delta t) / \left(1 - \frac{\overline{w'\theta'_{vs}}(t+\Delta t)}{\Delta\theta(t) w_*}\right) . \quad (44)$$

3. $\Delta\theta_v(t+\Delta t)$ is calculated from (37) using $(z_i(t) - z_i(t-\Delta t))$.

4. To get z_i we start with eq. (36) and assume that the local change of z_i can be calculated separately from the effects of vertical motion, advection and diffusion:

$$\frac{dz_i}{dt} = \left(\frac{d\Delta\theta_v}{dt} + \frac{d\theta_{vM}}{dt} \right) / \Gamma_L$$

The differential equation is now integrated with respect to time noting that $\theta_{vM}(t+\Delta t)$ is not yet known:

$$z_i(t+\Delta t) - z_i(t) + \left[(\Delta\theta_v(t+\Delta t) + \theta_{vM}(t)) - (\Delta\theta_v(t) + \theta_{vM}(t-\Delta t)) \right] / \Gamma_L$$

We now note that the second term in brackets is just the value of the free air temperature at height z_i at time t , and we may write the final form:

$$z_i(t+\Delta t) = z_i(t) + \left[(\Delta\theta_v(t+\Delta t) + \theta_{vM}(t)) - \theta_{vL}(z_i, t) \right] / \Gamma_L \quad (45)$$

All steps may then be repeated using updated values but it was found unnecessary to do so in practice.

Eq. (43) replaces (36) when $\Gamma_L \leq 0$. Otherwise eq. (43) is used as the upper limit to $\frac{\partial z_i}{\partial t}$. It should be noted here that although Table 1 was prepared using eq. (38) rather than eq. (42), the values of w_* during that experiment remained around 2 m sec^{-1} , so that the error in $\overline{w'\theta'_{vi}}$ resulting from this simplification is only a few percent.

The equation set (36), (37) and (42) has been compared with an equation offered by Deardorff in his first 1974 paper. The results of that comparison are displayed later in this paper (see Figures 10, 15, and 22). Examination of these figures shows that the equations presented here are somewhat better than the Deardorff equation in predicting the growth rate of the unstable boundary layer. The

Deardorff equation is formulated:

$$\frac{dz_i}{dt} = \frac{1.8 \overline{w'\theta'}_{vs} \left[1 + 1.1 \frac{u_*^3}{w_*^3} \left(1 - 3 \frac{fz_i}{u_*} \right) \right]}{z_i \Gamma_L + \frac{9w_*^2}{(g/\theta)_{vs}} z_i \left(1 + 0.8 \frac{u_*^2}{w_*^2} \right)} \quad (46)$$

This equation is basically a modification of eq. (35) (using (38) with a larger constant than 0.2) which also includes the case of $\Gamma_L \rightarrow 0$. In addition the Deardorff equation was formulated to include two cases where $\overline{w'\theta'}_{vs} \rightarrow 0$. The first is the case of a completely neutral atmosphere. In this case the equation predicts z_i to approach an equilibrium value of $0.33 u_* / f$. The other situation is the neutral layer capped by an inversion. In this case the equation is arranged to agree with some laboratory observations, where $z_i \ll 0.33 u_* / f$ -- not a very realistic atmospheric situation. Both of these cases come into play in the atmosphere only during very brief periods around sunrise and sunset, or possibly under very dense cloud cover, so the fact that they are neglected in (36), (37) and (42) is not considered a disadvantage. In fact the portions of the Deardorff equation applicable to these neutral cases was not tested at all in the 1974 paper, and have not been tested against atmospheric data at all. Furthermore the presence of these terms (specifically the term in brackets in the numerator) produces one of the major sources of error in the Deardorff equation under unstable conditions. Examination of figures 12, 17 and 23 presented later in this paper shows that when $z_i < 0.33 u_* / f$, the Deardorff equation causes z_i to rise too rapidly,

and when z_i is large compared to $0.33 u_* / f$, the boundary layer is predicted to grow too slowly. Also when u_* is large, as is the case for the O'Neill data (Figures 17 and 31), the rate of rise of z_i is seriously overpredicted by the Deardorff equation.

The other major source of error in this equation is the neglect of $\Delta\theta_v$. The inadequacy of eq. (35) due to neglect of the time rate of change of $\Delta\theta_v$ has been thoroughly discussed above; and the Deardorff equation suffers the same faults since it is based on eq. (35). The larger coefficient applied to $\overline{w'\theta'_v}$ was an attempt to ameliorate this problem without including $\Delta\theta_v$, however this treatment can only improve the mean value of dz_i/dt over a period in which some net change in $\Delta\theta_v$ occurs. The growth of the boundary layer will still be overpredicted when $\Delta\theta_v$ is growing rapidly, as in the morning, and will be underpredicted when $\Delta\theta_v$ is growing slowly or diminishing, as in the late afternoon.

The stable PBL height. The behavior of the boundary layer at night is not well understood. There is considerable disagreement about the true shape of the profiles of temperature and wind and their fluxes--even in the comparatively simple surface layer. Indeed, it has been suggested that the very stable PBL does not have a steady state solution at all, but fluctuates between turbulent and laminar flow. There is evidence (eg. Businger and Arya, 1974) that above the surface layer the Richardson number is maintained at very nearly its critical value. Under such conditions, the slight irregularities in an otherwise homogeneous natural surface probably function as the dominant cause of turbulence, and therefore may control the nature of the stable PBL. The picture presented is one of a very non-homogeneous

turbulent structure dependent on an irregular surface roughness. It is possible to imagine that the horizontal averaging processes routinely used in surface- and boundary -layer studies become inadequate under such conditions-- perhaps becoming increasingly meaningless as stability increases.

These difficulties notwithstanding, the present model requires a succinct parameterization of the horizontally averaged behavior of the stable PBL and of its depth. A number of theoretical and modelling studies (Zilitinkevich, 1972; Businger and Arya, 1974; Wyngaard, 1975) have found that the nocturnal boundary layer height may be proportional to the geometric mean of the Obukhov length and the neutral height parameter u_* / f , that is

$$z_i = a^* \left(\frac{u_* L}{f} \right)^{1/2},$$

where the constant a^* is of the order of unity. However Arya (1977) shows that the observed nocturnal inversion depth at Wangara is described poorly, if at all, by this relationship. Yu (1978) also tested this equation along with a few others including the familiar $z_i \propto u_* / f$. In this study it was concluded that the two diagnostic forms are preferable to the prognostic equation tested, but that none of the equations proved very adequate, particularly in the intermediate stability ranges.

Part of the problem of comparing a formulation for the nocturnal z_i with observations is to accurately define and locate a unique z_i in the observational data. A good estimate of z_i , when it exists in the data, is the top of the nocturnal inversion (above

which the temperature profile is close to adiabatic). Defined in this way, z_i is very likely to represent the level to which at least intermittent turbulence extends, because radiational effects alone, as Webb (1970) suggests, are not sufficient to seriously affect the temperature profile in the upper part of the nocturnal PBL. Therefore we seek an alternative means of describing the observed height of the inversion top which can be associated with the presence of turbulence.

The available evidence (e.g. Webb, 1970; Businger and Arya, 1974) appears to indicate that the Richardson number Ri approaches a critical value of 0.2 to 0.25 as z increases to approach the height L , and that above L , in the outer layer, the Richardson number is approximately constant with height and is near its critical value. Note that this latter finding for the outer layer is consistent with the assumption that the profiles of wind and potential temperature are linear in the outer layer. Based on this evidence the assumption is made that the PBL maintains a bulk Richardson number at a critical value which will be assigned a numerical value of 0.25, that is

$$Ri_B \equiv \frac{g}{\theta_{vMA}} \frac{(\theta_{vz_i} - \theta_{vs}) z_i}{|U|_{z_i}^2} = 0.25 \quad (47)$$

This equation is then used to determine z_i by iterative relaxation between the values of z_i and the values of θ_{vz_i} and $|U|_{z_i}$. The latter two quantities are determined from linear interpolation between grid points on the free atmosphere vertical grid maintained by the model. In reality, if the initial "guess" of the temperature

and wind speed are chosen to be the values at the level of z_i from the previous time step, more than two iterations were not found necessary. This is because θ_v and $|U|$ tend to increase correspondingly with height in the stable PBL (Webb, 1970), so that the ratio $(\theta_{vz_i} - \theta_{vs})/|U|_{z_i}^2$ is constant or changes only very slowly with height. The inclusion of the surface layer, where $Ri < 0.25$ in the calculation of z_i by eq. (47) is considered to be a reasonable approximation, since the selection of the constant 0.25 is somewhat arbitrary. One may interpret this constant as a mean value which includes lower values in the surface layer, and accounts for the observed presence of higher Ri values in the upper extremities of the nocturnal inversion.

As mentioned, the choice of 0.25 as the critical value of the bulk Richardson number is rather subjective. It is of course possible to have a layer of air with an overall bulk Richardson number much larger than 1 in which significant turbulence exists within thin layers where the local Ri is around 0.25. Such a structure was found by Woods (1969) in stable layers in the ocean. The observations by Woods led him to conclude that there are two critical values of local Richardson number--the familiar value of 0.25 for spontaneous initiation and maintenance of turbulence, and a second value of 1.0 up to which turbulence may exist inertially but will not develop spontaneously. A recent paper by Kondo, et al. (1978) strongly supports Woods' results through observations in the stable atmosphere. This study also found $Ri \sim 1.0$ to be an important threshold above

which turbulence is practically nonexistent. In addition $Ri \sim 0.25$ was found to be the critical value for continuous turbulence.

These considerations suggest that the choice for the critical bulk Richardson number should be somewhat larger than 0.25--perhaps 1.0. Therefore experiments were run using $Ri = 1.0$ in our model. Results showed that the calculated z_i was always much larger than observed, and that the calculated nocturnal PBL temperature structure was seriously in error. Apparently for the stable PBL, as parameterized here, it is necessary to insure the continuous presence of turbulence in a vertical column. With Ri_B as large as 1.0 there may be laminar layers separating independent layers of turbulence. Under such conditions very limited vertical transport through a deep layer is possible--there is little linkage with the earth's surface, therefore such layers should not be considered part of a boundary layer.

The transition periods. The period of boundary layer transition may be roughly defined as the period of time during which the turbulent lower portion of the atmosphere contains layers of both upward and downward heat flux. The observations of Kaimal, et al., (1976) for northerly winds in Minnesota suggest that in the evening the layer of negative heat flux propagates very rapidly downward from z_i to the surface in a matter of minutes. However in general the transition may take longer under some conditions, and may begin at the surface and propagate upward-- particularly during the morning transition. It is known that turbulence continues for some time after dark in the nearly adiabatic layer above the new nocturnal surface inversion. To illustrate a situation not included in the observations

of Kaimal et al., a nocturnal thunderstorm rooted in this turbulent adiabatic layer transfers large amounts of heat upward, while at the same time turbulence within the nocturnal inversion is transferring heat downward to the cool surface. More generally, since the primary thermal forcing for the atmosphere comes from the energy balance at the interface, one would expect the very lowest layers of the atmosphere to be the first to cool significantly in the evening and the first to warm in the morning. Above the lowest layers the temperature gradient should change sign reflecting the surface forcing at an earlier time before transition began. Since it takes time for turbulence to dissipate as well as for the influence of the surface to be transmitted upward, a turbulent layer through which the temperature gradient (and heat flux) changes sign can be expected.

At sunrise the onset of upward heat flux is transient and poorly defined at first. The heat flows upward only through a very shallow layer within the old nocturnal inversion. Furthermore the entire complex region of upward heat flow and decaying nocturnal inversion may be within the surface layer (if it can be defined). The value of $|L|$ at this time is very large and z_b has been restricted (see above) so that $z_b \leq 50$ m. In order to provide a smooth transition from a stable to an unstable PBL after sunrise, this rather deep surface layer is very useful. It provides a large "buffer" mass of air within which the transient unstable layer must establish itself before it is recognized numerically. As the surface begins to warm, $\overline{w'\theta'}$ vs θ_{vb} as calculated by (20) changes sign quickly, however as long as θ_{vb}

is larger than θ_{vs} , the heat flux at z_b , $(\overline{w'\theta'_{vb}})$, remains negative. By linking the definition of the overall stability of the PBL to the sign of $\overline{w'\theta'_{vb}}$, we delay the transition from stable to unstable PBL calculations until the unstable heated layer has reached a substantial depth and has become well established. This provides the stability necessary to effect a successful numerical transition from the equations and assumed profiles for the stable PBL to those for the unstable PBL. To reiterate, it is not until the heat flux at the top of the "surface layer" (50 m.) changes sign that we transfer the calculations of z_i , θ , u , v , etc. to the set of equations which apply for the unstable PBL.

The situation as modelled at sunset is very similar. The change in sign of $\overline{w'\theta'_{vb}}$ triggers the switch to the stable equations. Once this occurs, z_i drops very rapidly from its daytime value of ~ 1 to 2 km to a nighttime value of a few hundred meters. This differs from the morning transition where z_i changes very little during transition. As z_i drops rapidly, a nearly adiabatic layer is left above the nocturnal z_i . This layer contains residual turbulence which may affect the true height of the nocturnal PBL, however this residual turbulence is not treated by the present model. The amount of error introduced by neglecting turbulence in this "inertial" layer is uncertain. The calculated values of eddy diffusivity determined by Orlanski et al. (1974) in the inertial layer dropped only gradually overnight and were still larger than the "background" or free air minimum values at sunrise. Wyngaard (1975) and Yamada and Mellor (1975), using higher order closure models, found turbulence above

the stable layer to become negligible after a few hours. The effect of any residual turbulence will be to enhance mixing in the boundary layer and to reduce the strength of the nocturnal inversion and increase its depth. However, the magnitude of this effect has yet to be determined.

One additional problem peculiar to the sunset transition exists. When $\overline{w'\theta'_{vb}}$ changes sign, the temperature gradient is nearly zero, therefore the stable z_i equation (eq.(47)) gives unreasonably large values of z_i for the first few minutes. In order to circumvent this difficulty, the stable PBL is required to be no larger than its neutral counterpart. That is, when the PBL is stable we require

$$z_i \leq 0.3 u_{*b} / |f| \quad f \neq 0$$

where u_{*b} is the friction velocity at z_b , and f is the coriolis parameter. One additional restriction on z_i is imposed for numerical stability. A minimum value of 60 meters is set for z_i so that the PBL contains enough mass that small fluctuations in the heat balance do not cause wild temperature changes.

2. Temperature wind, and moisture.

After some basic approximations the time rate of change of an arbitrary atmospheric variable X is described by eq. (1):

$$\frac{dX}{dt} = \frac{\partial}{\partial z} (\overline{-w'X'}) + Q ,$$

where Q represents all sources and sinks of X . Neglecting advection and the source and sink terms, and writing the time derivative in

finite difference form with a simple first order difference scheme, eq. (1) may be written

$$\frac{X_s(t) - X_s(t-\delta t)}{\delta t} = \frac{\partial}{\partial z} (\overline{w'X'}). .$$

The term on the right hand side is evaluated at some unspecified intermediate time between t and $t-\delta t$ by virtue of the order of calculations. The values of $\overline{w'X'}$ used to evaluate the vertical eddy transport term are calculated (from eqs. (24), (25), (26), (32), (33), (34), and/or (44)) based on the layer-averaged atmospheric X -values from the previous time step ($t-\delta t$), and on the new interface layer values $X_{s(t)}$. At this point we take the layer-average of the above equation through the layer z_1 to z_2 , where z_1 is the upper boundary of that layer (e.g. z_i for the outer layer). The layer-averaging is performed at time t by applying the following operator:

$$\left[\right]_{\text{LAV}(t)} = \frac{1}{(z_2 - z_1)(t)} \int_{z_1(t)}^{z_2(t)} \left[\right] dz.$$

Assuming horizontal homogeneity of the vertical fluxes, the resulting equation is

$$X_{\text{LAV}(t)} - \frac{1}{(z_2 - z_1)(t)} \int_{z_1(t)}^{z_2(t)} X(t-\delta t) dz = \frac{\overline{w'X'}_{z_1} - w'X'_{z_2}}{(z_2 - z_1)(t)} \delta t$$

Now the layer-average of $X_{(t-\delta t)}$ is not readily evaluated in terms of known quantities. The values of $X_{LAV(t-\delta t)}$ are known for the various layers but the boundaries of these layers do not necessarily coincide with the boundaries required at time t . Therefore in order to evaluate the layer average of $X_{(t-\delta t)}$ for the required layer, a properly constructed average of the known values of $X_{LAV(t-\delta t)}$ from several layers must be developed. Assuming that density is constant with height in the region considered, the layer-averaged operator as defined is mass-weighted, and the mass-weighted layer-average of $X_{(t-\delta t)}$ may be written

$$\int_{z_1(t)}^{z_2(t)} X_{(t-\delta t)} dz = (z_2 - z_1)_{(t-\delta t)} X_{LAV(t-\delta t)} + \delta z_2 X_{2AV} - \delta z_1 X_{1AV}$$

where $\delta z_2 = z_2(t) - z_2(t-\delta t)$, $\delta z_1 = z_1(t) - z_1(t-\delta t)$, X_{2AV} is the average value of $X_{(t-\delta t)}$ applicable to the layer δz_2 , and X_{1AV} is defined similarly to X_{2AV} . The final expression then becomes (48).

$$X_{LAV(t)} = \frac{(z_2 - z_1)_{(t-\delta t)} X_{LAV(t-\delta t)} + \delta z_2 X_{2AV} - \delta z_1 X_{1AV}}{(z_2 - z_1)_{(t)}} - \frac{\overline{w'X'}_{z_2} - \overline{w'X'}_{z_1}}{(z_2 - z_1)_{(t)}} \delta t.$$

The specific evaluation of (48) for PBL temperature, moisture, and wind is discussed below, then the complete solution of eq. (1) including source and sink terms for each variable, is discussed.

The PBL is divided into two layers, the surface layer and the mixed or outer layer. Layer averaged values of each variable are

which is determined by an approximate interpolation between X_M and X_S . The interpolation is performed assuming that the profile of X is described by Paulson's integrated profile equations.

To reach the comparison values \tilde{X}_{MA} we begin with eq. (31) re-written for an arbitrary variable X at an unspecified height z :

$$X(z) = X_S + \frac{f'(z, z_0)}{f'(z_b, z_0)} (X_M - X_S).$$

The symbolism X_M is used instead of X_b since for unstable conditions the two values must be equal if X is to be continuous at z_b . This symbolism shows that the comparison values \tilde{X}_{MA} are coupled with the outer layer above through the equations to be derived. For this situation the Paulson profiles are used:

$$f'(z, z_0) = \ln \frac{z}{z_0} + \Psi_X(z)$$

$$\Psi_H = 2 \ln \left(\frac{1+\eta}{2} \right), \quad \eta = \left(1 - 9 \frac{z}{L} \right)^{1/2}$$

$$\Psi_U = -\ln \left(\frac{1+\xi^2}{2} \right) - 2 \ln \left(\frac{1+\xi}{2} \right) + 2 \tan^{-1} \xi - \frac{\pi}{2},$$

$$\xi = \left(1 - 15 \frac{z}{L} \right)^{1/4}.$$

Using the definition of the layer averaged value \tilde{X}_{MA} we may write

$$\tilde{X}_{MA} = \frac{1}{z_b - z_0} \int_{z_0}^{z_b} X(z) dz = z_s + \frac{X_M - X_S}{(z_b - z_0) f'(z_b, z_0)} \left[\int_{z_0}^{z_b} \ln \frac{z}{z_0} dz + \int_{z_0}^{z_b} \Psi_X(z) dz \right].$$

calculated for both layers. The outer layer average is delineated by the subscript M, and the surface layer average by MA. Because the assumed profiles are different in stable and unstable conditions, the two stability cases are discussed separately.

The unstable surface layer. In the surface layer all variables (θ , u , v , q) may be treated identically. The lower boundary, z_o , does not change. The value z_o is used for all quantities (rather than z_θ and z_q for consistency). The upper boundary (z_b) is quite fictitious in that there is a vigorous exchange of mass across it. Because of this, it is assumed for simplicity that when z_b falls, the resultant mass leaving the surface layer carries with it the mean properties of the entire surface layer rather than the statistical properties of the narrow layer at the top of the surface layer. Thus eq. (48) for all variables becomes

$$X_{MA}(t) = \frac{(z_b(t-\delta t) - z_o) X_{MA}(t-\delta t) + \delta z_b X_{2AV}}{z_b(t) - z_o} - \frac{\overline{w'X'}_b - \overline{w'X'}_s}{z_b(t) - z_o} \delta t, \quad (49)$$

where

$$X_{2AV} = \begin{cases} X_{MA}(t-\delta t) & \delta z_b < 0 \\ X_M(t-\delta t) & \delta z_b > 0 \end{cases}$$

Because the accuracy of this equation is not perfect, it is possible for the surface layer X values to become decoupled from the mixed layer above, especially when z_b is constant or decreasing in value. Therefore it is found convenient to provide a comparison value of X_{MA}

After integration holding the fluxes constant the final results become,
for $X=(\theta, q)$,

$$\begin{aligned} \tilde{X}_{MA} = X_s + \frac{X_m - X_s}{(z_b - z_o) \left(\ln \frac{z_b}{z_o} - 2 \ln \lambda_b \right)} z_b \ln \frac{z_b}{z_o} - (z_b - z_o) + \\ \frac{8L}{9} \left(\lambda_b^2 - \lambda_o^2 \right) \ln \lambda_b - \left(\lambda_o^2 - \lambda_b^2 \right) \ln \lambda_o + \lambda_b - \frac{\lambda_b^2}{2} - \lambda_o + \frac{\lambda_o^2}{2} , \quad (50) \end{aligned}$$

$$\lambda = \frac{1+\eta}{2} ,$$

and for the wind, assuming direction does not change through the surface layer,

$$\begin{aligned} \tilde{u}_{MA} = \frac{u_M}{(z_b - z_o) \left(\ln \frac{z_b}{z_o} - \ln \mu_b - 2 \ln v_b + 2 \tan^{-1} \xi_b - \frac{\pi}{2} \right)} \times \\ \left[z_b \ln \frac{z_b}{z_o} - \left(1 - \frac{\pi}{2} \right) (z_b - z_o) + \frac{L}{15} (4A + 16B - 2C) \right] \quad (51) \end{aligned}$$

where

$$A = (\mu_b^2 - \mu_o^2) \ln \mu_b - (\mu_o^2 - \mu_b^2) \ln \mu_o - \frac{\mu_b^2}{2} + \mu_b + \frac{\mu_o^2}{2} - \mu_o ,$$

$$B = (2v_b^4 - 4v_b^3 + 3v_b^2 - v_b) \ln v_b - (2v_o^4 - 4v_o^3 + 3v_o^2 - v_o) \ln v_o -$$

$$\frac{v_b^4}{4} + \frac{v_o^4}{4} + \frac{v_b^3}{3} - \frac{v_o^3}{3} - \frac{v_b^2}{2} + \frac{v_o^2}{2} + v_b - v_o ,$$

$$C = (\xi_b^4 - 1) \tan^{-1} \xi_b - (\xi_o^4 - 1) \tan^{-1} \xi_o - \frac{\xi_b^3}{3} + \frac{\xi_o^3}{3} + \xi_b - \xi_o ,$$

$$\mu = \frac{1 + \xi^2}{2} , \quad \nu = \frac{1 + \xi}{2} .$$

For future reference we consolidate (50) and (51) into a general form which may also apply to stable conditions:

$$\tilde{X}_{MA} = X_s + \frac{X_M - X_s}{B} \cdot A \quad (52)$$

If the value of X_{MA} determined from eq. (49) strays too far from \tilde{X}_{MA} , the value of \tilde{X}_{MA} is used, and the necessary adjustment in order to conserve the total PBL quantity of X is added to X_M (see below). Eqs. (50) and (51) in effect assure that the surface layer and the mixed layer do not become decoupled. The maximum allowed difference between X_{MA} and \tilde{X}_{MA} is 0.5°C for θ , 10 cm sec^{-1} for u and v , and 0.02 g kg^{-1} for q .

The unstable mixed layer. In the unstable mixed layer the mean value X_M is also assumed to be the true value at all points within the layer. At the top of the mixed layer the turbulent fluxes, by definition, vanish. However there is turbulent entrainment of air into the PBL from above which must be accounted for. This can be done by one of two exactly equivalent methods, the "bulk" method in which the properties of the slab of air entrained during an increment of time are combined in a weighted average with the mean properties already existing within the mixed layer, or the

turbulent transfer method in which the turbulent flux $\overline{w'X'_i}$ is assumed to have some finite value immediately below z_i . Tetroon measurements have shown large measured turbulent fluxes to exist near z_i which are explained by the entrainment process (Deardorff, 1973). Thus the turbulent transfer representation of entrainment appears to be more physically descriptive, however the bulk method accomplishes the same transfer of properties without being concerned with the mechanism of the transfer. The bulk method is then particularly suited to describe the transfer of nearly "inert" properties of the atmosphere whose turbulent behavior does not affect the entrainment process itself. In the case of the unstable mixed layer, entrainment is primarily controlled by the heat flux, $\overline{w'\theta'_{vi}}$, and the wind and moisture may be considered inert quantities to a good approximation. Therefore, since the value of $\overline{w'\theta'_{vi}}$ is available from eq. (42), the value of $\theta_{vM}(t)$ is calculated using the turbulent transfer method. This is accomplished in the framework of eq. (48) by recalling that eq. (37) states

$$\overline{-w'\theta'_{vi}} = \Delta\theta_v \frac{\partial z_i}{\partial t} ,$$

which in finite difference form may be written

$$-\delta t \overline{w'\theta'_{vi}} = \Delta\theta_{v(AV)} \delta z_i ,$$

where $\Delta\theta_{v(AV)}$ is the mean value of $\Delta\theta_v$ during the time δt in which z_i is changing by an amount δz_i . Now we note that $\Delta\theta_{v(AV)}$ is given by the difference between θ_{vM} in the mixed layer and the average

value of the free air θ_v just above z_i during the time increment δt .

The latter is symbolized by θ_{v2AV} . In equation form we have

$\Delta\theta_{v(AV)} = \theta_{v2AV} - \theta_{vM}(t)$, which allows us to write

$$-\delta t \overline{w'\theta'_v}_{vi} = \delta z_i \theta_{v2AV} - \theta_{vM}(t)(z_i(t) - z_i(t-\delta t)) \quad (53)$$

Now if, in eq. (48), we let $X=\theta_v$, $z_2=z_i$, and $z_1=z_b$, and we multiply both sides of (48) by $(z_i-z_b)(t)$, then we may apply eq. (53).

Noting first that $\overline{w'\theta'_v}$ at z_i is by definition zero, then adding the left side of (53) to the last term on the right side of (48), subtracting the right side of (53) from the first term on the right of (48), and rearranging, we reach the equation for the mean virtual temperature of the unstable outer layer:

(54)

$$\theta_{vM}(t) = \frac{(z_i-z_b)(t-\delta t) \theta_{vM}(t-\delta t) - \delta z_b \theta_{v1AV}}{z_i(t-\delta t) - z_b(t)} - \frac{\overline{w'\theta'_v}_{vi} - \overline{w'\theta'_v}_{vb}}{z_i(t-\delta t) - z_b(t)} \delta t + \Delta\theta_M.$$

Here θ_{v1AV} is the surface layer value of θ_v which is mixed into the outer layer when z_b drops. Its value must be identical to X_{2AV} in eq. (49) for $X=\theta_v$. The quantity $\Delta\theta_M$ represents the correction added to the mixed layer when the surface layer value θ_{vMA} is restrained by $\tilde{\theta}_{vMA}$. Eq. (54), simply stated, assumes that z_i is held constant during the time step, and allows the calculated turbulent entrainment to bring heat into the layer in place of the bulk method.

Finally, since the equation set (37), (44) and (45) determines the mass entrainment rate, $\partial z_i / \partial t$, without consideration to the

entrainment of momentum or moisture, the values of $u_M(t)$, $v_M(t)$, and $q_M(t)$ can be treated as inert quantities and are determined by the bulk entrainment method. This means that the values of $\overline{w'u'_i}$, $\overline{w'v'_i}$, and $\overline{w'q'_i}$ are set at zero, and, for $X = u, v$, and q , eq. (48) becomes

$$X_{M(t)} = \frac{(z_i - z_b)(t - \delta t) X_{M(t - \delta t)} + \delta z_i X_{3AV} - \delta z_b X_{2AV}}{(z_i - z_b)(t)} + \frac{\overline{w'X'_b}}{(z_i - z_b)(t)} \delta t + \Delta X_M, \quad (55)$$

where

$$X_{3AV} = \begin{cases} X_{M(t - \delta t)} & \delta z_i < 0 \\ \frac{X_L(z_i(t)) + X_L(z_i(t - \delta t))}{2} & \delta z_i > 0 \end{cases}$$

and X_L is the free atmosphere value, X_{2AV} is as defined in (35), and ΔX_M is defined equivalently to $\Delta \theta_M$ in (54).

Transition periods. Two minor contingencies must be accounted for during the transition between the stable and unstable regimes. First, when the unstable PBL becomes very nearly neutral, there is the possibility that the sign of $\theta_M - \theta_{MA}$ does not agree with the direction of the heat flux indicated by $\overline{w'\theta'_{vb}}$. In this case, the heat is redistributed such that $\theta_M = \theta_{MA}$ and the entire PBL is considered neutral. Secondly, at sunrise on the first time step in which the unstable equations are used, the profiles of $X (= \theta, u, v, q)$ are such that $X_M \neq X_b$. In order to initialize the proper assumed unstable profile, the quantity X is similarly redistributed so that $X_M = X_{MA}$.

The stable PBL. Two features distinguish the calculation of the stable X values from the unstable calculations. First, little is known about the nature of "entrainment" at z_i under stable conditions. There is no consistent temperature "jump", and in many cases there is not even a clearly defined change in temperature gradient at z_i . Indeed, z_i itself is often hard to define since there are no reliable distinguishing features in the wind or moisture profiles either. Furthermore the z_i equation we have chosen for stable conditions (eq.(47)) is not prognostic, which implies that turbulence may spontaneously form or disappear within some layer in response to changing conditions beneath. With such sudden changes within a layer permitted in the model, the bulk treatment of entrainment is preferred for all variables including virtual potential temperature.

The other fundamental difference between the stable and unstable calculations is the non-zero slope of the X profiles within the outer layer. During unstable conditions $X = X_M$ everywhere within this layer, however at night both X_M and $(\frac{\partial X}{\partial z})_M$ must be determined. As a result, the X_{LAV} calculation used for the unstable case produces an infinite family of stable profiles. A third equation (in addition to equations for X_M and X_{MA}) is needed in order to determine the one profile in the family which is continuous at z_b . In other words, an equation is needed which requires that X_b , extrapolated upward from X_s and X_{MA} , must be equal to the X_b extrapolated downward from $X_L(z_i)$ and X_M .

Noting that the stable outer layer profiles are assumed to vary linearly with height, that the stable surface layer profiles are assumed to vary with height as described by eq. (52), and that all variables may be treated the same here, the set of three simultaneous equations to be solved for X_M , X_{MA} and X_b are:

$$X_M(t) = (X_b + X_L(z_i))/2.0 \quad (56)$$

$$X_b = X_s + \frac{(X_{MA} - X_s)(z_b - z_o) \left(\ln \frac{z_b}{z_o} + a' \frac{z_b}{L} \right)}{z_b \ln \frac{z_b}{z_o} - (z_b - z_o) + \frac{a'}{2L} (z_b^2 - z_o^2)}, \quad a' = \begin{cases} 6.35 & \text{for } X=(\theta_v, q) \\ 4.7 & \text{for } X=u \end{cases} \quad (57)$$

$$X_{MA}(t)(z_b - z_c)(t) = \delta t \overline{w'X'}_s + X_{MA}(t-\delta t)(z_b - z_o)(t-\delta t) + \quad (58)$$

$$X_M(t-\delta t)(z_i - z_b)(t-\delta t) - X_M(t)(z_i - z_b)(t) +$$

$$(X_{4AV}(t-\delta t) + X_{4AV}(t)) \delta z_i$$

Eq. (56) describes the linear change of X through the outer layer with no jump at z_i , (57) extrapolates upward from X_{MA} and X_S to get a value of X_b (which must equal the value used in (56)), and (58) is simply a mass-weighted statement of the conservation of X during the time increment in question. Finally we define

$$X_{4AV}(t-\delta t) = \begin{cases} \frac{1}{2} [X_L(z_i(t-\delta t)) + X_L(z_i(t))] & \delta z_i > 0 \\ 0 & \delta z_i < 0 \end{cases}$$

$$X_{4AV}(t) = \begin{cases} 0 & \delta z_i > 0 \\ \frac{1}{2} [X_L(z_i(t-\delta t)) + X_L(z_i(t))] & \delta z_i < 0 \end{cases}$$

The source and sink terms. Having determined the vertical exchange terms for all variables, we return to the complete prognostic equation for X (eq. 1). After layer-averaging and neglecting horizontal advection the expression becomes

$$\frac{\partial X_{LAV}}{\partial t} = \frac{X_{LAV}(t) - X_{LAV}(t-\delta t)}{\delta t} + Q_{LAV}$$

Now, for $X=q$, the vertically averaged sources and sinks, Q_{LAV} of moisture are negligible assuming no condensation. The only source of change of potential temperature which needs to be considered is caused by radiative processes, which will be covered in section E below.

For momentum, the Coriolis and geostrophic terms must be considered. The coriolis term provides a mechanism for exchange of momentum between the u and v components, and the vertically averaged geostrophic wind term provides the primary source of the momentum which is constantly dissipated at the surface. The interaction of these two terms with the vertical exchange term warrants some analysis.

Detailed numerical experiments by Wyngaard et al. (1974) have shown that in an unstable PBL with no geostrophic shear, the vertical profiles of momentum flux are very nearly linear, as is assumed here, despite the interactions permitted by the Coriolis effect. The assumption of linearity is more correct the stronger the instability. On the other hand, under baroclinic conditions the flux profiles become extremely non-linear even for weak geostrophic shear, and it would appear at first glance that important features of the PBL wind

structure may be missed using the gross vertical averaging employed here. But Wyngaard et al. (1974) show that the actual calculated wind shear is small compared to the geostrophic shear even for moderately weak instability ($z_i/L = -50$). This evidence suggests that the use of a vertically averaged geostrophic wind is acceptable for baroclinic conditions in the unstable PBL, and that the vertically averaged winds obtained in this way will closely follow the actual wind profile. Therefore the assumptions applied here under unstable conditions, that $U_g(z)$ may be represented by U_{gLAV} , that $U(z) = U_M$ in the mixed layer, and that the momentum flux profiles are linear, may be considered valid assumptions even for baroclinic conditions.

Under stable stratification much less is known about the stress profiles or the theoretical shape of the wind profile. It is likely that the stress profiles are highly nonlinear, and it is possible, as mentioned earlier, that no practical "steady state" exists. The observations do not rule out the reasonableness of the linear profile of wind in the outer layer that is assumed here. Nevertheless the calculated layer-average wind components u_M and v_M should be interpreted far less strictly for stable conditions than they may be for unstable conditions.

3. The cloud-topped PBL.

Strictly as a crude first approximation to test the response of the model to cloud formation, an inert cloud is permitted to form below z_i when the humidity reaches 90%. As yet no provision has been made for the formation of partial cloud cover, or for the

influence of latent heat release on the fluxes of heat, moisture, or momentum in the PBL. The only effect considered is that upon the surface and atmospheric radiation budget. When present, the cloud is assumed to reflect 60% of the short wave radiation, and to be an opaque blackbody to longwave radiation. To determine the presence of this cloud beneath z_i and to find the height of its base, z_c , the following iterative equation is used:

$$P_c = 10^6 / \left\{ \frac{-\theta_{VM}}{5419} \left(\ln \frac{P_c \times 1.11 q_M}{3800} - 19.84 \right) \right\}^{3.5}, \quad (59)$$

when P_c is the pressure at cloud base from which z_c is obtained through the hydrostatic equation. z_c only exists when $P_c > P_i(z_i)$. Eq. (59) is a rapidly converging form of the Clausius-Clapeyron equation with P given in dynes cm^{-2} and q in gm gm^{-1} . Since θ_{VM} is assumed to represent the virtual potential temperature throughout the mixed layer, this equation is obviously only intended for use during unstable periods.

D. The free atmosphere.

Above z_i information about temperature, moisture, and wind is stored to provide environmental conditions through which z_i must rise and from which the PBL gets its characteristics by entrainment. The information comes, at the time of initialization, from a "raw" sounding which may consist of any number of randomly distributed pressure levels. These data are stored, and in addition an interpolated sounding with values every 100 meters from z_i up to 4 km AGL is created. Dummy values of the variables are in these grid points

from z_i down to the surface. It is with this 100 meter grid that the bulk of the model interacts directly. However all modifications to the free atmosphere due to inertial oscillations, radiation, and detrainment from a falling z_i are made to both the 100 meter grid and the raw sounding grid. Thus maximum flexibility is maintained in interaction with any large scale model from which the raw sounding is obtained.

The model assumes a linear variation of all variables when interpolating between points on the 100 meter grid. For example, when $X_L(z_i)$ is calculated, the value is determined by assuming a linear change of X between the first grid point above z_i and the point immediately below z_i . At this lower point a fictitious value of X is stored which remains unchanged until z_i passes downward past that level. This assures accurate values of Γ_L , $X_L(z_i)$, etc. when needed. Since the 100 meter grid extends only to 4 km, z_i is not permitted to pass above that level.

At each time step the following calculations are performed at each grid point above z_i :

$$\frac{\partial q_j}{\partial t} = 0 \quad (60)$$

$$\frac{\partial \theta_{vj}}{\partial t} = Q_{LWj}$$

$$\frac{\partial u_j}{\partial t} = F (v_j - v_g) + K \frac{\partial^2 u_j}{\partial z^2}$$

$$\frac{\partial v_j}{\partial t} = F (v_g - v_j) + K \frac{\partial^2 v_j}{\partial z^2}$$

where Q_{LWj} is the long wave radiative flux divergence which is discussed in the next section. The value of K , the eddy diffusivity, is set at $5000 \text{ cm}^2/\text{sec}$, which allows only a weak vertical diffusion of the wind components. The only other modification to these values occurs, as mentioned, when z_i falls below a grid point. When this occurs the PBL is considered to have detrained air without change in its properties. Thus the grid point takes on the values of θ , u , v , and q which had existed at that level within the PBL on the previous time step. Again, both the 100 meter and the raw grid are modified in this way so that control may be readily returned to a large scale model routine at any time.

E. The radiation calculations.

A complete radiative cooling calculation has been written based on the empirical formulae of Sasamori (1968). The atmosphere is divided into a variable number of layers and a cooling rate is determined for each. The lowest two layers are always the surface and outer layers of the PBL, and the remaining free atmosphere layers generally coincide with the levels of the raw input sounding. When a cloud is present it is treated as a blackbody and independent cooling rates are determined above and below. The raw sounding, the 100 meter grid, and the values of θ_M and θ_{MA} are all modified following the results of the radiation calculation.

The calculation itself accounts for the influence of both water vapor and carbon dioxide. It is assumed that CO_2 absorbs only in the $15 \mu\text{m}$ region where the overlapping H_2O absorption is given by

Sasamori (1968). The transmissivity of the mixture of gasses is assumed, following Yamamoto (1952), to be given by the product of the transmissivities of the individual gasses.

In addition a crude parameterization has been included which accounts for the absorption of short wave radiation by water vapor. It begins with the assumption that 12% of the solar constant is absorbed by water vapor whenever the sun is above the horizon (see Chapter III, A.1.). At low solar elevation angles the decreased intensity on a horizontal surface is assumed to be offset by the increased optical depth or path length of water vapor in each layer. A layer absorbs energy in amount proportional to the fraction of the total atmospheric water vapor it contains. The resulting parameterization is as follows for an arbitrary layer of thickness Δz :

$$\frac{\Delta T_{SW}}{\Delta t} = \frac{0.12 I_o}{\bar{\rho} C_p \Delta z} \cdot \frac{\Delta U_W}{U_W}$$

where U_W is the effective total optical depth of water vapor given by

$$U_W = \frac{1}{g} \sum_j \bar{q}_j \frac{\bar{p}_j}{p_o} \Delta p_j, \quad p_o = 1000 \text{ mb.}$$

F. Applicability to non-homogeneous terrain

A considerable amount of work has been done with solutions of surface layer systems over abrupt changes in surface roughness (e.g. Rao et al., 1974; Taylor, 1970; Peterson, 1971). Unfortunately these studies do not generally consider the effects above the surface layer nor do they examine a wide range of stabilities. The stable

PBL has again been neglected. Studies pursuing the effect on the PBL of a change in surface slope, or of a gradual change in roughness are limited to one recent exploratory study by Lo (1977). However a few conclusions may be drawn from the work which has been done. It is the general consensus that equilibrium is reestablished to a height $h \approx 0.01x$ at a distance x downstream from a sudden roughness change under neutral conditions. This height appears to be larger for unstable conditions and possibly smaller for stable stratification. In the unstable mixed layer during free convection the effect of changes in surface conditions theoretically becomes small. Mesoscale studies such as the sea breeze model of Pielke (1973) have used a rather fine grid mesh ($\Delta x = 11\text{km.}$) across variable terrain without considering the effects of inhomogeneous surface conditions on the PBL formulation, and any detrimental effects have gone undetected. Finally, the most common natural form of inhomogeneity is the generally homogeneous surface strewn with random obstacles such as trees, houses, fences, roads, rocks, ponds, gullies and small hills. It is suggested that with a horizontal grid spacing much larger than the obstacles themselves (i.e. a few kilometers), these obstacles may be readily included in a horizontal mean roughness \bar{z}_0 , (Fiedler, et al., 1971, as referenced in Deardorff, 1972b; Kung, 1963, as referenced in Arya, 1977; Thompson, 1978) and the surface may be considered homogeneous.

In conclusion, the following tentative recommendations are made: For complete accuracy the minimum horizontal grid spacing should be approximately $100|L|$ for unstable conditions and at least $100 z_i$

for neutral and stable conditions. However if no abrupt changes in surface conditions occur or if the abrupt changes occur only infrequently along the trajectory of the airflow, a considerably finer grid may be used without serious difficulties.

G. Initialization and numerical solution

When this model is used as a PBL parameterization for a meso-scale 2- or 3- dimensional study, a large part of the initialization is provided by the parent model. For example the raw sounding simply consists of the values from a vertical column of grid points. The parameters required for this sounding are pressure, temperature, mixing ratio, u , v , and w wind components, and the geostrophic winds U_g and v_g . In addition to the sounding, 23 other variables must be initialized from the parent model, stored at each horizontal grid point, or mathematically represented as functions of horizontal space. These are T_s , θ_{vM} , θ_{vMA} , u_M , v_M , u_{MA} , v_{MA} , q_M , q_{MA} , q_s the soil moisture W , dew accumulation D , z_i , z_b , z_o , L , $\partial z_i / \partial t$, $\Delta\theta_v$, cloud cover parameter c , biomass mc_s , albedo a , soil temperature T_{15cm} , and soil conductivity k . Other miscellaneous quantities which must be provided are the time t , latitude ϕ , day number d , time step δt , and the slope of the surface $\frac{dh}{ds}$. From experience it has been found that the selection of initial values of such basic quantities as θ , u , v , q , and z_i is not critical to the solution after about an hour of simulated time. Given a reasonable set of input values, the model will quickly seek its own "equilibrium". Initial values used in the experiments reported here are given in the appendix.

As a result of the effort to maintain numerical simplicity and brevity there are no nonlinear terms in the non-advective (horizontally homogeneous) portion of this model except for the vertical diffusion of wind above z_1 which is stable for time steps up to one hour. A simple Euler or forward time differencing has been used and there are no other easily recognized theoretical restrictions to the time step. A time step of 3 minutes was used for all experiments reported here. The full calculations for one time step require about 0.2 seconds on a CDC 6400, more than half of which is consumed by the radiation flux routine. It will be possible to lengthen the practical time step and improve the calculation speed in the future with the use of improved coding and a more sophisticated time difference scheme.

As a review of the equations used in the solution, an outline of the order of the calculations is presented.

- 1). The initial data is read and the raw sounding is interpolated to the 100 meter grid.
- 2). The surface energy budget is compiled, one component at a time, after which the new surface temperature is calculated from eq. (6).
 - a) the incoming solar radiation component is determined by eq. (10).
 - b) the complete radiation calculation is performed, the temperatures at all levels are modified, and H_{\downarrow} is determined for the net longwave component given by eq. (7).

- c) The latent heat flux is calculated from eqs. (19) and (20).
 - d) The sensible heat flux is obtained from eqs. (33) and (34).
 - e) The soil heat flux term is parameterized by eq. (23).
- 3). The momentum flux at z_0 is determined from eq. (32).
 - 4). The surface layer heat, moisture, and momentum fluxes and the height z_b are determined with the use of eqs. (24-27).
 - 5). The height of the PBL is determined either from the equation set (37), (41), (43), (44), and (45) or when the stratification is stable, from the smaller value of z_i determined by eq. (47) or $0.3 u_{*b}/|f|$.
 - 6). The existence of a cloud below z_i is ascertained using eq. (59).
 - 7). The values of $\overline{X_L}$ to be entrained when z_i rises are determined, or the large scale is modified as z_i falls.
 - 8). The surface and outer layer mean temperature, wind component, and moisture vertical exchange terms are calculated from eqs. (49-58).
 - 9). The wind calculations are completed by inclusion of the coriolis and geostrophic terms, and the free atmosphere wind oscillation is calculated.
 - 10). In place of step (9) control may be returned to the parent mesoscale model for calculation of the complete advective equations for θ , q , u , v , following which we return to

step (1). Otherwise for the one dimensional experiments performed here, the time step is advanced, values are printed, and we return to step (2).

H. Application to a parent model.

The techniques for applying the model developed here to a parent 2- or 3-dimensional mesoscale or global scale model will vary depending on the specific details of the parent model, however some general considerations are given here which should be applicable to most models. We present three basic modes of interaction between parent model and PBL parameterization which will be defined as they are presented.

1. Partial Application. Many of the concepts presented in this report are perfectly amenable to use out of context. Such things as the interface temperature calculation, any of the surface energy components, or the technique for calculating z_i may be borrowed individually and applied to other models with little difficulty.

2. Direct Adaption. This technique implies taking the PBL parameterization developed here and incorporating it into an existing or new model with as little increase in data storage and computation as possible. It requires storage or specification of the 23 variables needed to initialize the PBL model, but the sounding of wind, temperature, and moisture are interpolated from the parent model grid each time the PBL model is called (see figure 5). This method provides vertical resolution which is only as good as the parent model above z_i . Thus the behavior of the PBL, as it is affected by entrainment

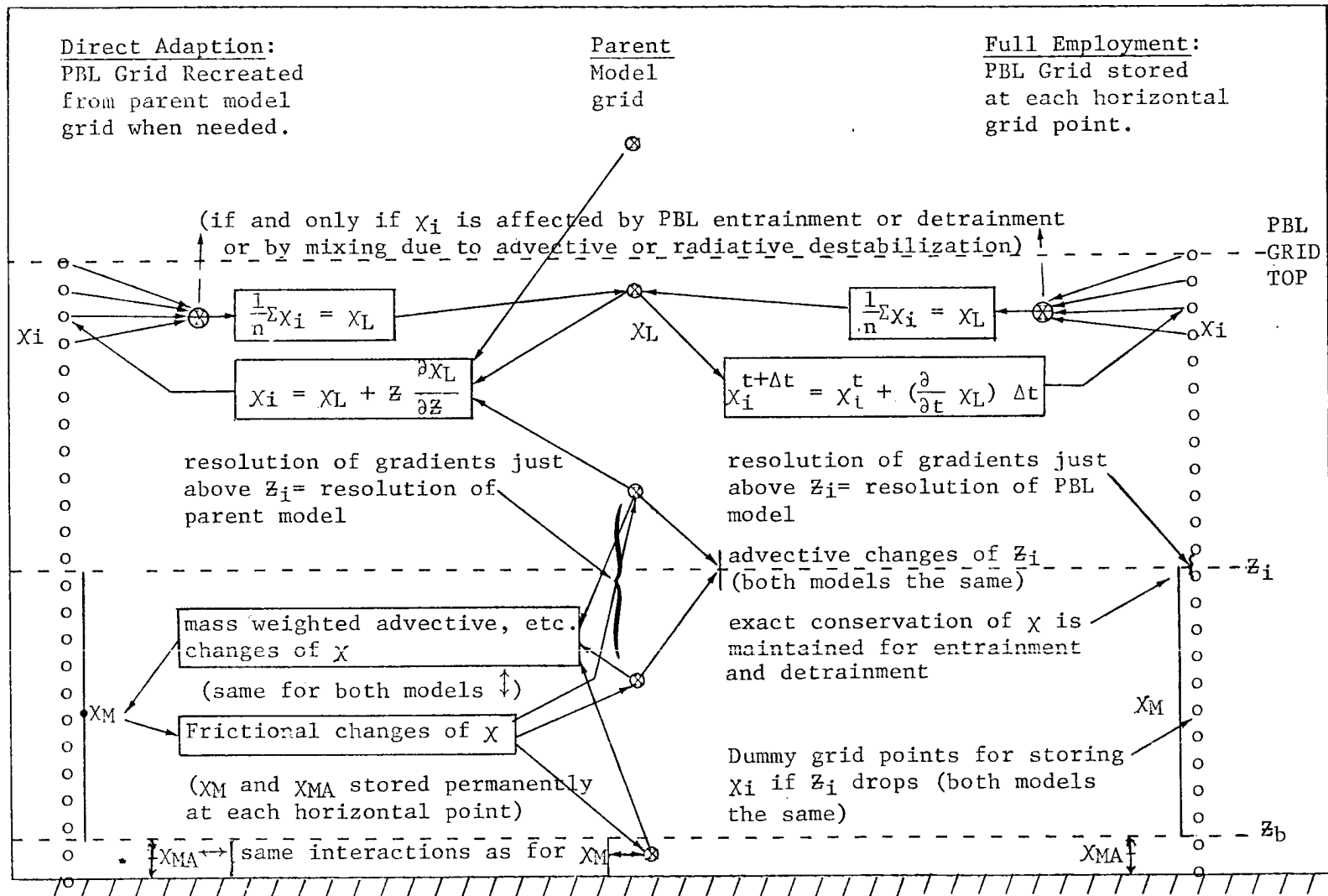


Figure 5. Schematic of some interactions between parent model and two forms of application of the PBL model.

through z_i , is generally less accurately described than by the full employment method discussed below.

3. Full Employment. This method requires greater data storage capacity in order to provide better vertical resolution above z_i . The added storage required is to hold possibly 20-40 values each of θ_v , u , v , and q at every horizontal grid point--however the u , v , and q values could probably be treated as in the direct adaption method with comparatively little added error. Then only a vertical column of θ_v values would be required. This is a new and untried idea and it may be found that the cost in computer storage exceeds the benefit of the more accurate description of the PBL behavior. Figure 5 displays the differences between this and the direct adaption method--which are primarily above z_i . Below z_i it is envisioned that in both techniques the parent model grid points, if any, are used to determine advective changes of the layer averaged variables X_M and X_{MA} , but the profiles of X are controlled by the PBL model and its parameterization of frictional effects. If the parent model contains enough vertical resolution that at least one point above the surface is nearly always within the PBL, one might consider tying the prescribed depth δz of that layer to the value of z_i . This would make the advective calculation of X_M much more exact. The radiative divergence calculation as modelled here is based on the parent model grid values above z_i and on T_M and T_{MA} below z_i .

The parameterization presented in this report provides some special advantages to the mesoscale and global scale modeller. The storage of the mean values X_M and X_{MA} independent of the grid point

values in the parent model provides improved resolution of the PBL without adding more advective calculations. Similarly above z_i the 100 meter grid which is maintained by the PBL model adds no advective calculations (even in the full employment method) but provides better resolution of the entrainment and detrainment processes. Finally the accurate representation of surface temperature--even if no other part of the model is applied--can improve the quantitative results of any model.

IV. TESTING THE MODEL

Because of the versatility and relative simplicity of the model developed here it has been possible to perform tests under a variety of conditions, and to vary a number of parameters in order to check the sensitivity of the model to them. The first part of this chapter discusses the four basic cases that have been modelled, then in the latter part the responses of the model to various "stimuli" are discussed.

A. Comparison with observations and with other models.

It is felt that any boundary layer model or parameterization which is to be considered useful in describing a wide range of conditions should first be carefully tested under a wide range of conditions. Many models in the literature are compared against one set of observations in one case study and then are "let loose" into the scientific community. Such models run the risk of having been inadvertently "tuned" to one particular data set, and they may be far less accurate in another situation. To avoid this, the present model has been tested against four distinct periods of observational data from two different data sets, and has been, at the same time, compared with the calculations of other models which have used the same data. The case studies chosen are the following:

- 1). Day 33 of the Wangara experiment (Clarke, et al., 1971), which was a clear winter day at about 35°S with dry soil and light winds. Other models which have used this data, and which are discussed below are those due to Deardorff (1974a), Wyngaard and Coté

(1974), and Pielke and Mahrer (1975). The former two are high order closure models and the latter is an eddy viscosity type PBL parameterization designed for use in a mesoscale model.

2). General observation period 2 at O'Neill, Nebraska (Lettau and Davidson, 1957). This was a clear, hot breezy summer day near 42° N with fairly moist soil.

3). General observation period 5 at O'Neill, Nebraska-- a clear hot windy pair of days in late summer with dry soil and with possible cold advection and considerable moisture advection from a large irrigated region upwind. Another study of this period, which is used for comparison here, is the one dimensional micrometeorological model of Sasamori (1970).

4). Day 16 of the Wangara experiment was a partly cloudy winter day with dry soil but high relative humidity, and with an approximately linear change of both components of the geostrophic wind with time through the period.

The specific initial conditions and input sounding used for each of these cases are presented in the appendix. In general the runs were initialized to pre-dawn values and the computer integration began before sunrise. The one exception is the first day of O'Neill period 5 which was initialized at noon.

1. Wangara, day 33.

The data from day 33 of the Wangara experiment are without doubt the most widely used observations for comparison with boundary layer models. On that day there were perfectly clear skies and practically unchanging synoptic conditions. Figure 6 shows the energy budget

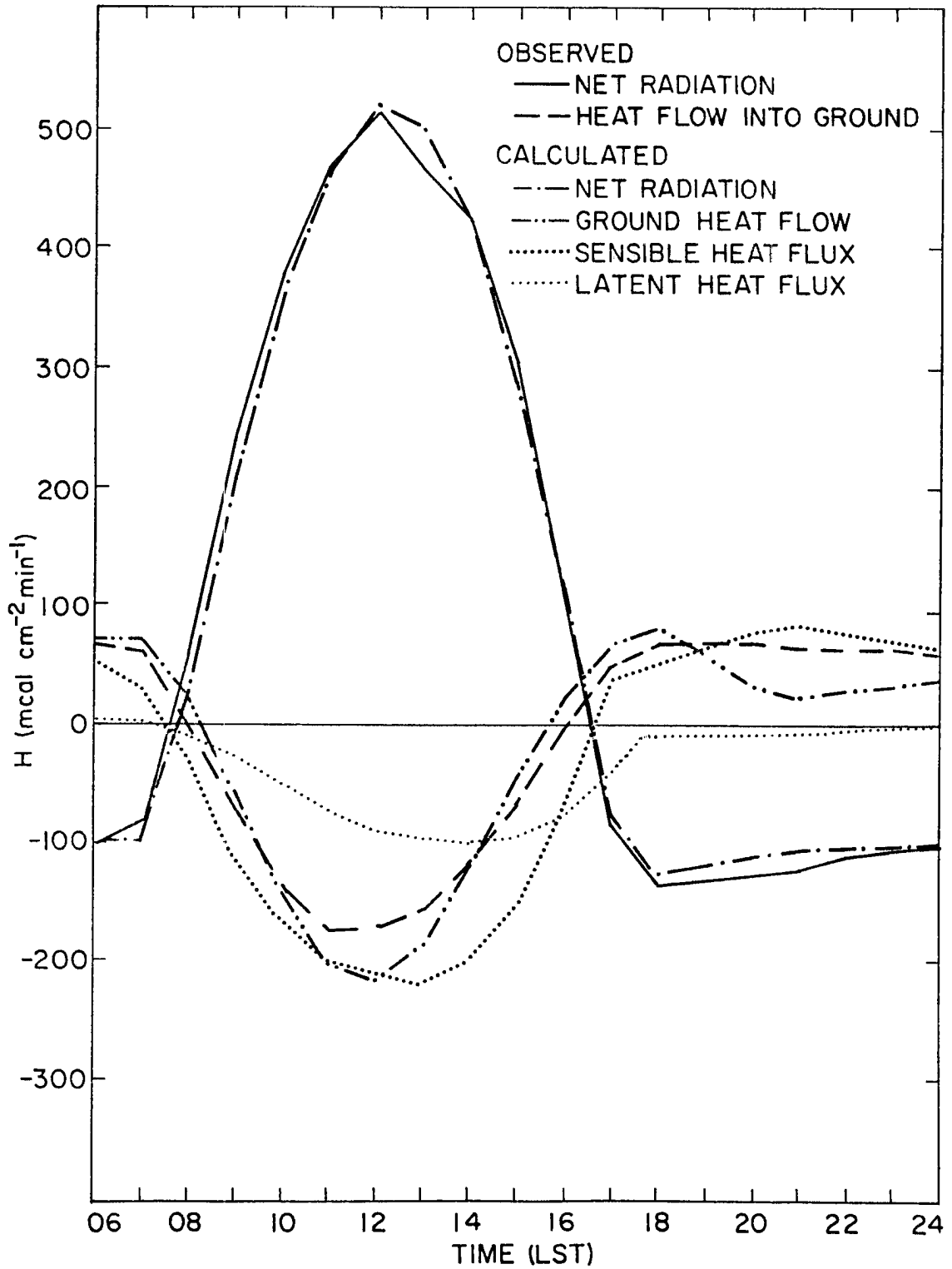


Figure 6.) Surface energy budget-Wangara 33.

components for the period 0600 to 2400 local standard time at Hay, N.S.W., Australia on 16 August, 1967. Observations were made of only two of the components, the net radiation and soil heat flux. The net radiation, which is the basic driving force of the PBL, is simulated very accurately by the model. The ground heat flow is somewhat less well described by the present parameterization, particularly around noon and after sunset. The sensible and latent heat flows seem to be modelled reasonably. In preliminary tests of this day it was found that in order to reproduce the heating rate in the PBL which is observed, an evaporation of about 0.7 mm. of soil moisture and/or dew is required under conditions of no net subsidence through the day. Any subsidence would cause further warming and thus further increase the amount of evaporation required. The latent heat flux as modelled in Figure 6 yields the needed amount of evaporation, but in order to evaporate that much soil moisture using the present parameterization, a soil moisture of about 40% of field capacity was required. This is somewhat larger than expected since the investigators (Clarke, et al., 1971) felt that the soil moisture was near the wilting point--about 10 to 15 percent of field capacity. There are five possibilities which can explain the need for a greater soil moisture in the parameterization, all of which probably have some influence on the results: 1). The evaporation formulation used here may underestimate evaporation somewhat under conditions of dry soil and light winds. 2). During the frontal passage a few days earlier, little precipitation fell at Hay but more precipitation may have fallen to the east. The air modified by this moister soil may then

have been advected westward on day 33. 3). Desert plants are very deep rooted and tap moist layers deep beneath the surface. Thus they may continue to transpire significant amounts of moisture even though the soil appears very dry. 4). The wind flow on this day was light from the east. With this trajectory, the air reaching the radiosonde observation site at Hay has followed the Murrumbidgee river for a considerable distance. Dr. D.H. Lenschow (personal communication) reports that the flood plain of the Murrumbidgee is a rather wide, tree covered wetland surrounded by areas of irrigated pastureland. Based on this description it would appear that a 40% soil moisture value is not at all unreasonable for air with a long fetch along the river. 5). The high values of mixing ratio observed near the surface at night over the site coupled with cold temperatures, light winds, and clear skies could have caused a heavy dew/frost deposition on the morning of day 33. The evaporation of this moisture can seriously affect the surface energy budget. This last possibility however does not appear to be able to explain the entire effect, because a special test was run in which the soil moisture was set at 15% and 0.7 mm of dew was allowed to evaporate; and the results did not completely agree with observations. This test is discussed further in section B.2 of this chapter.

Figures 7 compare the profiles of virtual potential temperature as observed and as calculated by the present model. The profiles simulated by our model are quite accurate at all times. At 1200 data are available also for the models of Pielke and Mahrer, and of Deardorff. Their results are not plotted since the figures here

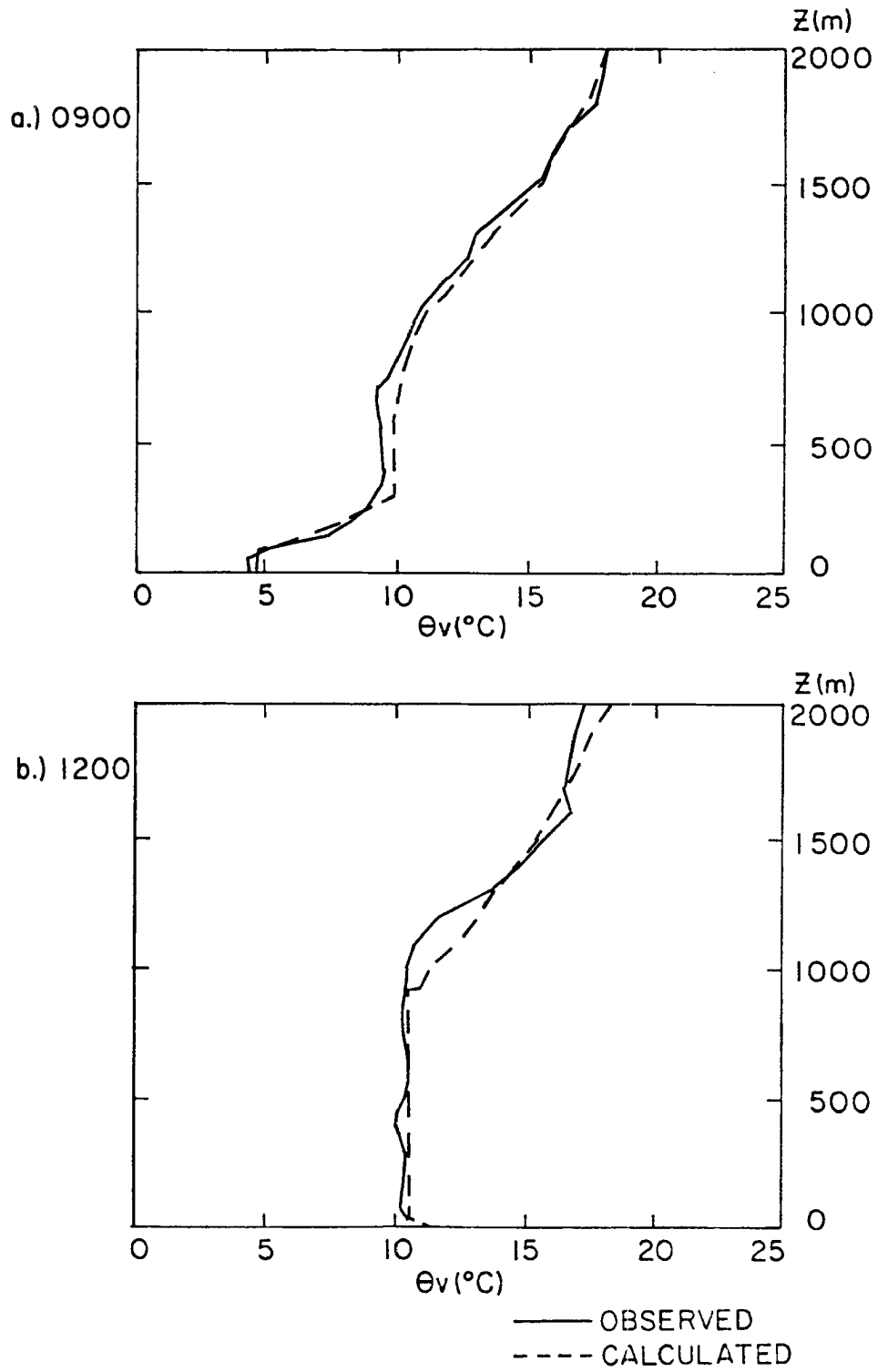


Figure 7.) Virtual potential temperature profiles-Wangara 33.

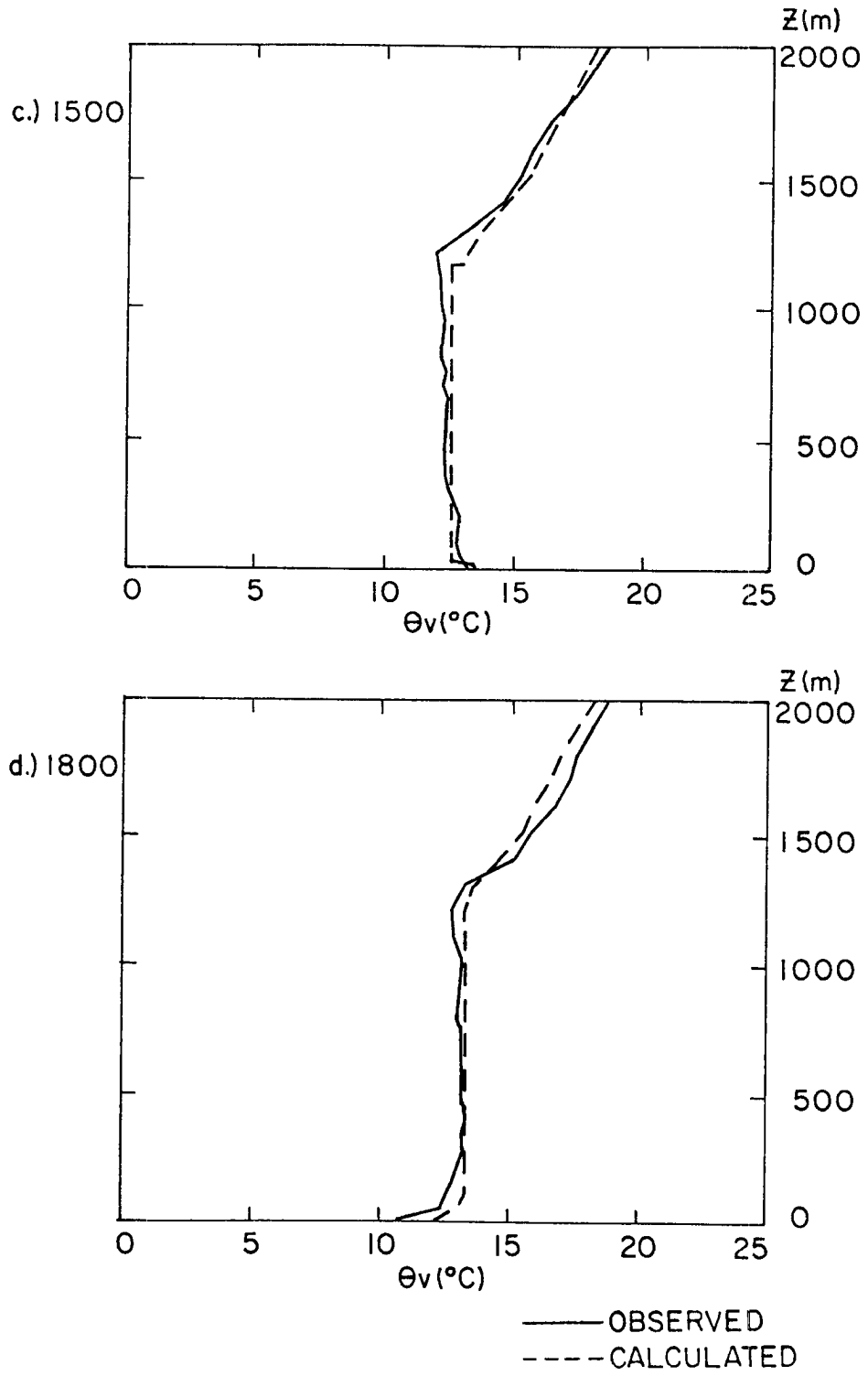


Figure 7.) (Continued)

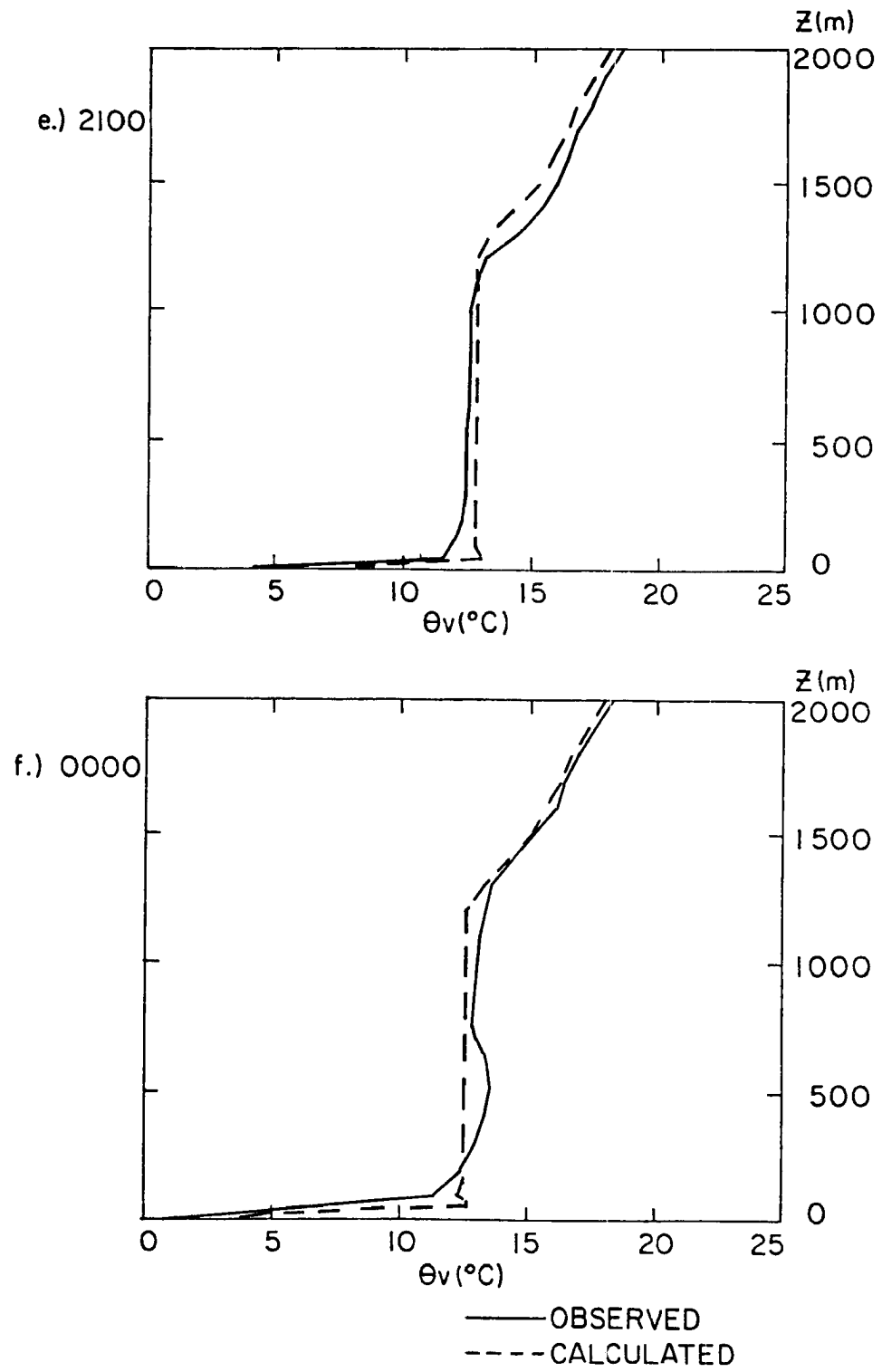


Figure 7.) (Continued)

present virtual potential temperature while the other two models report potential temperature. The PBL potential temperature profile is about equally well represented by our model and by Pielke and Mahrer (both models are generally within 1°C of the observed values). It should be noted, however, that our model was initialized at 0600 and had run for six hours of simulated time, including the transition through sunrise. The other models were initialized at 0900 and had run for only three hours. It seems surprising that the extremely sophisticated model of Deardorff is about 1°C too warm in the PBL after 3 hours. As the day progresses, that model continues to warm too rapidly and strays further from the observed profiles. Obviously it is not the primary function of the Deardorff model to simulate the horizontally averaged gross quantitative features of the PBL, however its relative failure points out an important fact, which will be further expanded upon later: The most sophisticated model imaginable will not perform well unless at its foundation is an accurate surface energy budget. The unstable PBL is not primarily controlled by the detailed nature of the turbulence but by the thermodynamic forcing applied by the earth's surface.

The temperatures at and near the surface are compared in Figure 8. The agreement is quite good except for somewhat too warm values during the nighttime hours. This may be a result of insufficient radiational cooling as calculated by the Sasamori empirical formulae. Other possible contributing factors may be the error in the assumed shape of the nocturnal temperature profile which could affect the sensible heat flux into the lower PBL, and the somewhat

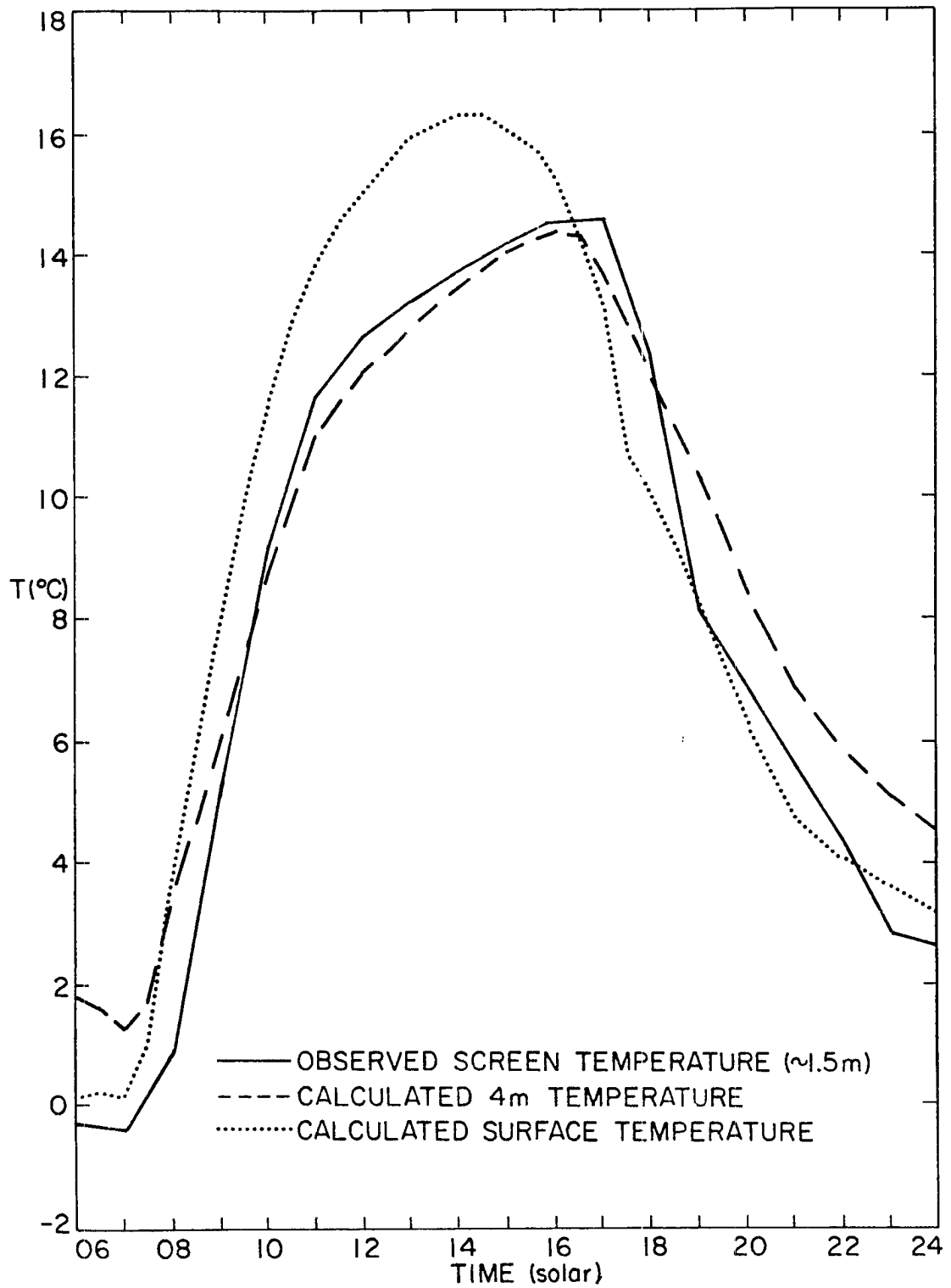


Figure 8.) Ground level temperature-Wangara 33.

too high wind speeds calculated by the model after sunset. The fact that the calculated ground heat flow (Figure 6) is less than observed is probably primarily a result of the excessive warmth at the surface.

Figures 9 present the ground level winds, as observed and as simulated. Generally there is good agreement in the wind speeds although some of the calculated trends may appear out of phase with observations. The wind speeds become somewhat too high after sunset which, as mentioned, may contribute to keeping the surface temperatures too warm. The calculated wind direction simulates the observations as well as or better than Deardorff's model.

There are some basic difficulties in dealing with wind observations which make it nearly impossible for any model to closely simulate real data. The calculated wind profiles represent horizontal averages, the equivalent of which would require many hours of continuous observation in the field. This problem will be discussed in detail in section B of this chapter. However the calculated wind profiles should only be considered loosely verified by the observations.

With the preceding discussion as background, some wind profiles are compared in Figures 10. Also presented are the calculations of Pielke and Mahrer. It appears that the models agree between themselves about as much as either agrees with the observations. It should be remembered that above z_1 our model simply calculates an inertial oscillation of the wind about the geostrophic, assuming no advection and a minimum of damping.

The moisture profiles for this day appear in Figure 11. The calculated moisture profiles are consistently too high although

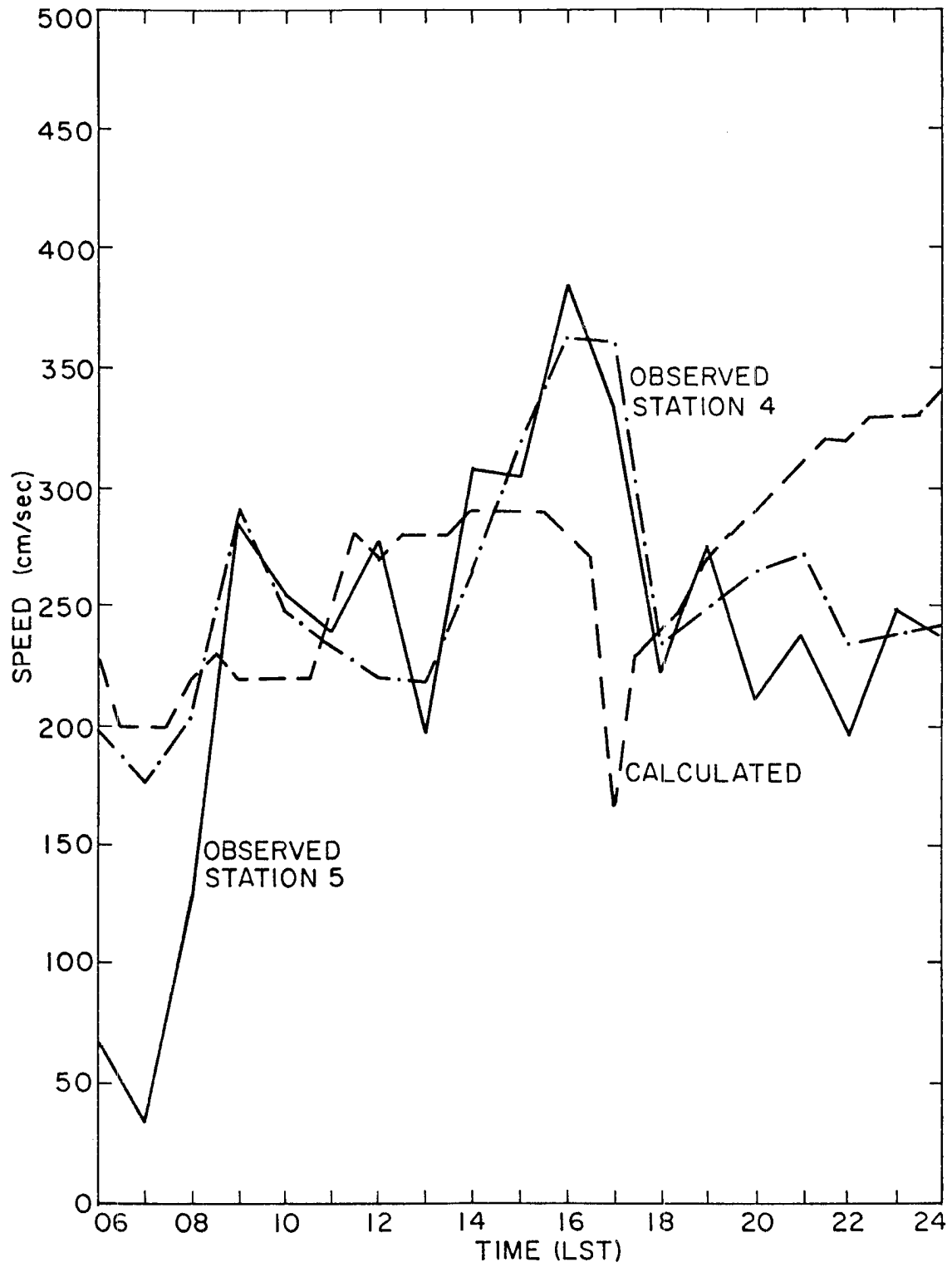


Figure 9a.) 4-meter wind speed-Wangara 33.

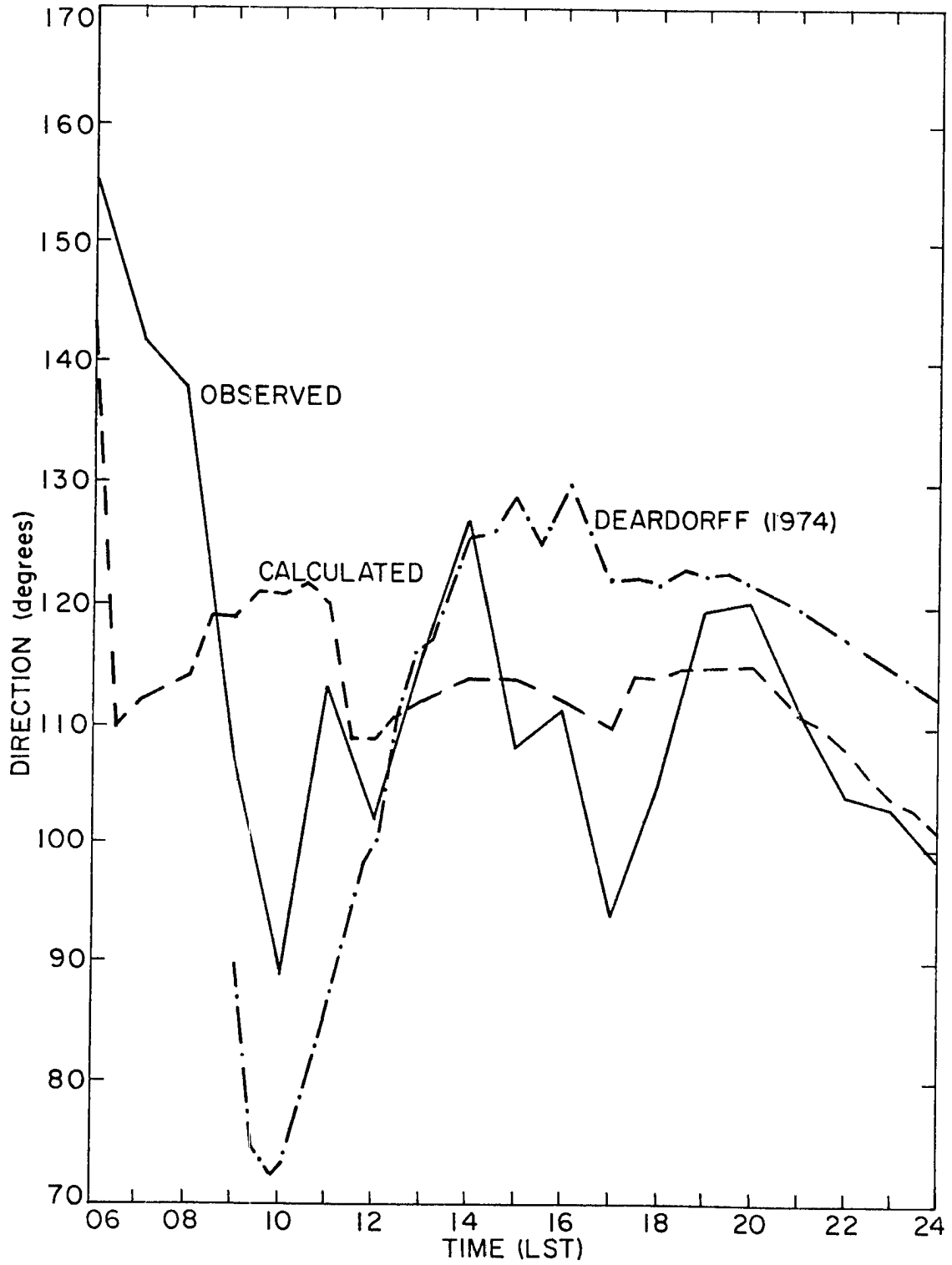


Figure 9b.) Surface layer wind direction-Wangara 33.

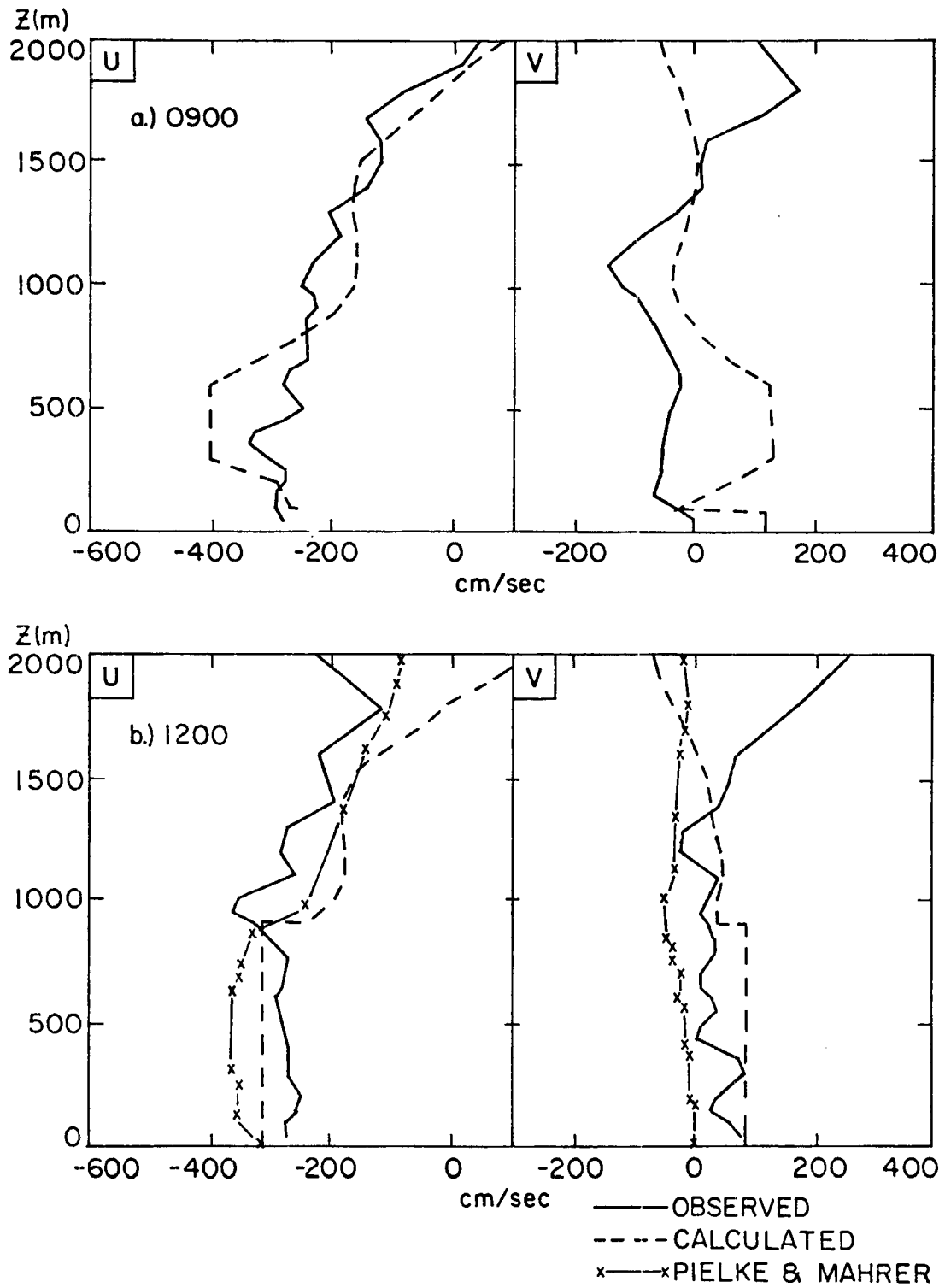


Figure 10.) Wind profiles-Wangara 33.

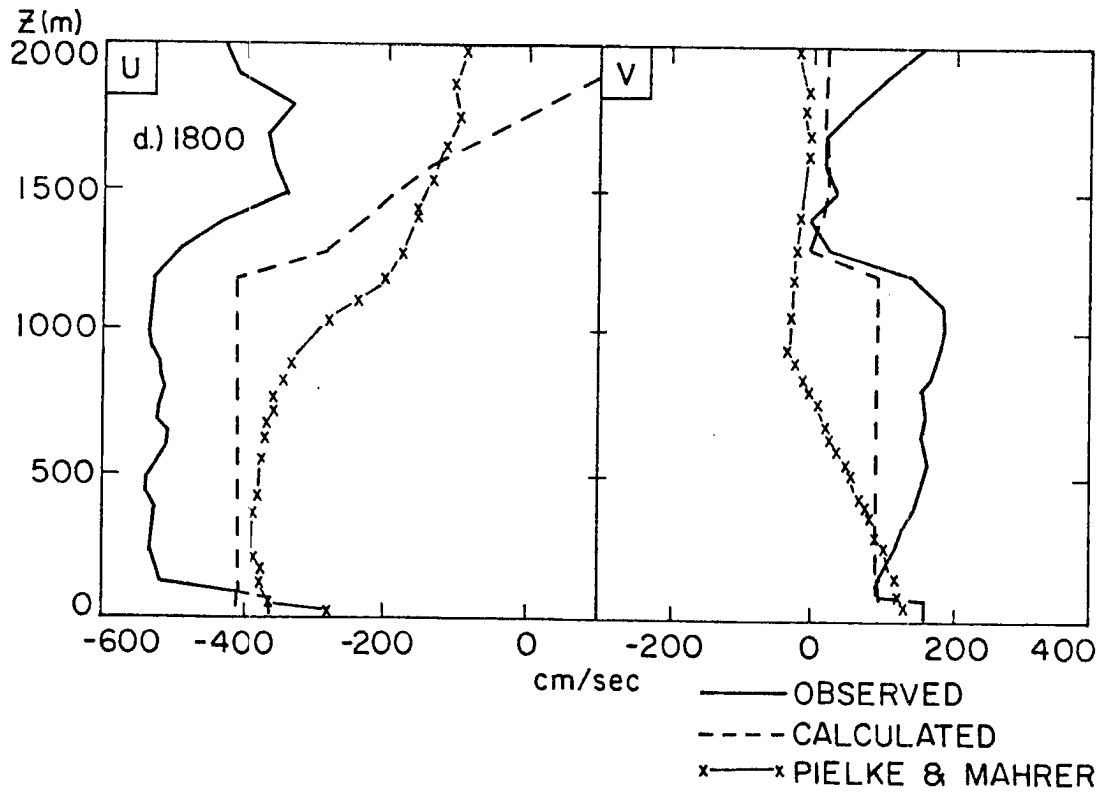
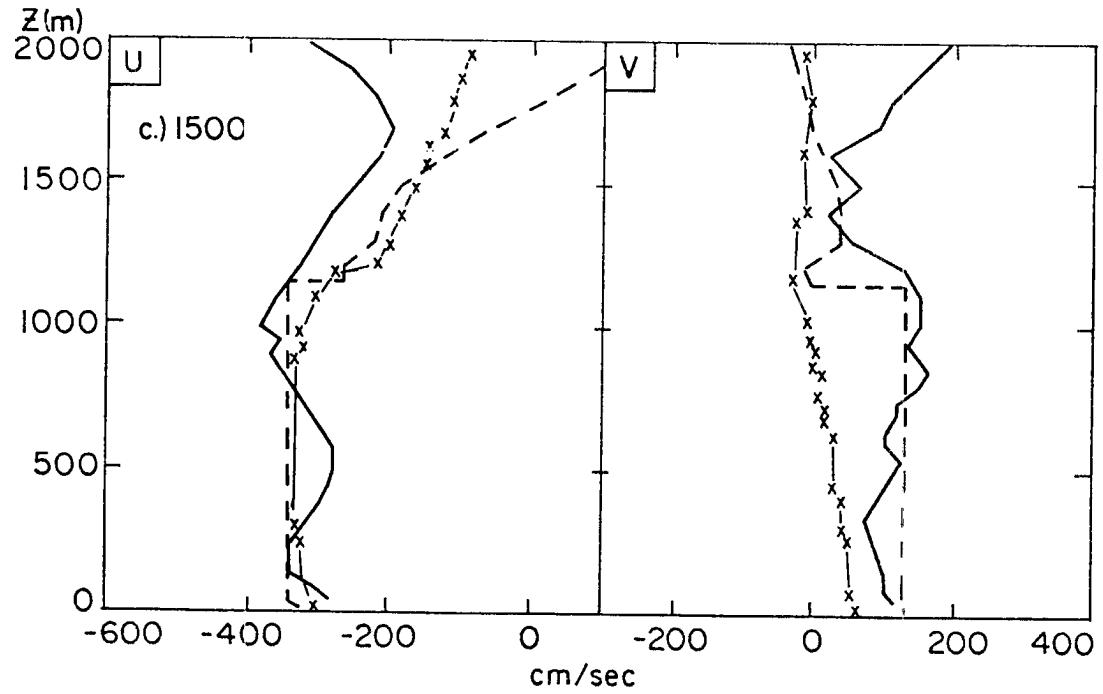


Figure 10.) (Continued)

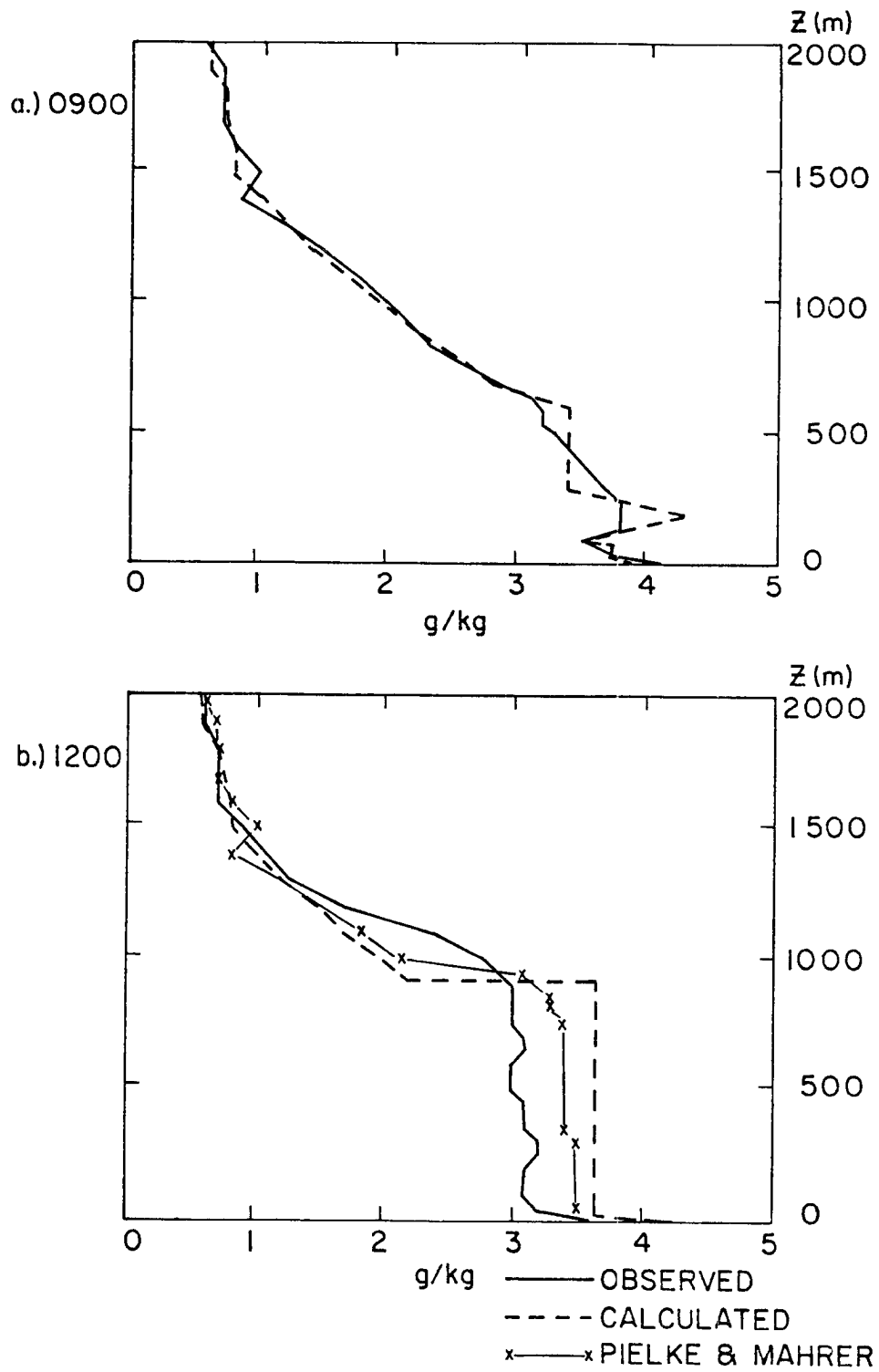


Figure 11.) Moisture profiles-Wangara 33.

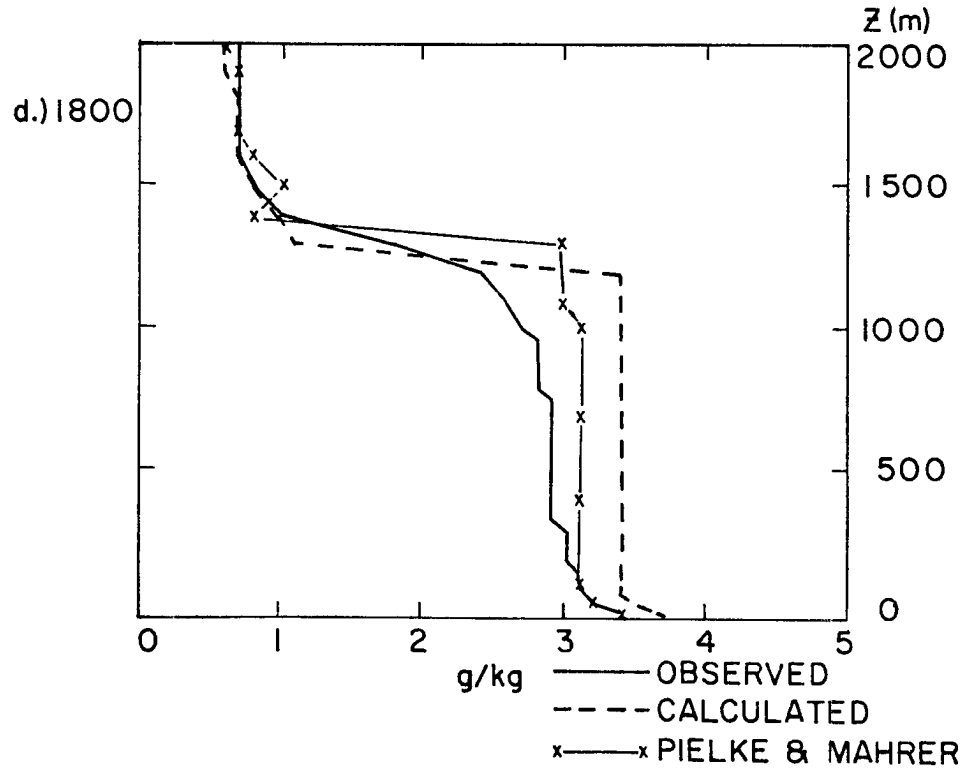
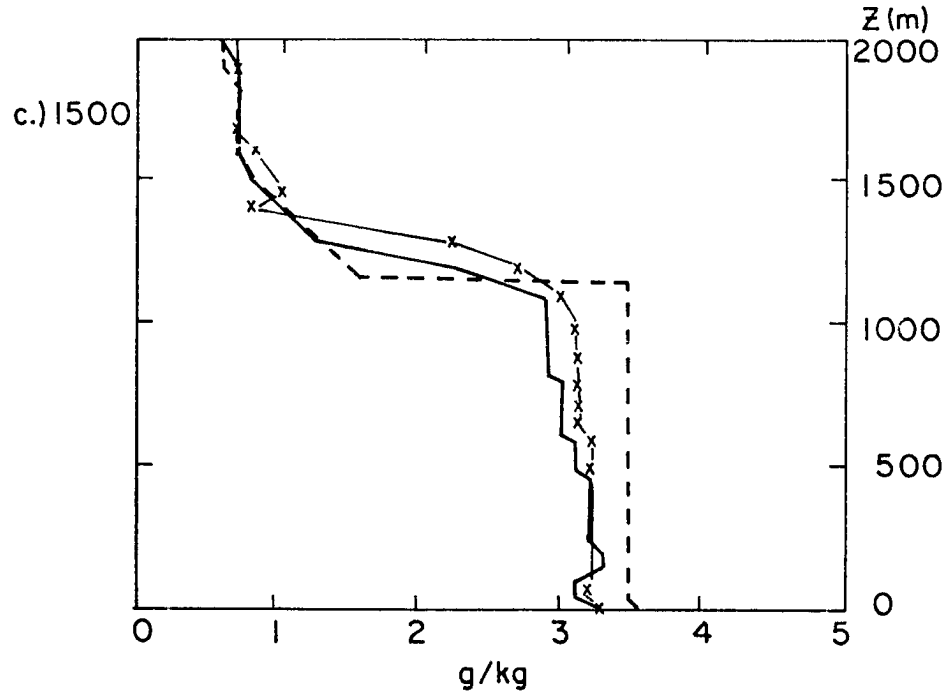


Figure 11.) (Continued)

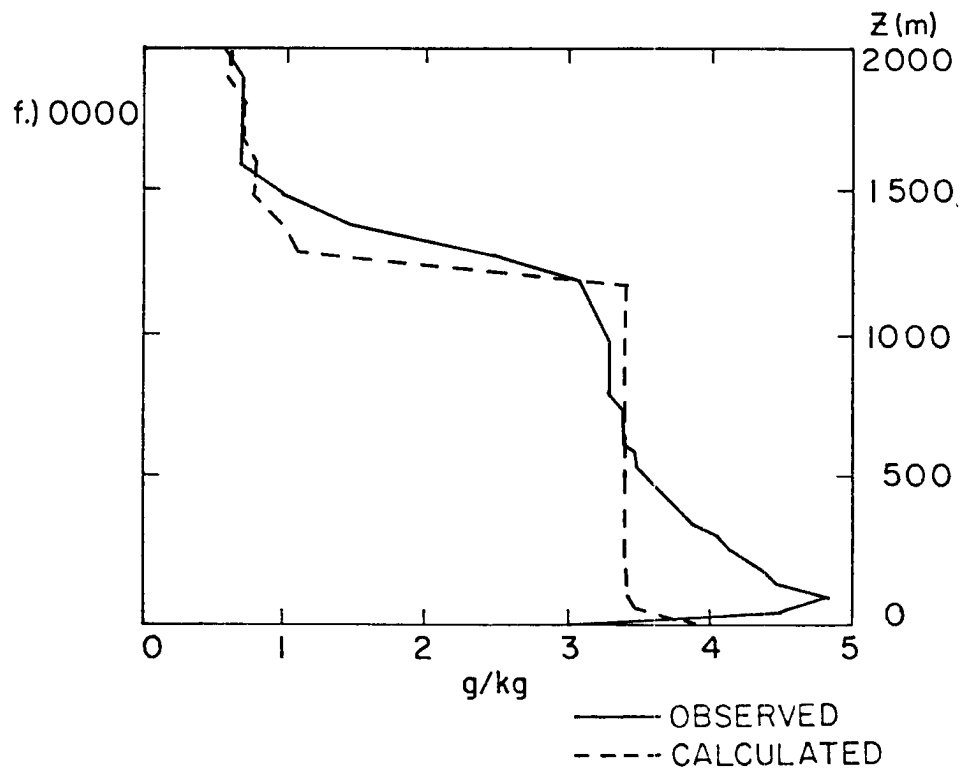
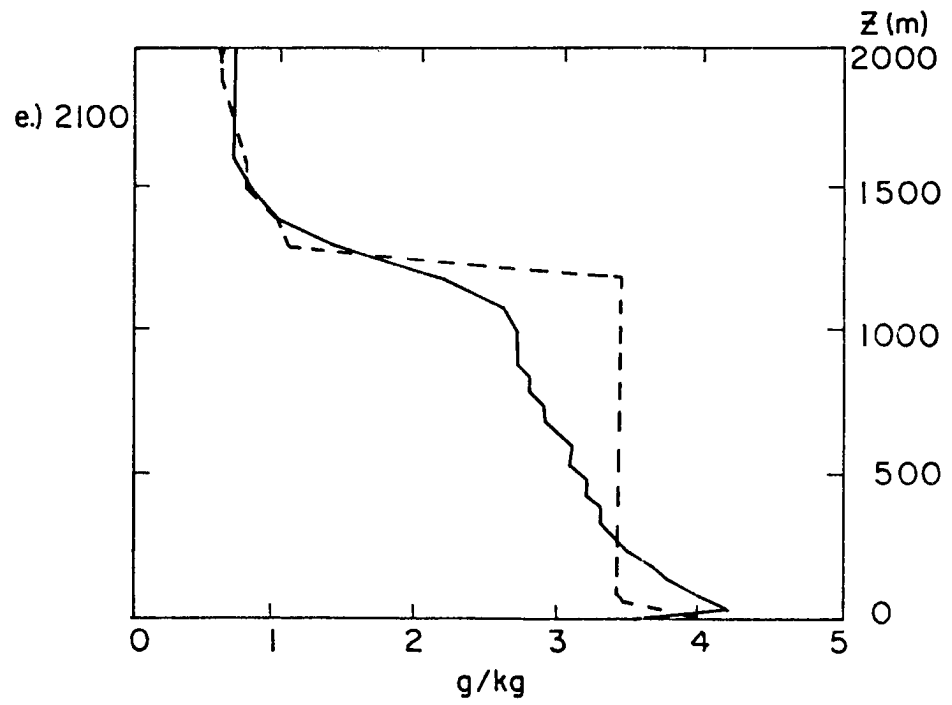


Figure 11.) (Continued)

profile shapes are very comparable. There are two causes for this result. First the somewhat high soil moisture assumed for our model may have introduced excessive moisture into the atmosphere during the course of the day. However this effect should be additive and most prominent in the afternoon. In fact the discrepancy between calculated and observed values is greatest at noon. This points to the second, and probably the more important cause for the discrepancy. The model was initiated before sunrise when the moisture in the lower atmosphere was quite abundant. The Wangara data displays a quite regular pattern of strong moisture inflow after sunset (see Figures 11e and 11f) and rapid drying after sunrise. Thus it is suspected that the initialized values of moisture are more representative of the nocturnal moisture abundance rather than the daytime conditions. The apparent dry advection immediately after sunrise is not accounted for.

Finally the calculated height of the boundary layer is compared with the observed boundary layer height in Figure 12. The observed values are estimated from the temperature and moisture profiles. At 1800 two observed values are plotted--the top of the inertial well mixed layer and the top of the developing nocturnal inversion. Here again the two high-order-closure models are the least accurate because they have failed to carefully model the surface heat input. Of all the models shown, the model developed in this study, with its new predictive equation for the unstable z_i , appears to be the closest to the observations. Using the Deardorff equation, our model over-predicts it in the afternoon. The model of Pielke and Mahrer is also

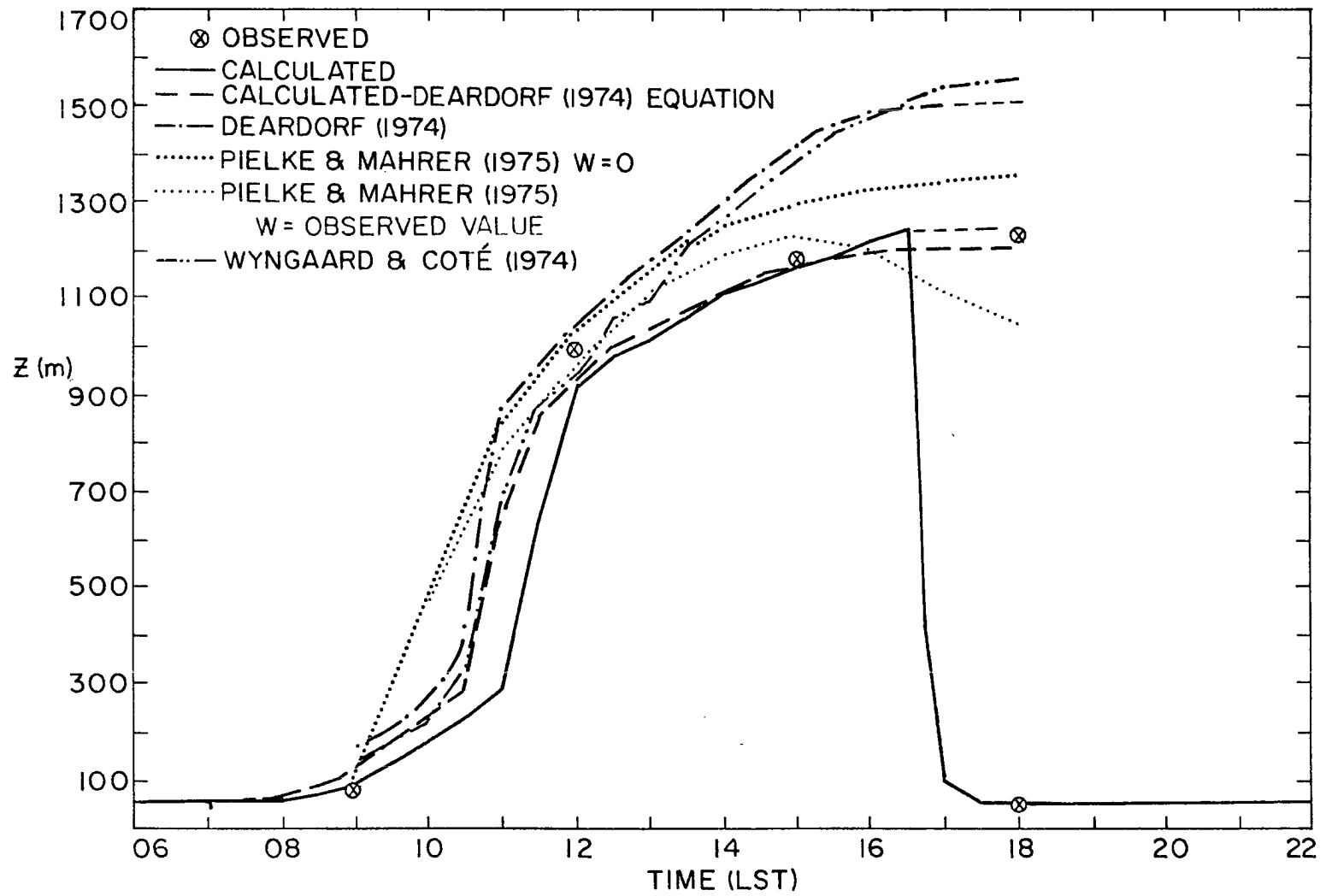


Figure 12.) Boundary layer height-Wangara 33.

fairly accurate when the observed vertical motion is taken into account, however the quality of the reported vertical wind speeds for the Wangara experiment is questionable, since the values are derived from four pibal point wind soundings. There is evidence that some subsidence may have been occurring, but the Pielke and Mahrer calculations indicate that the reported magnitudes are too large.

2. O'Neill, Nebraska; Period 2.

General observation period 2 at O'Neill covers the period from before sunrise to midnight on August 13, 1953. The weather was clear and hot with brisk southerly winds in advance of an approaching cold front which reached the area near midnight. Figures 13 show a comparison of the various calculated components of the surface energy budget with the observations of three different scientists at the site. The degree to which the three observations differ provides a good qualitative estimate of the measurement error for the various components. All the calculated values appear to lie well within the limits of the observational error except possibly after sunset, and generally agree very well with the mean of the observed values. Note that the largest observational uncertainty occurs in the estimation of evaporation. With such discrepancies in the observations, it is easy to understand why evaporation is difficult to model.

The potential temperature profiles are presented in Figures 14. The unstable PBL is very accurately modelled throughout the day. By 1600 local solar time, the boundary layer had broken into a deep, nearly dry adiabatic layer, and the PBL top was not clearly defined

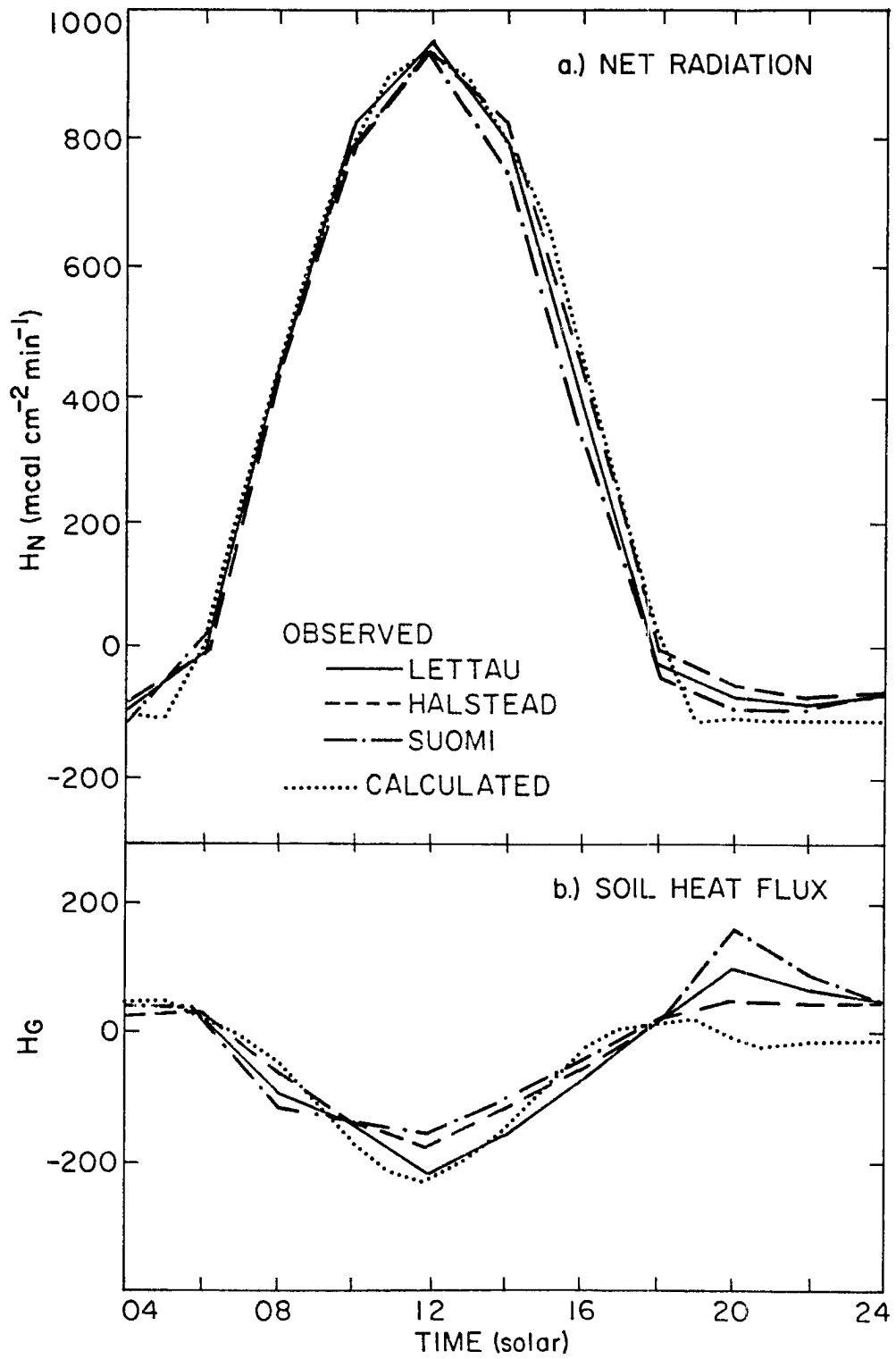


Figure 13.) Surface energy budget-O'Neill general observation period 2.

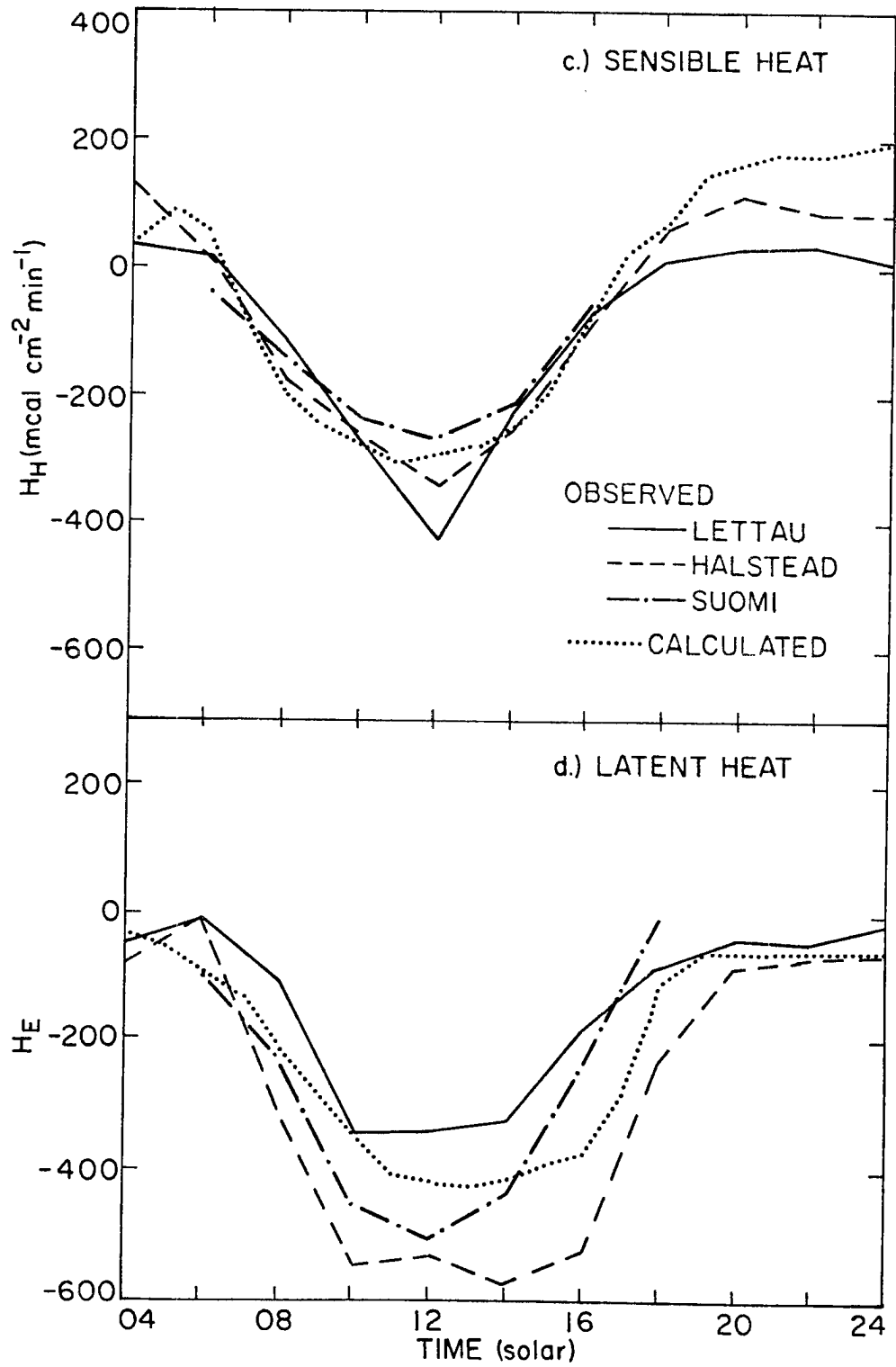


Figure 13.) (Continued)

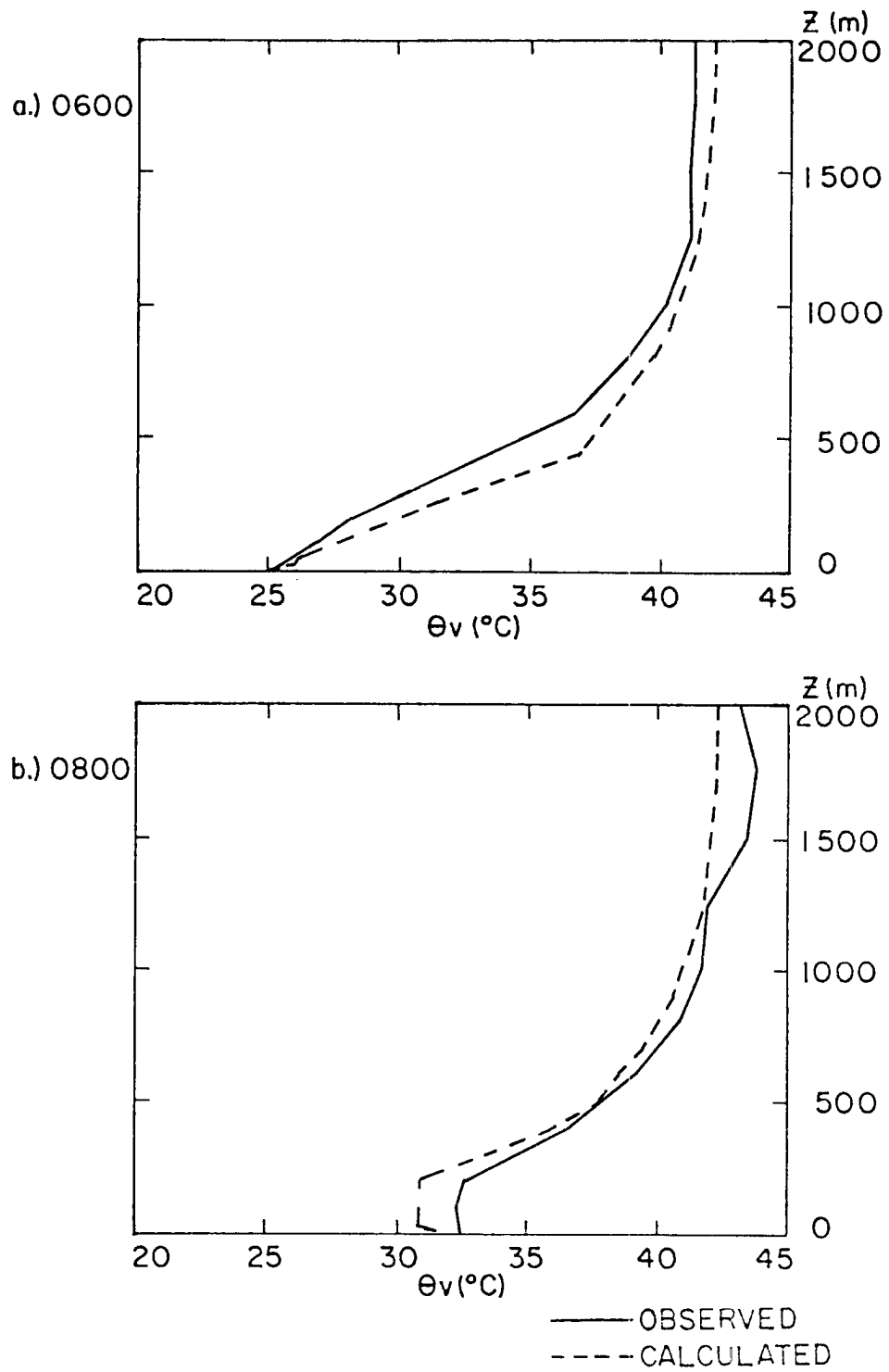


Figure 14.) Virtual potential temperature profiles-
O'Neill general observation period 2.

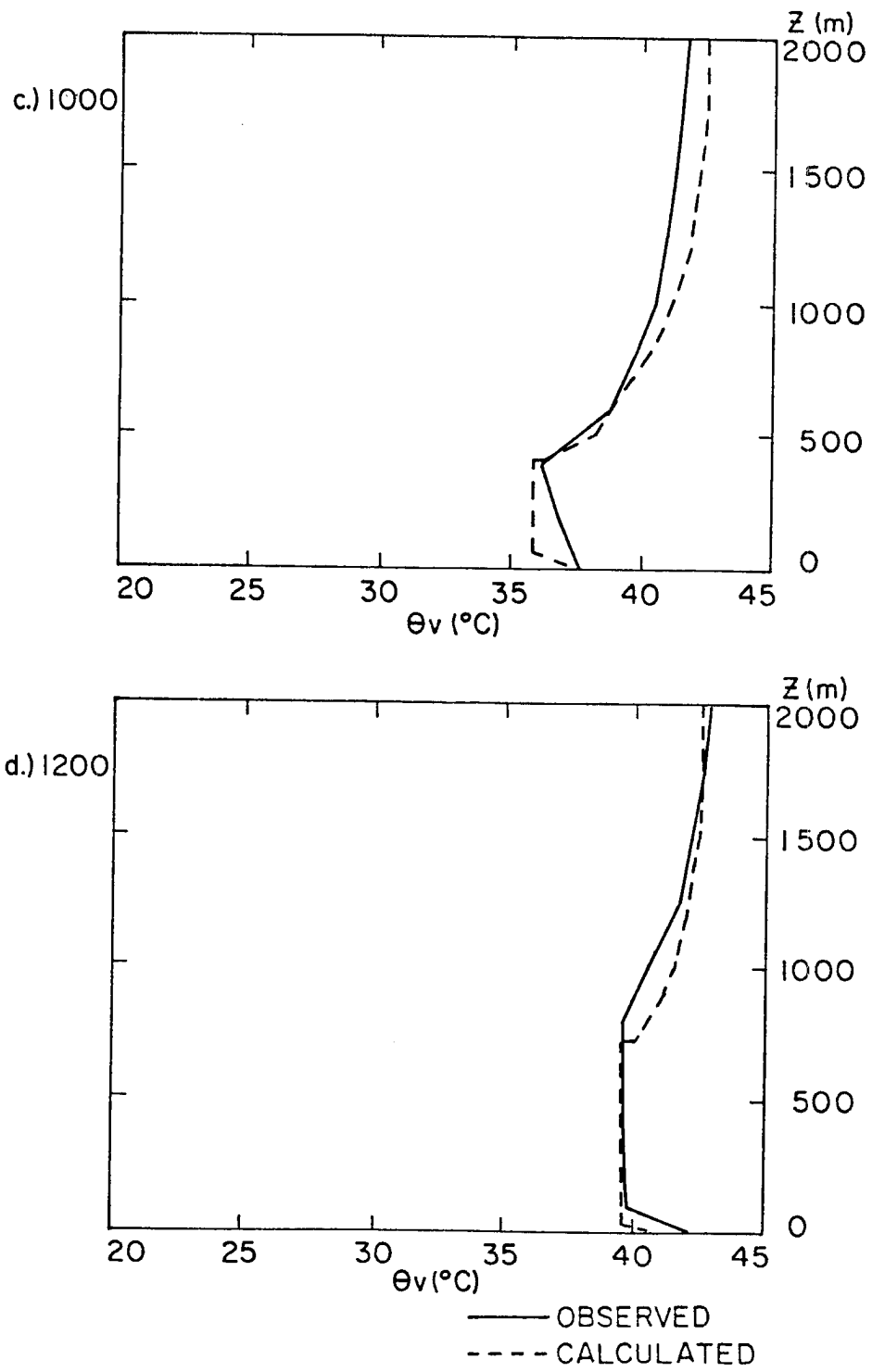


Figure 14.) (Continued)

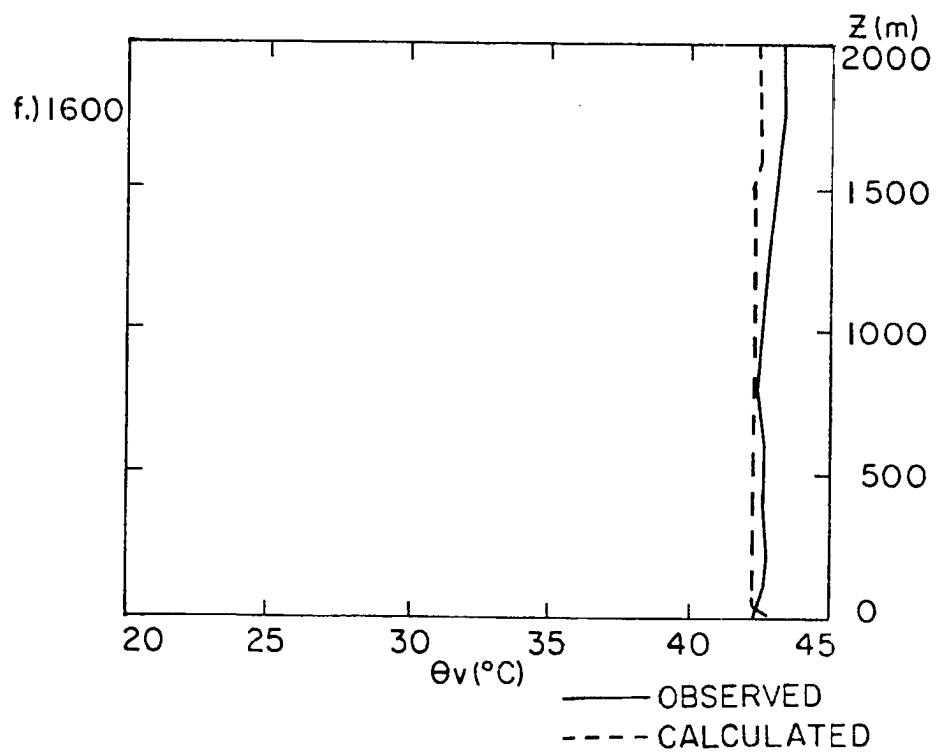
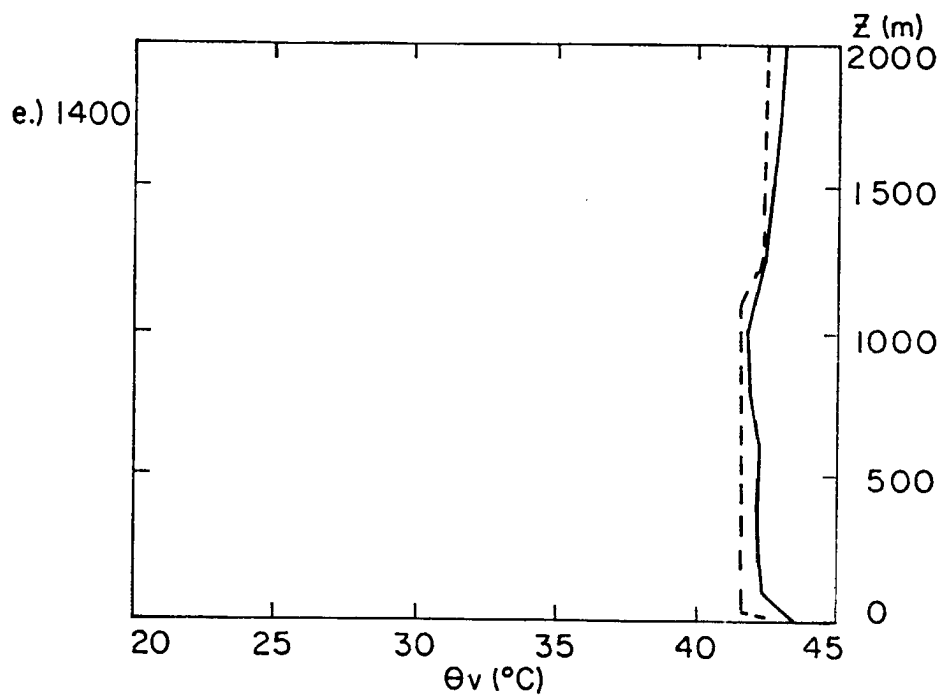


Figure 14.) (Continued)

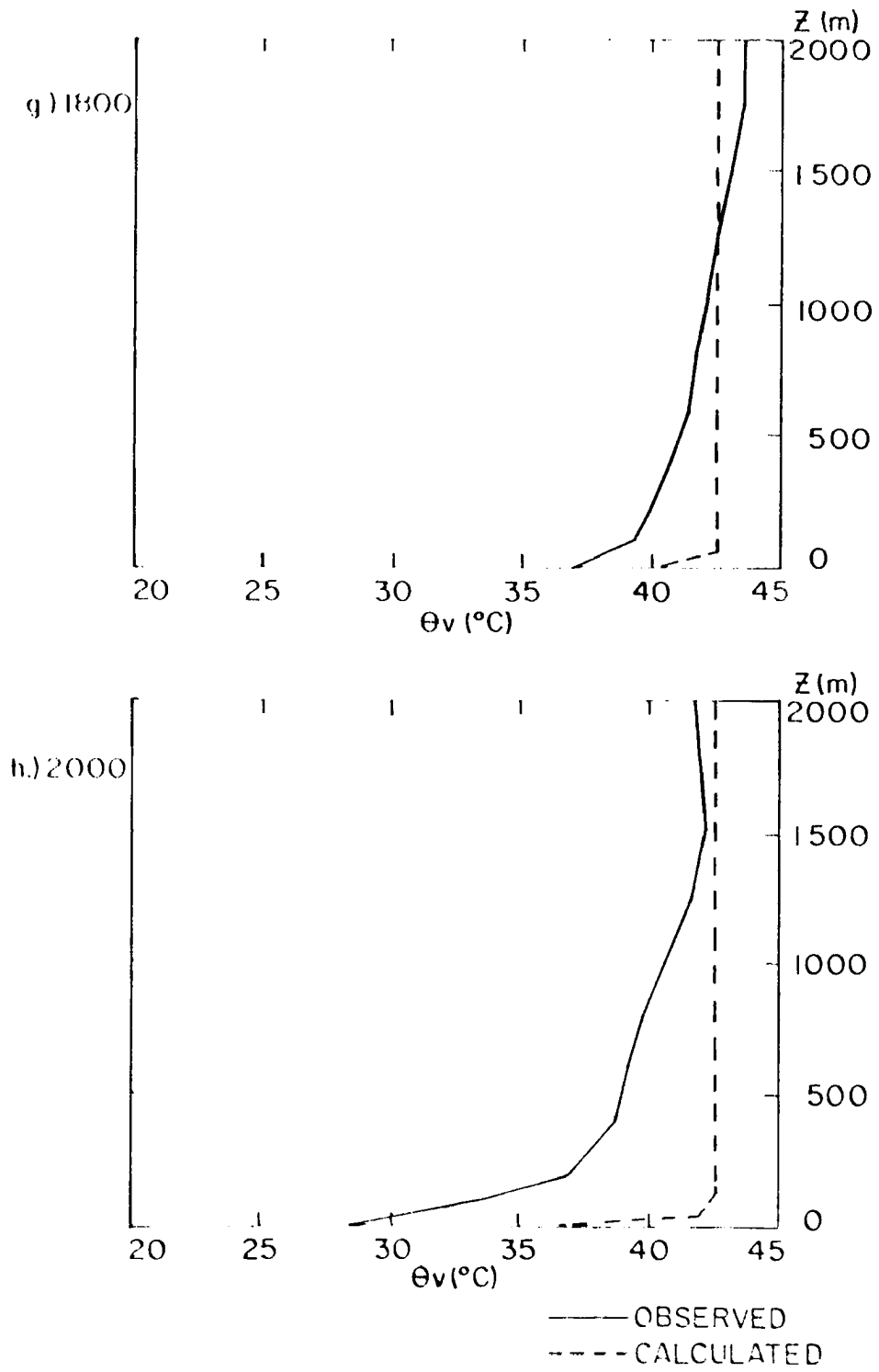


Figure 14.) (Continued)

in the observations. By 1800 cooling had begun near the surface, and the model is slow at developing the nocturnal stable layer. However it is believed that cold advection was taking place in the observational data as a cold front was entering the area. In Figure 15 the observed temperatures at various levels near the surface are plotted along with the calculated temperature of the interface layer and the calculated temperature at four meters. The discrepancy between the calculated values and their true counterparts is everywhere less than 3°C except for a serious failure of the model to cool as much as is observed after sunset. This is not as good as one would have hoped, but it is an acceptable margin of error for a short term forecast from a one-dimensional PBL model which cannot account for horizontal advective effects. Part of the nocturnal problem may also be that discussed in the Wangara day 33 case.

The near-surface wind speed and direction are shown in Figure 16. The speeds during the unstable hours seem to be rather well simulated by the model, but the values are too large during the stable hours. The modelled wind direction is too westerly at all times. This is likely to be a result of the fact that the O'Neill site lies on a gently sloping plain. Although the incline is so slight as to be imperceptible ($\sim 1:600$), it has an important influence on the airflow under diabatic conditions. Besides influencing the wind direction, the sloping surface is probably the primary cause of the strong low level jet observed almost nightly in the summer at O'Neill.

Figure 17 compares the observed and predicted height of the PBL. As mentioned, the observed value of z_1 in the late afternoon is

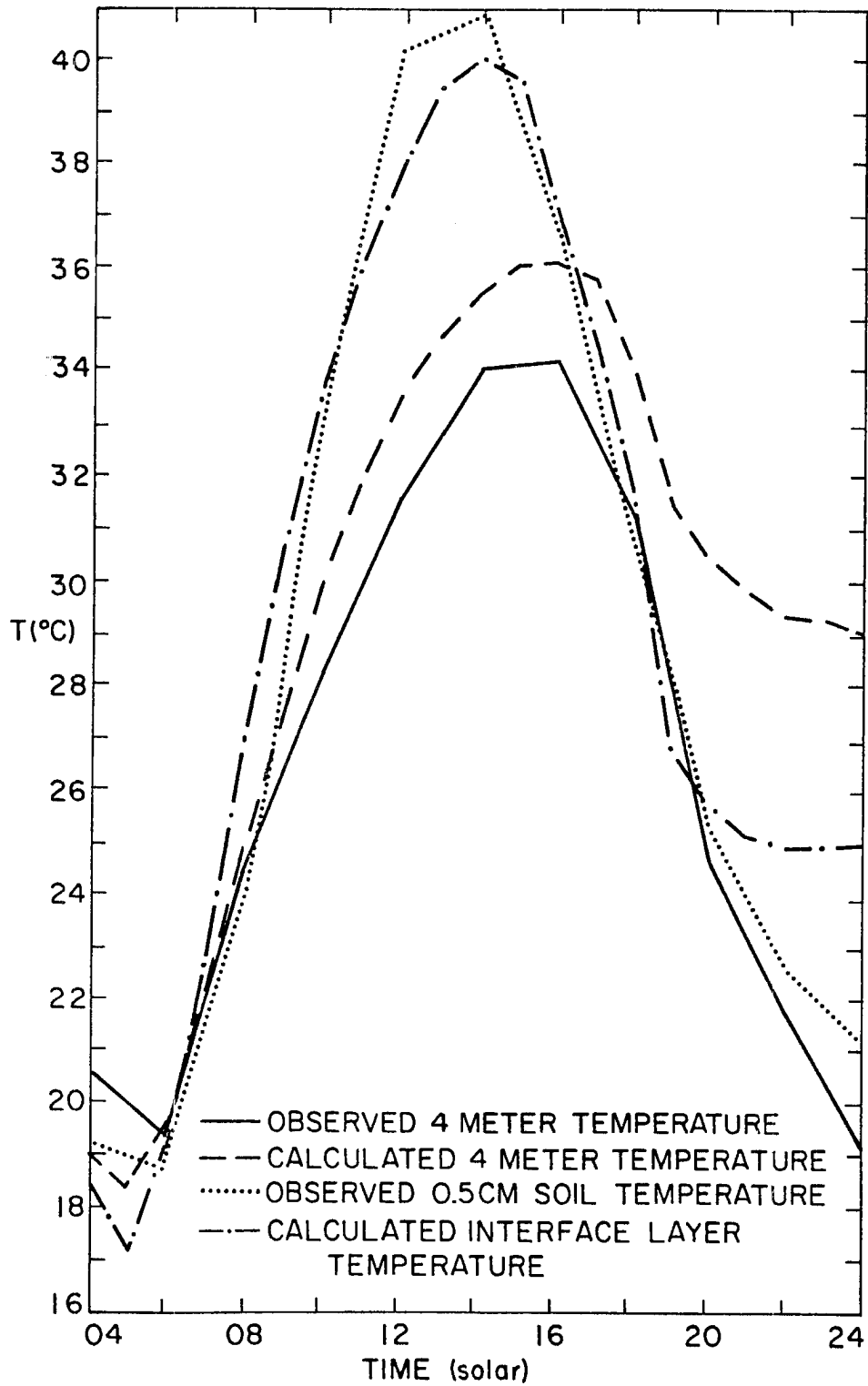


Figure 15.) Ground level temperature-
O'Neill general observation period 2.

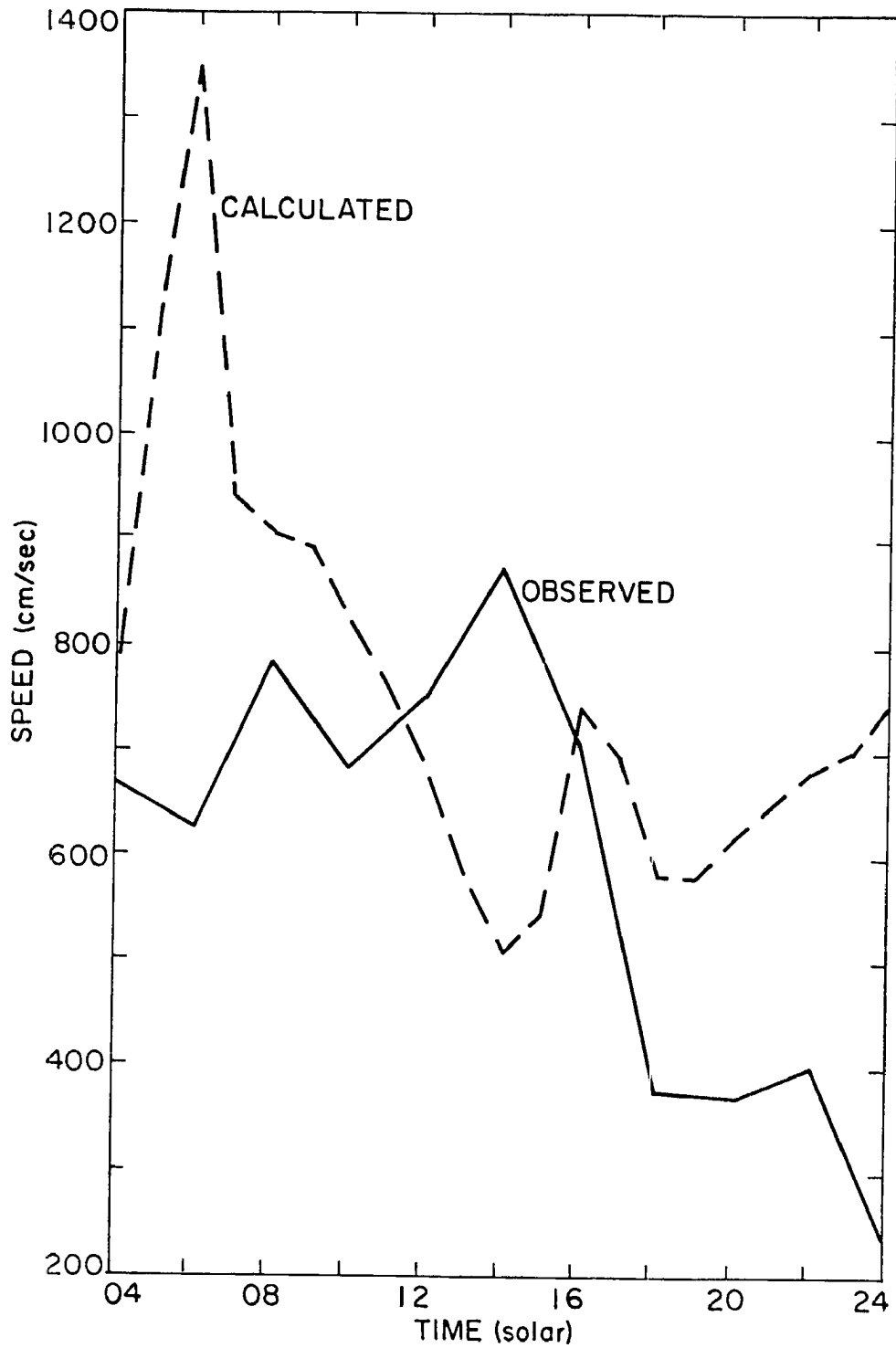


Figure 16a.) 4-meter wind speed-
O'Neill general observation period 2.

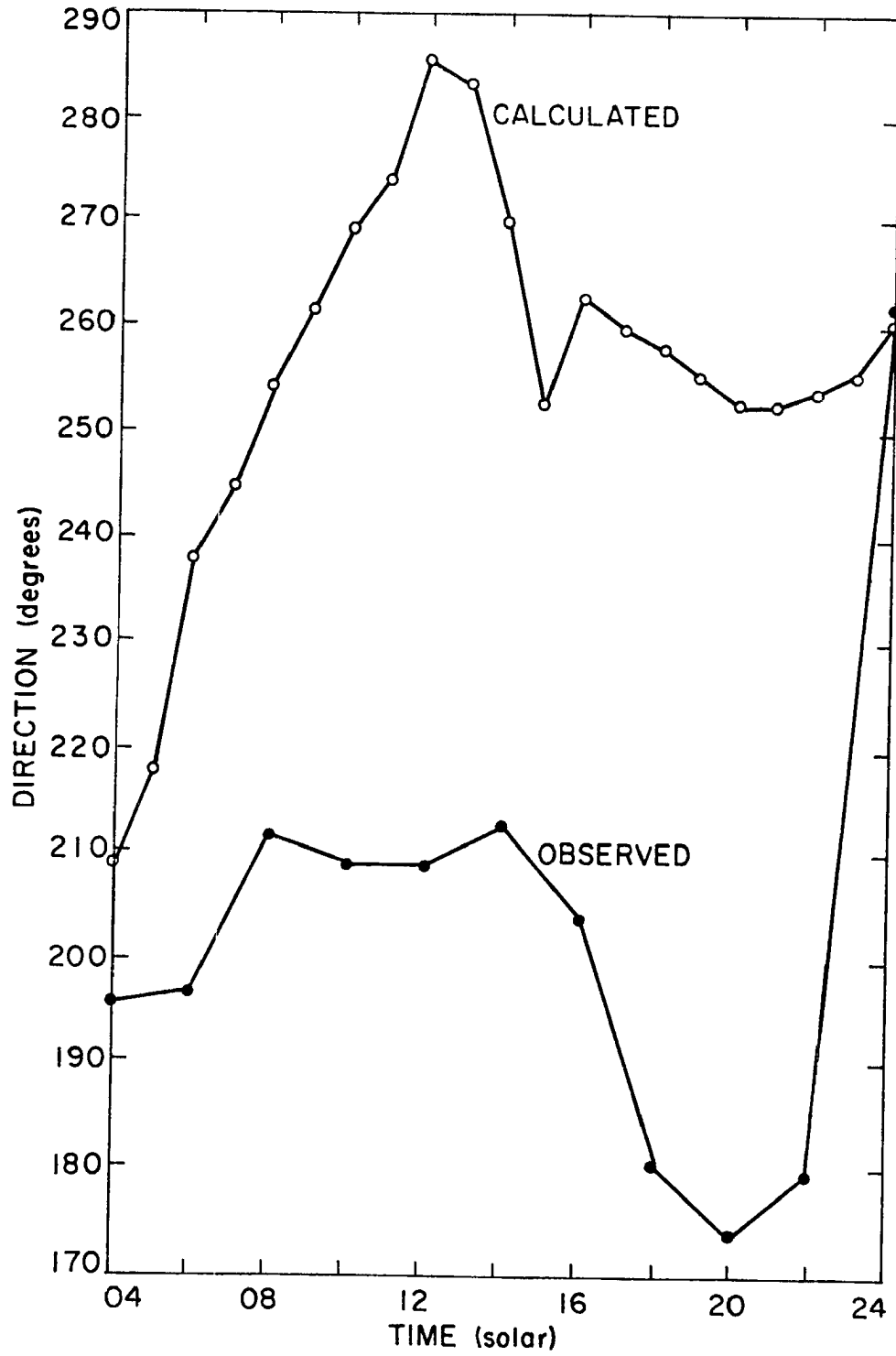


Figure 16b.) Surface layer wind direction-
O'Neill general observation period 2.

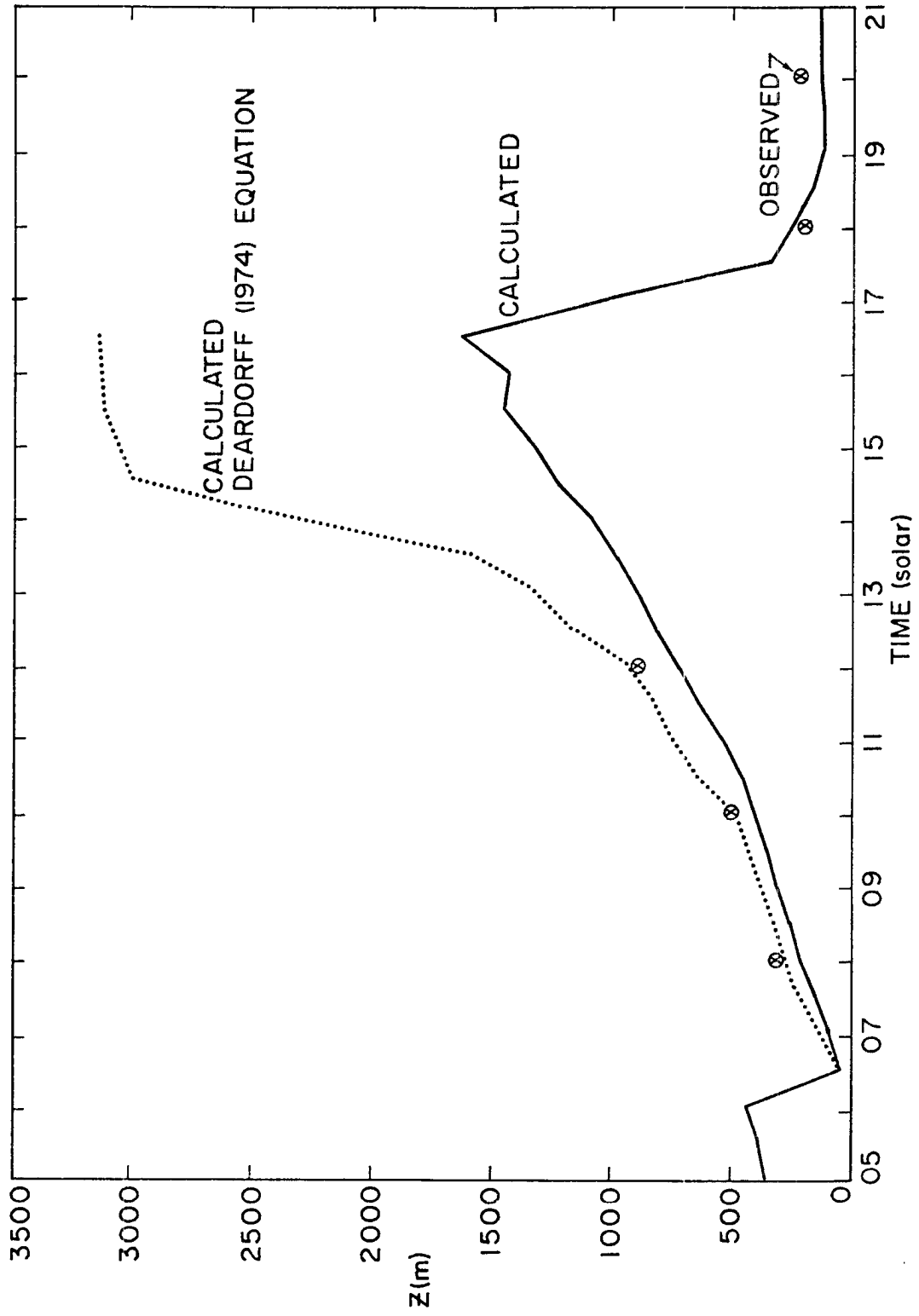


Figure 17.) Boundary layer height-O'Neill general observation period 2.

difficult to determine because of the presence of a deep nearly dry adiabatic layer above about 2 km. However, where the observations are available, the agreement is very good. The Deardorff equation, based on the quantities as modelled, predicts z_i well in the morning. The discrepancy between the two predicted curves increases in the afternoon because, as discussed earlier, the Deardorff equation tends to overpredict z_i when u_* is large.

3. O'Neill, Nebraska; Period 5

General observation period 5 has been used by a number of authors to verify their PBL models. Among these are Estoque (1963), Shaffer and Long (1975), and Sasamoni (1970). Some of Sasamoni's results are presented here for comparison. The weather during this 32 hour period from noon August 24, 1953 to 2000 the next evening, was clear, warm, windy and dry. The soil was very dry at the site, and very little evaporation was observed. However, preliminary tests showed that in order to produce the correct quantitative results, a strong cold advection and/or moisture advection must be accounted for. Examination of the synoptic maps show very little, if any, temperature advection, therefore a search was made for moisture sources upstream of the O'Neill site (i.e. to the SSW). Unfortunately it was found that the soil in the region was extremely dry as a result of an almost total lack of precipitation for several weeks. The area of dry soil extended through the entire central and eastern portions of the states of Nebraska and Kansas. However a broad area of irrigated cropland exists across south central Nebraska generally centered on the Platte River (Schickedanz, 1976). Within this region approximately 20% of

the land area was actually irrigated. The irrigated region extends southwestward into western Kansas and then southward along the high plains into Texas. The northernmost extent of the irrigated region reaches to within 100 to 150 km of the O'Neill site, so that on this day, when the moisture was being advected by strong $10-20 \text{ m sec}^{-1}$ low level winds, there is approximately a $2\frac{1}{2}$ hour fetch across dry soil before the air reaches the observation site.

As a result of this source of moisture upstream, the strict requirement of horizontal homogeneity necessary for a one-dimensional model is rather severely violated. When the model calculations are performed assuming a very dry soil, the surface energy budget is excellently simulated, but the PBL is "overheated" because of the lack of latent heat consumption. On the other hand, when the soil is assumed to be moist, the calculated evaporation is much greater than observed but the PBL temperature and moisture profiles are modelled very well. Therefore, the Figures below present the results of three model runs, one for the local dry soil ($W/W_s \approx 0.28$), one for moist soil ($W/W_s \approx 0.6$), and one in which patchy irrigation is simulated. This latter experiment assumes 20% of the land upstream is irrigated, as reported for the area in the 1950's by Schickedanz (1976). The value of W/W_s is set at 0.35 for four time steps and then at 1.0 for the fifth. This procedure continues until $2\frac{1}{2}$ hours before the time the model is intended to simulate. For the last $2\frac{1}{2}$ hours W/W_s is fixed at 0.287 to simulate the final fetch over unirrigated land. Three such experiments were run with target times of 1200, 1400, and 1600 solar time on the second day of general observation period 5.

Figures 18 present the calculated surface energy budget for dry soil, the three observed curves, and the results of the model of Sasamori. The calculated net radiative and ground heat fluxes fit the observations quite well, while the calculations of Sasamori are somewhat less accurate. The sensible heat flux is well simulated by both models (except, of course, in the moist soil case). There is considerable discrepancy between the three observed latent heat flux curves and all values are rather small. The calculated values for the present model overestimated the evaporation on the first day when an attempt was made to strike a compromise between the dry soil and the moisture advection. However on the second day the dry soil case predicts the evaporation rate quite reasonably while the moist soil case grossly overestimates the local evaporation. The evaporation rate for the irrigation upstream case is not shown because of its erratic nature. As could be expected most of the evaporation occurs during the one time step in five during which $W/W_s = 1.0$. While the air is over these "irrigated patches" the evaporation rate far exceeds the potential evaporation rate for saturated soil. This is because the boundary layer is warmed and dried while passing over the dry "patches", and when the air reaches the saturated soil a tremendous moisture gradient develops. It is interesting to note that the temporally averaged evaporation rate over the irrigated land is about 20% greater than that for the moist soil case even though the soil moisture averages 15% less in the irrigation case (See table 4). Sasamori's evaporation parameterization, which is based on the bare soil model of Phillip (1957), breaks down once the moisture is removed from a thin layer of soil near the surface.

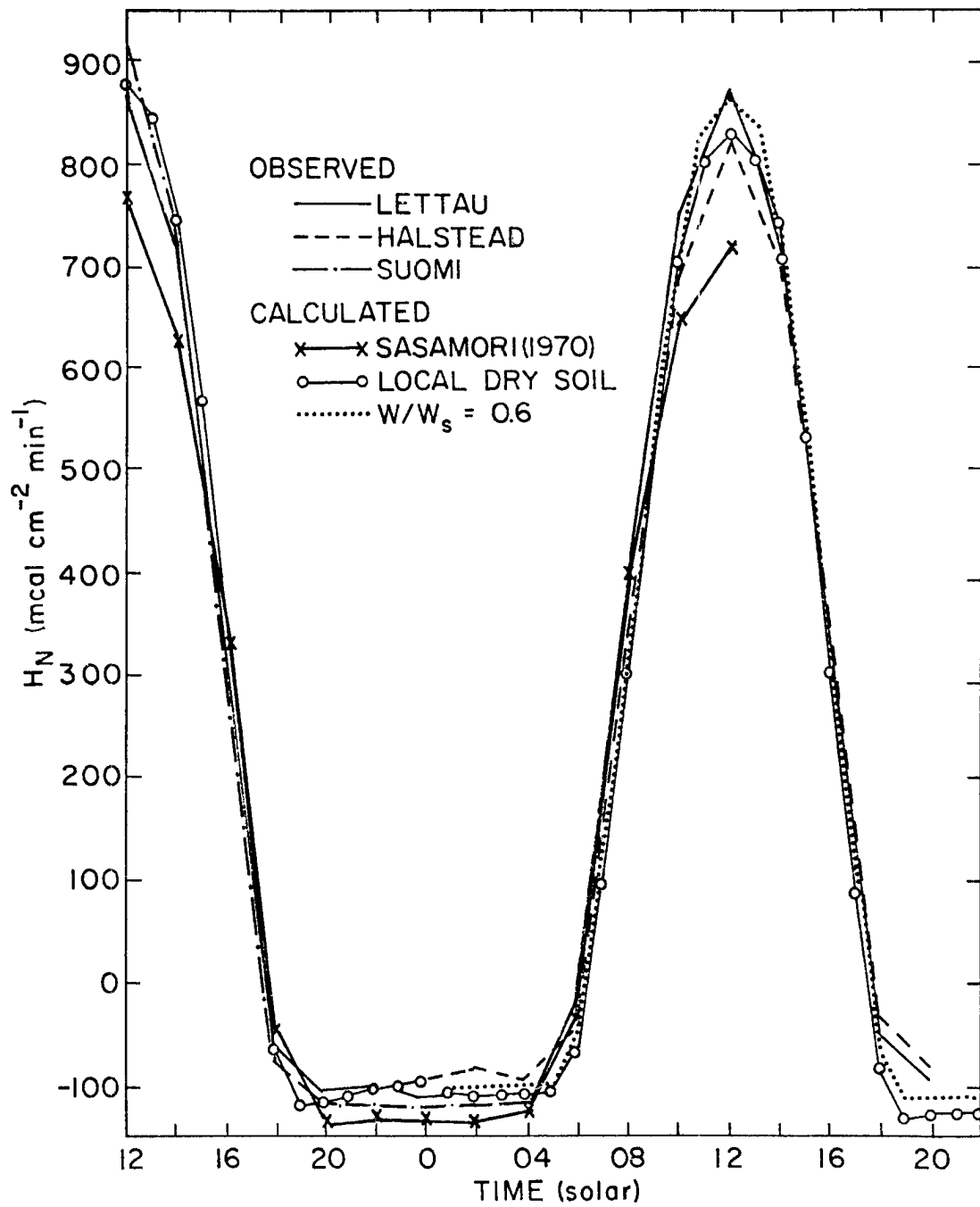


Figure 18a.) Net radiation-
O'Neill general observation period 5,

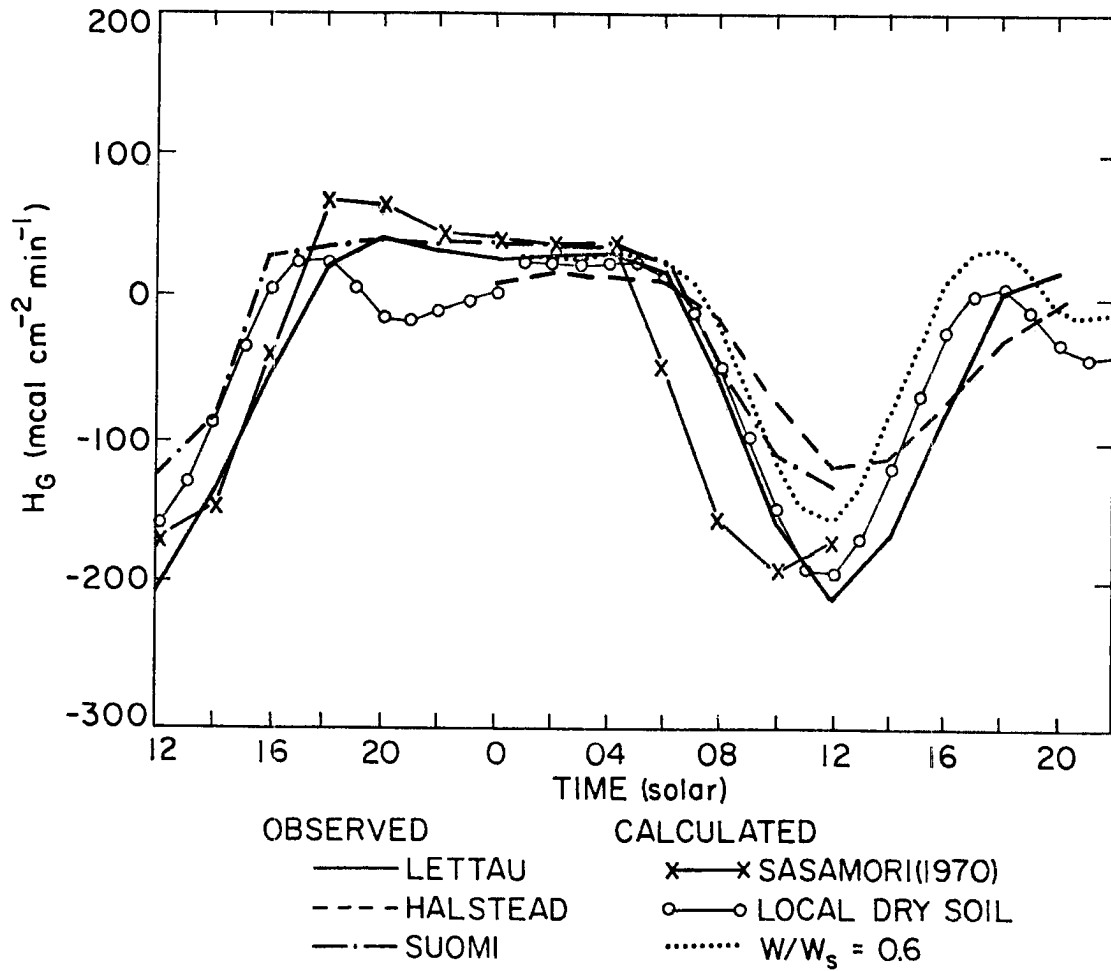


Figure 18b.) Soil heat flux-
O'Neill general observation period 5.

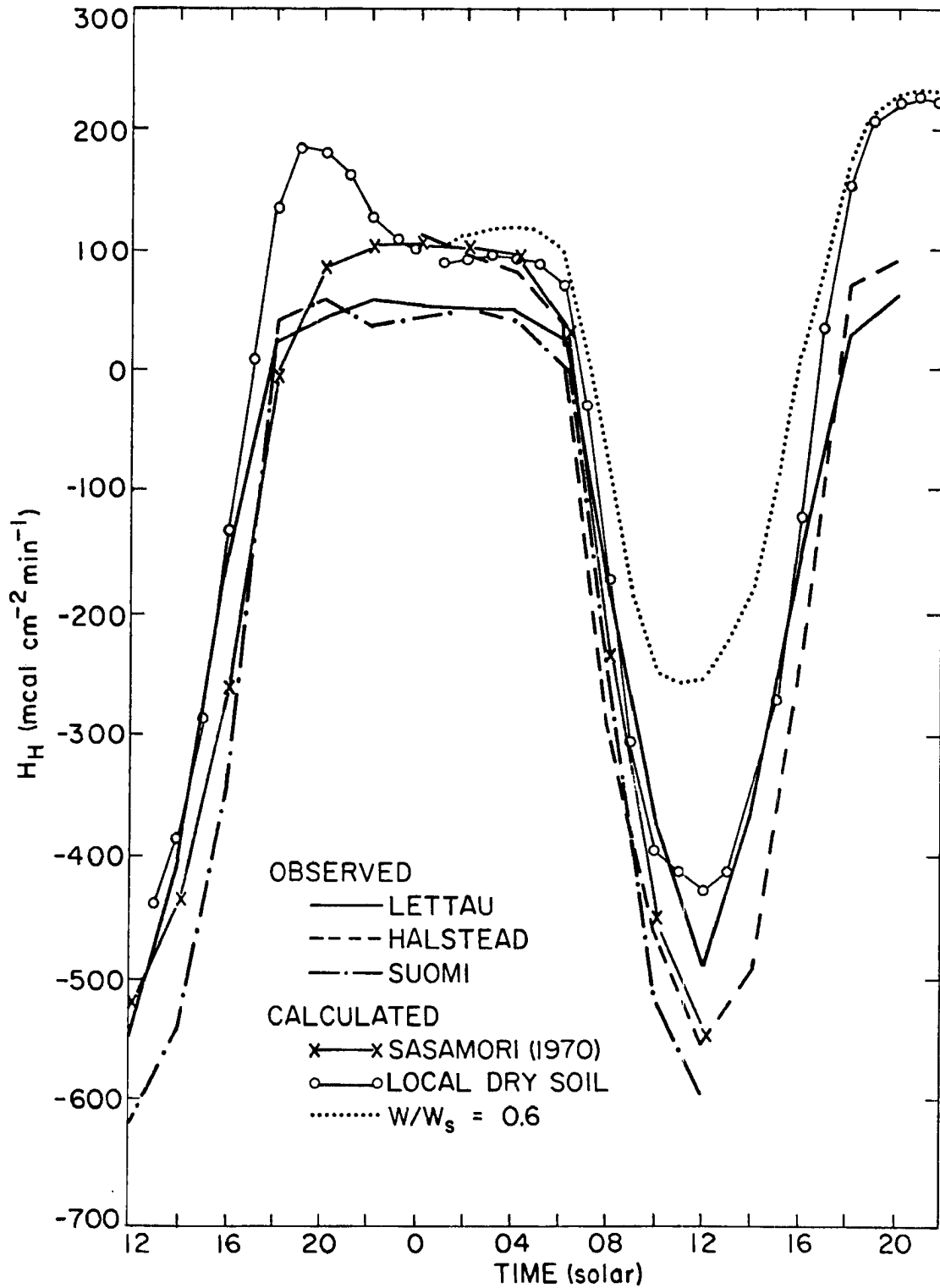


Figure 18c.) Surface sensible heat flux-
O'Neill general observation period 5.

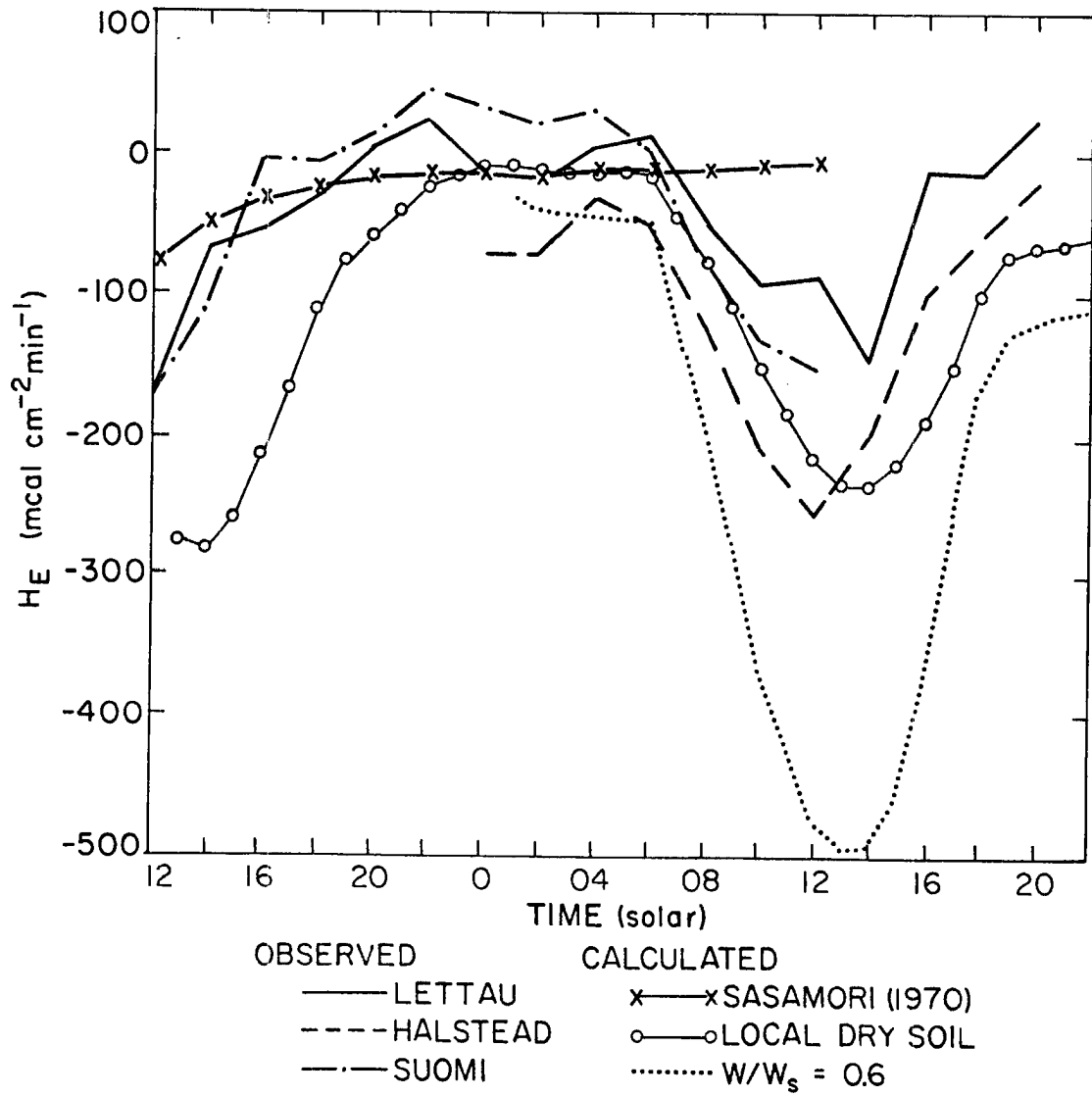


Figure 18d.) Surface latent heat flux-
O'Neill general observation period 5.

Table 4. Temporally averaged soil moisture and evaporation rate for the period 1030-1130 on the second day of general observation period 5.

Experiment	Average W/W_s	Average H_E ($\text{mcal cm}^{-2} \text{min}^{-1}$)
Dry Soil	0.281	187.0
Moist Soil	0.585	423.4
Irrigation upstream	0.500	506.4

The potential temperature profiles for each of the three cases are compared to the observations in Figures 19. Note that the model was re-initialized at midnight after the first day in order to fit the pre-dawn profiles for the second day. This was necessary because some turbulent or advective mechanism, probably the very strong nocturnal low level jet, wiped out the inertial dry adiabatic layer overnight. During the second day the moist soil and irrigation models simulate the observed potential temperature profiles quite well while the dry soil profiles become much too warm. Note that the irrigation case keeps the boundary layer cooler just as well as the moist soil case does, even though the former has a $2\frac{1}{2}$ hour fetch over dry soil before reaching the target time. At night, when the evaporation is nearly nil, there is little difference between the dry and moist soil calculations. Both models cool the low level air too little, possibly as a result of a failure to correctly model the strong low level jet or as a result of the other factors discussed previously.

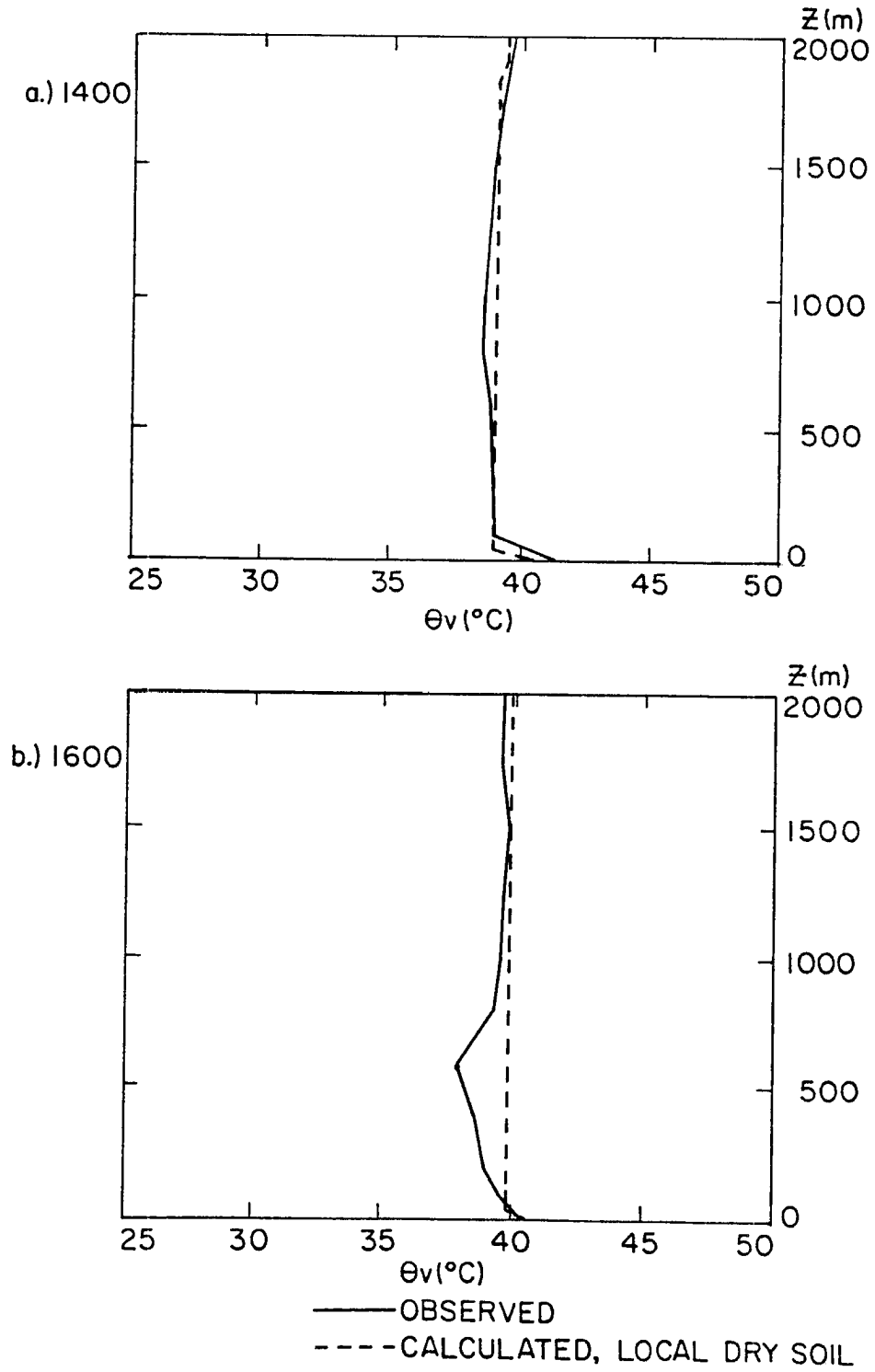


Figure 19.) Virtual potential temperature profiles-
O'Neill general observation period 5.

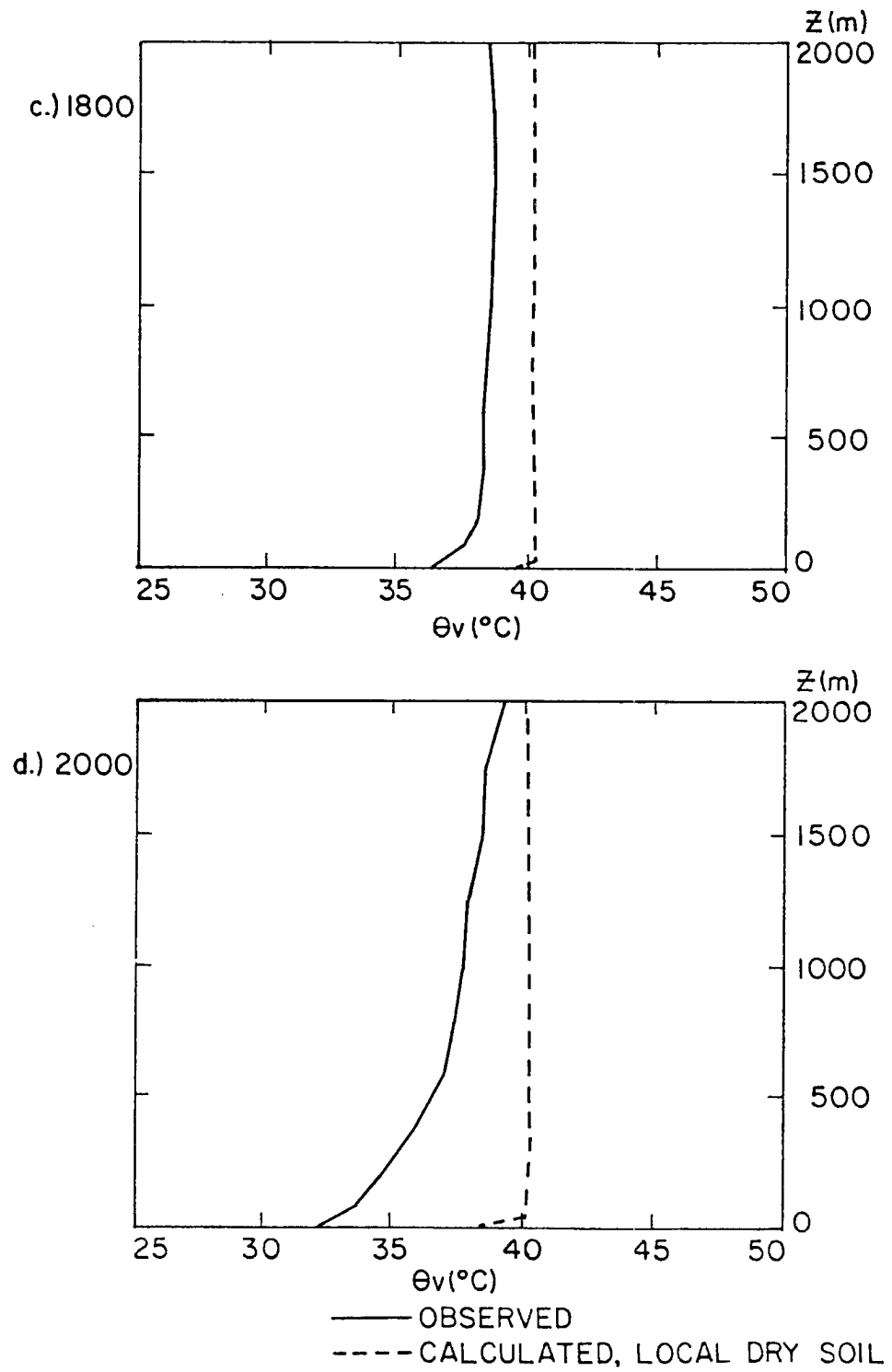


Figure 19.) (Continued)

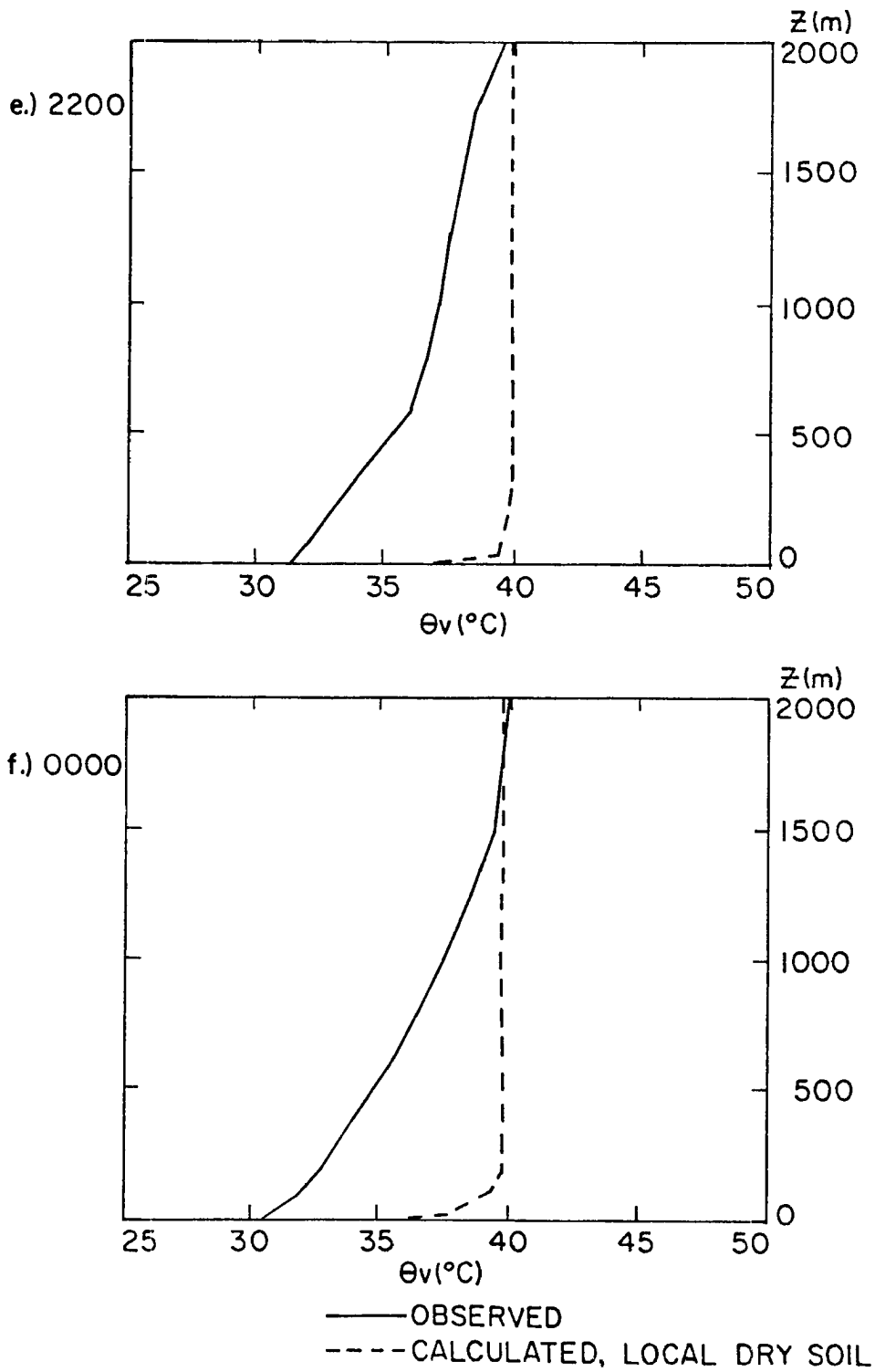


Figure 19.) (Continued)

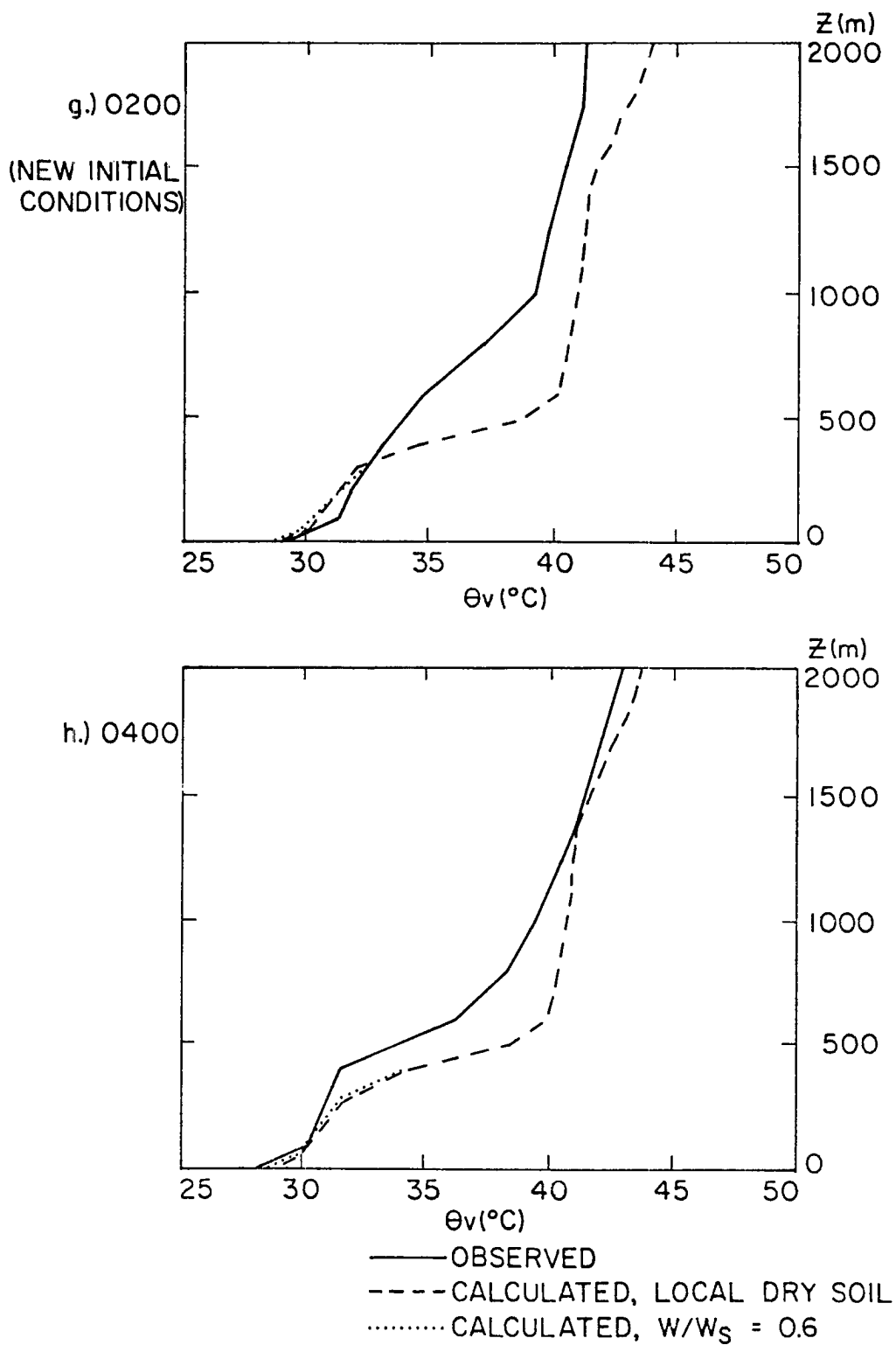


Figure 19.) (Continued)

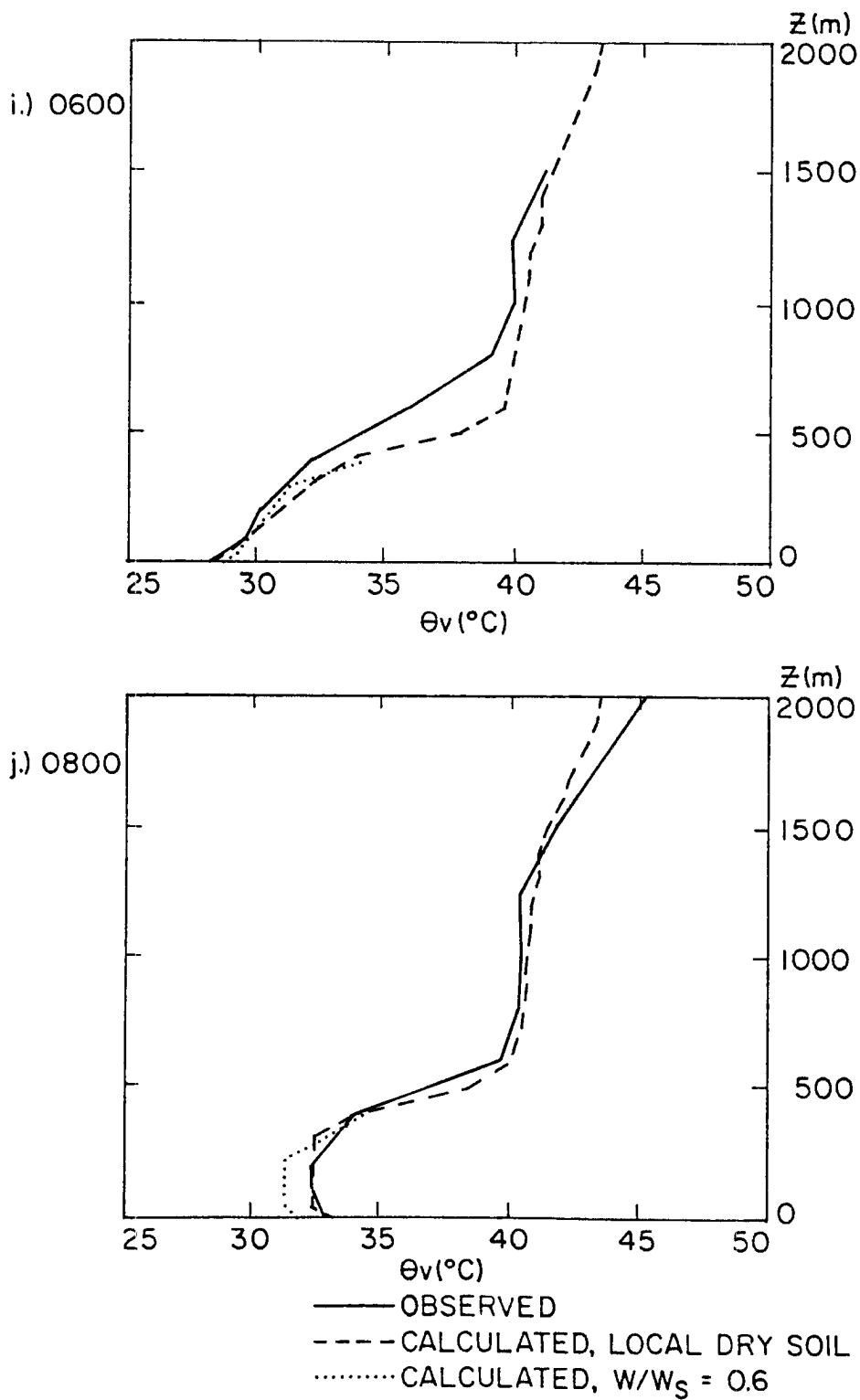
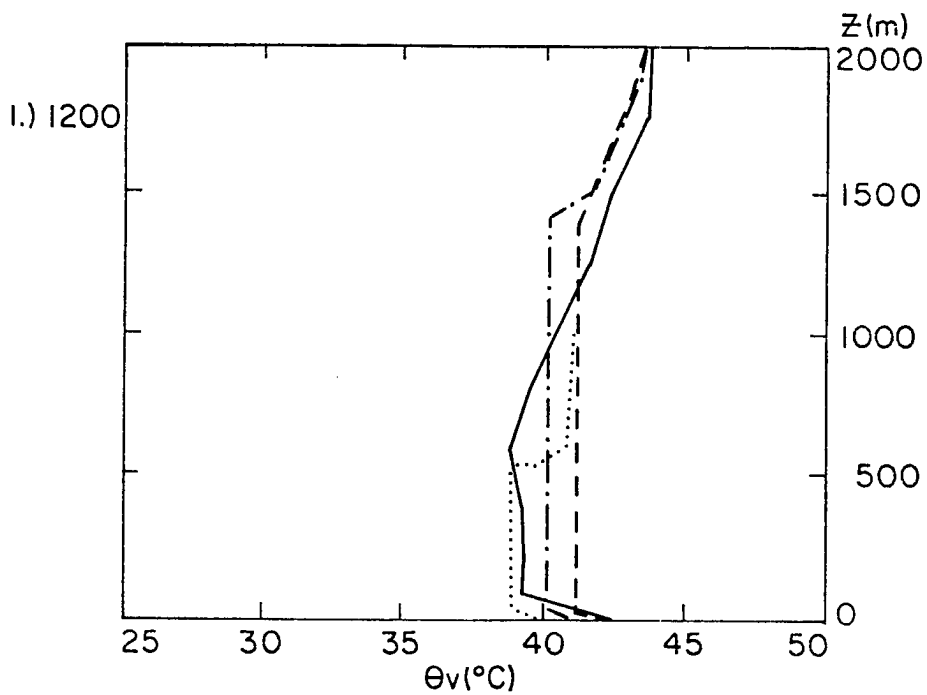
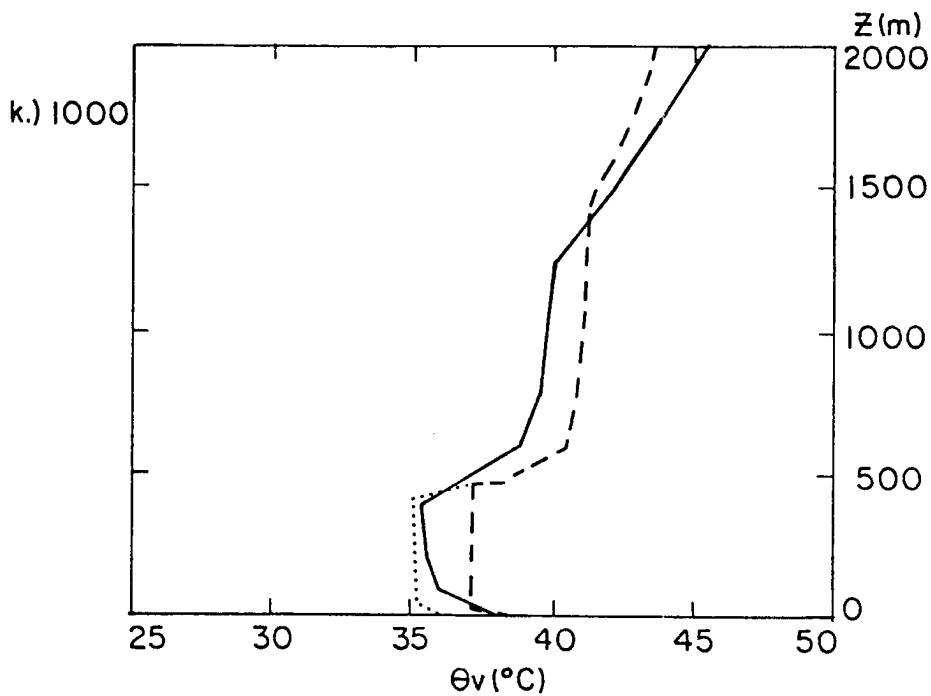
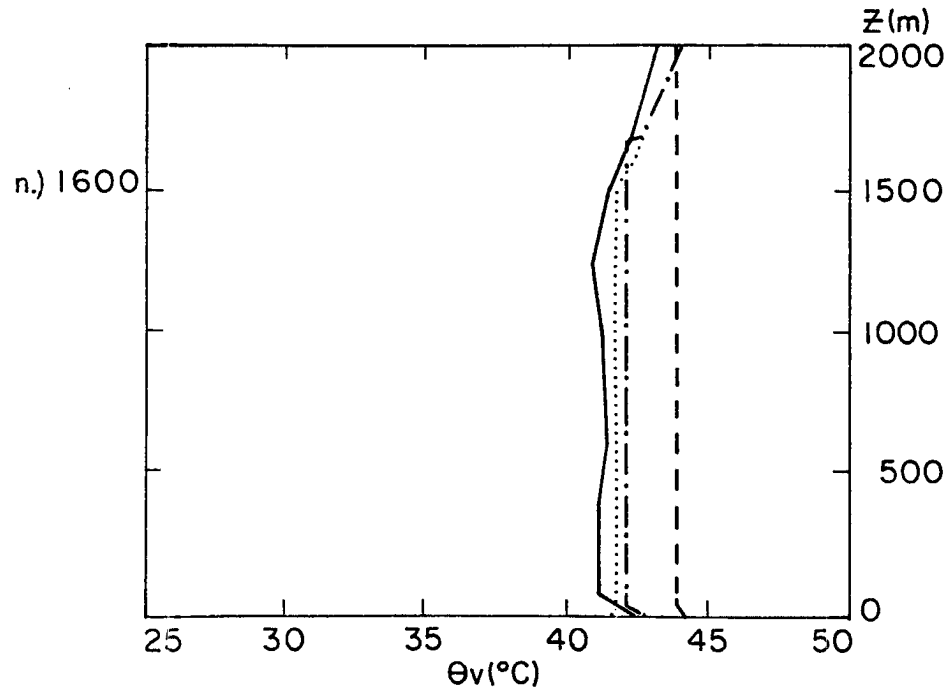
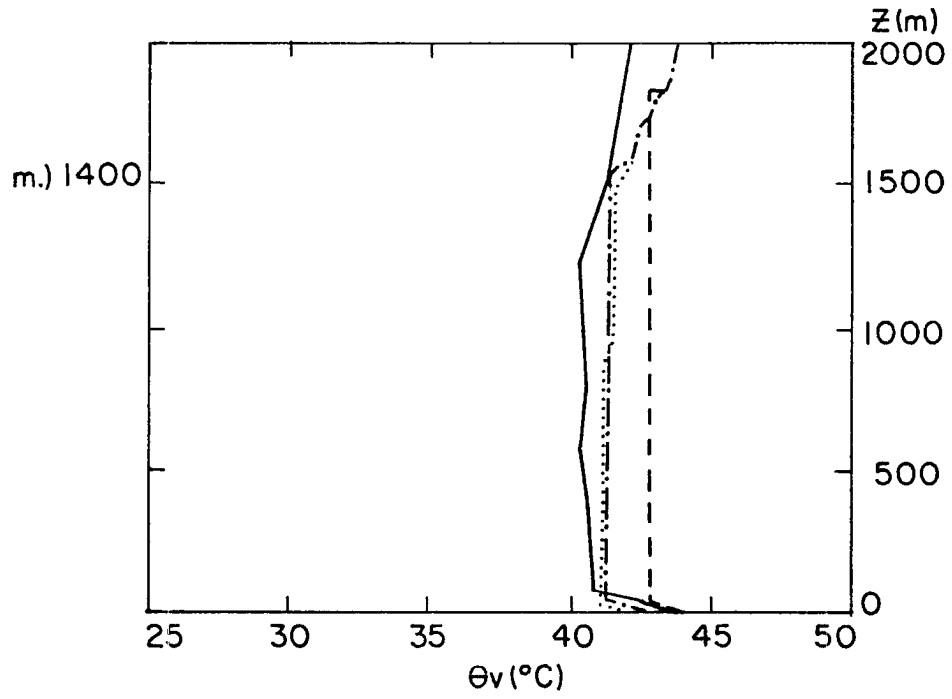


Figure 19.) (Continued)



- OBSERVED
- - - CALCULATED, LOCAL DRY SOIL
- CALCULATED, $W/W_s = 0.6$
- · - · - CALCULATED, IRRIGATION UPSTREAM

Figure 19.) (Continued)



- OBSERVED
- CALCULATED, LOCAL DRY SOIL
- CALCULATED, $w/w_s = 0.6$
- .-.- CALCULATED, IRRIGATION UPSTREAM

Figure 19.) (Continued)

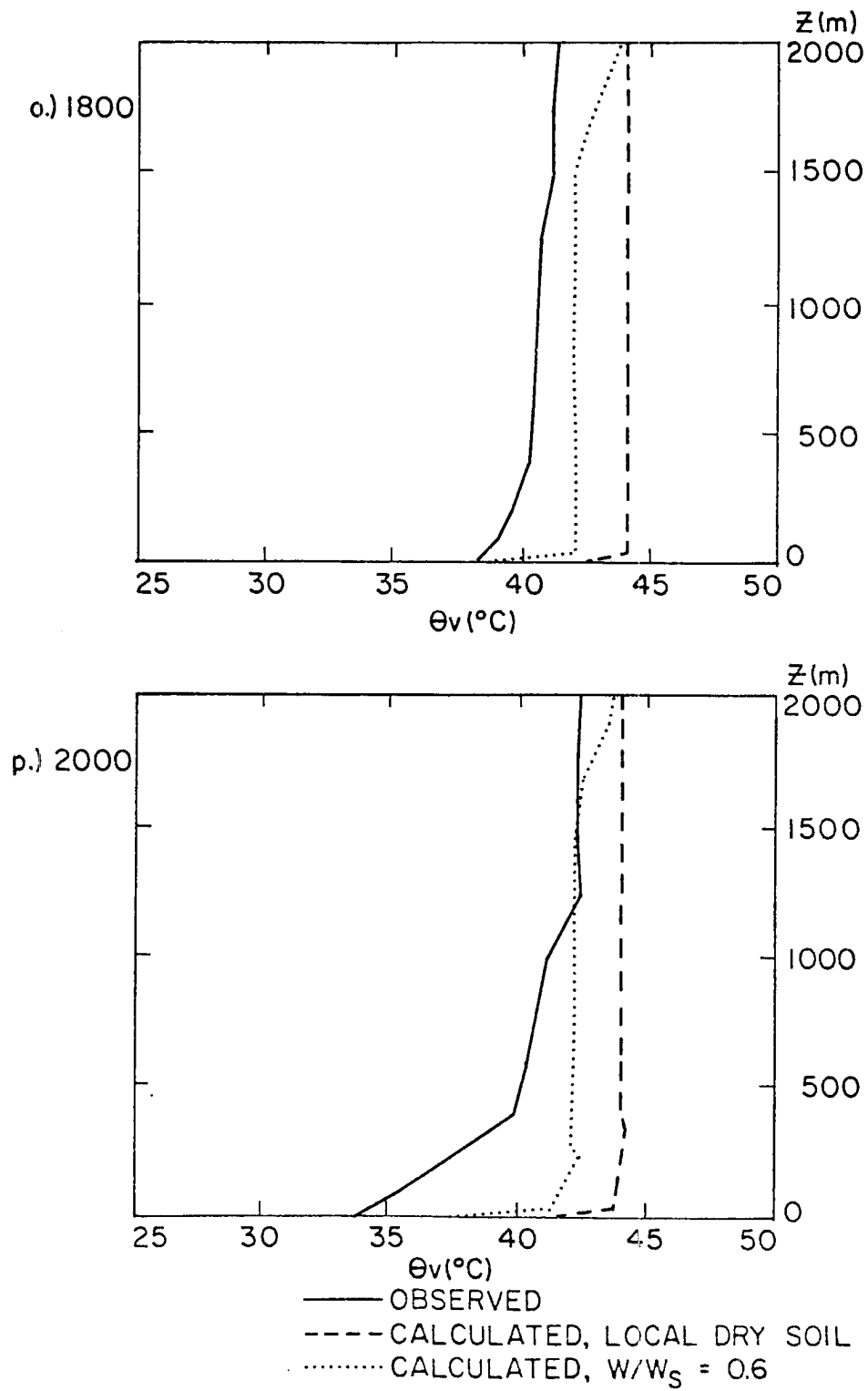


Figure 19.) (Continued)

Figures 20 show the observed near-surface temperatures and the calculated temperatures for dry soil. On the first day the attempted soil moisture compromise seems relatively inadequate. On the second day, in the daylight hours, the calculated surface temperature very closely fits the observed soil temperature at 0.5 cm. depth, but the 4 meter calculated temperature is correctly modelled by the moist soil case. This appears to indicate that the effects of the observed cool moist advection are felt very close to the surface during periods of strong mixing.

Figures 21 depict the 4 meter wind speed and direction as calculated and as observed. The agreement is fair at best, with the calculated wind directions again too westerly. There is little difference between the dry and moist soil cases.

The moisture profiles for the dry, moist, and irrigated calculations are compared with the observations in Figures 22. The agreement is best between the irrigated soil case and the observed profiles. These figures are rather strong evidence for the hypothesis that the air over the site had indeed advected from the region of irrigation to the south.

Finally Figure 23 presents the z_i calculations for dry and moist soil. The important features to note here are the good agreement between the moist soil z_i and the observations on the second day, and the rather large daytime differences between the dry and moist soil calculations. The Deardorff equation appears to overpredict z_i on this day.

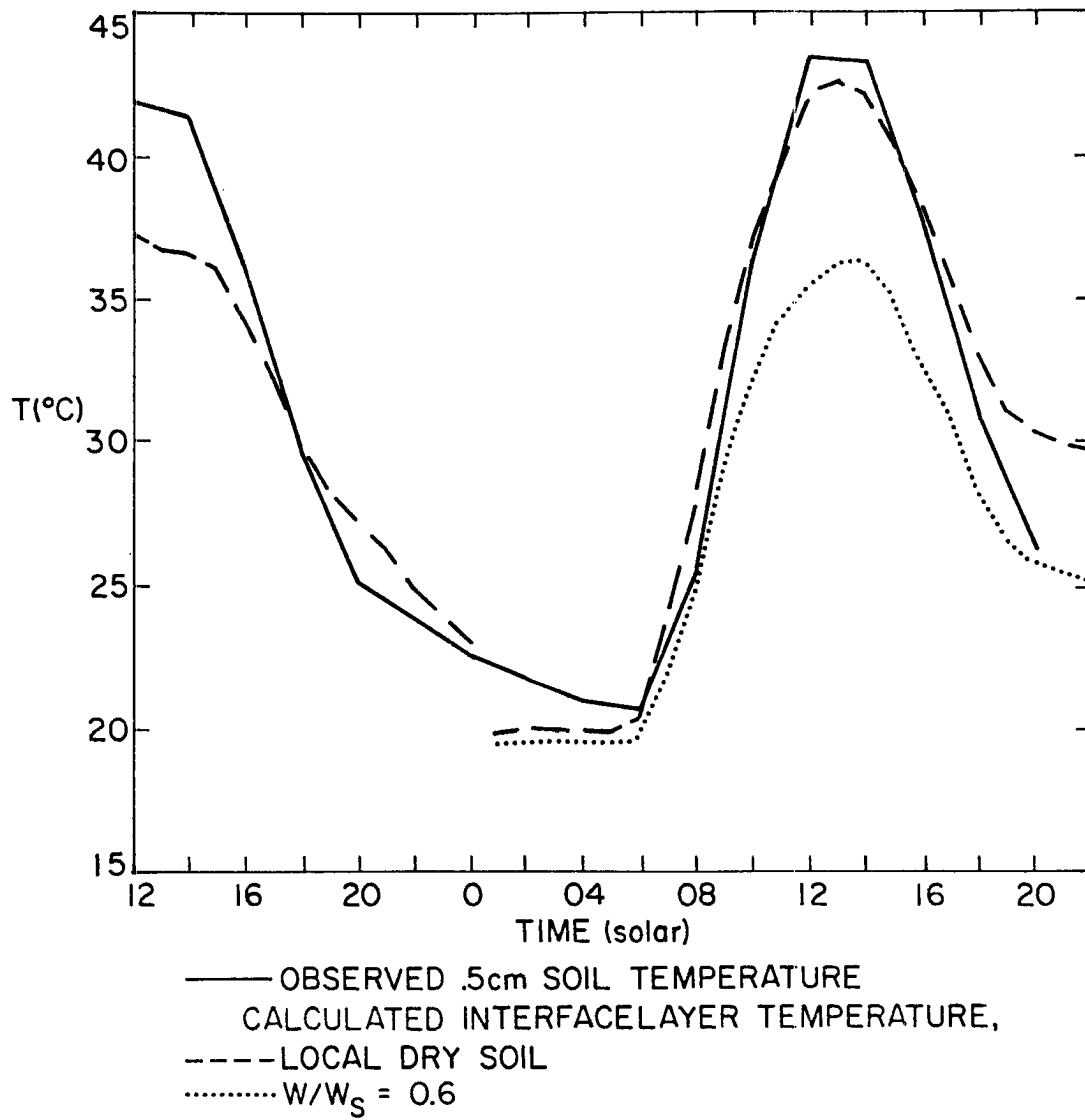


Figure 20a.) Surface temperature-
O'Neill general observation period 5.

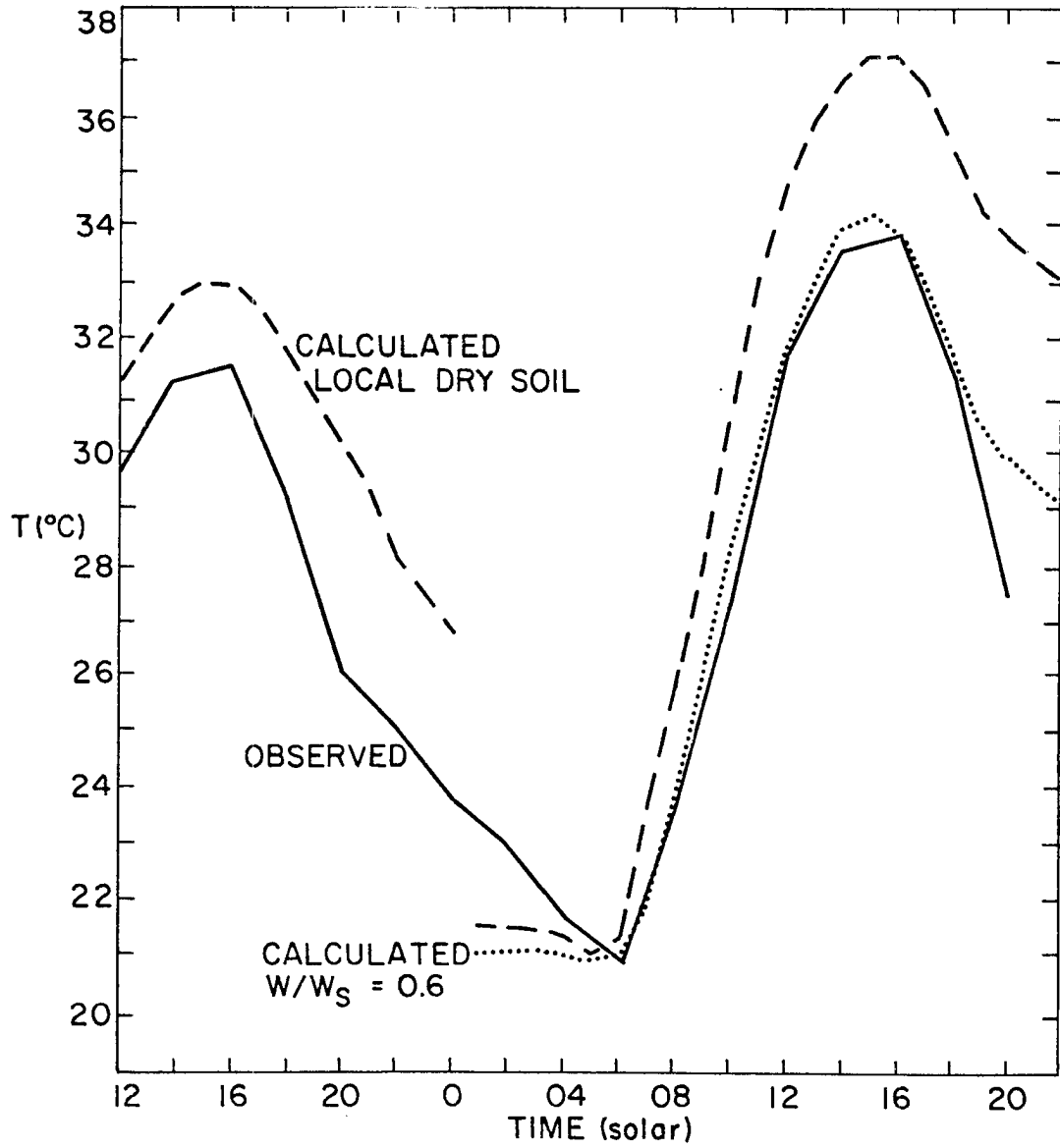


Figure 20b.) 4-meter temperature-
O'Neill general observation period 5.

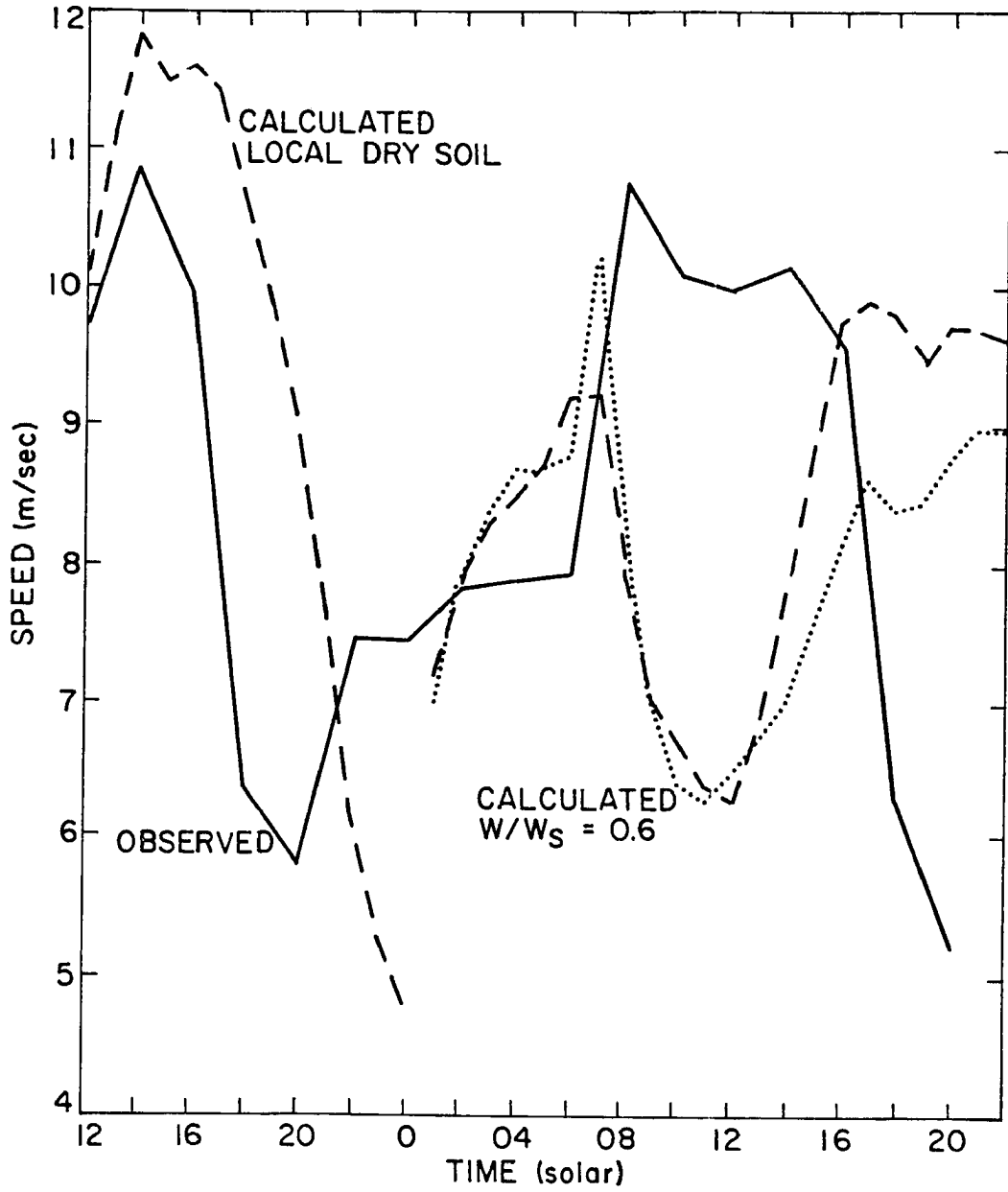


Figure 21a.) 4-meter wind speed-
O'Neill general observation period 5.

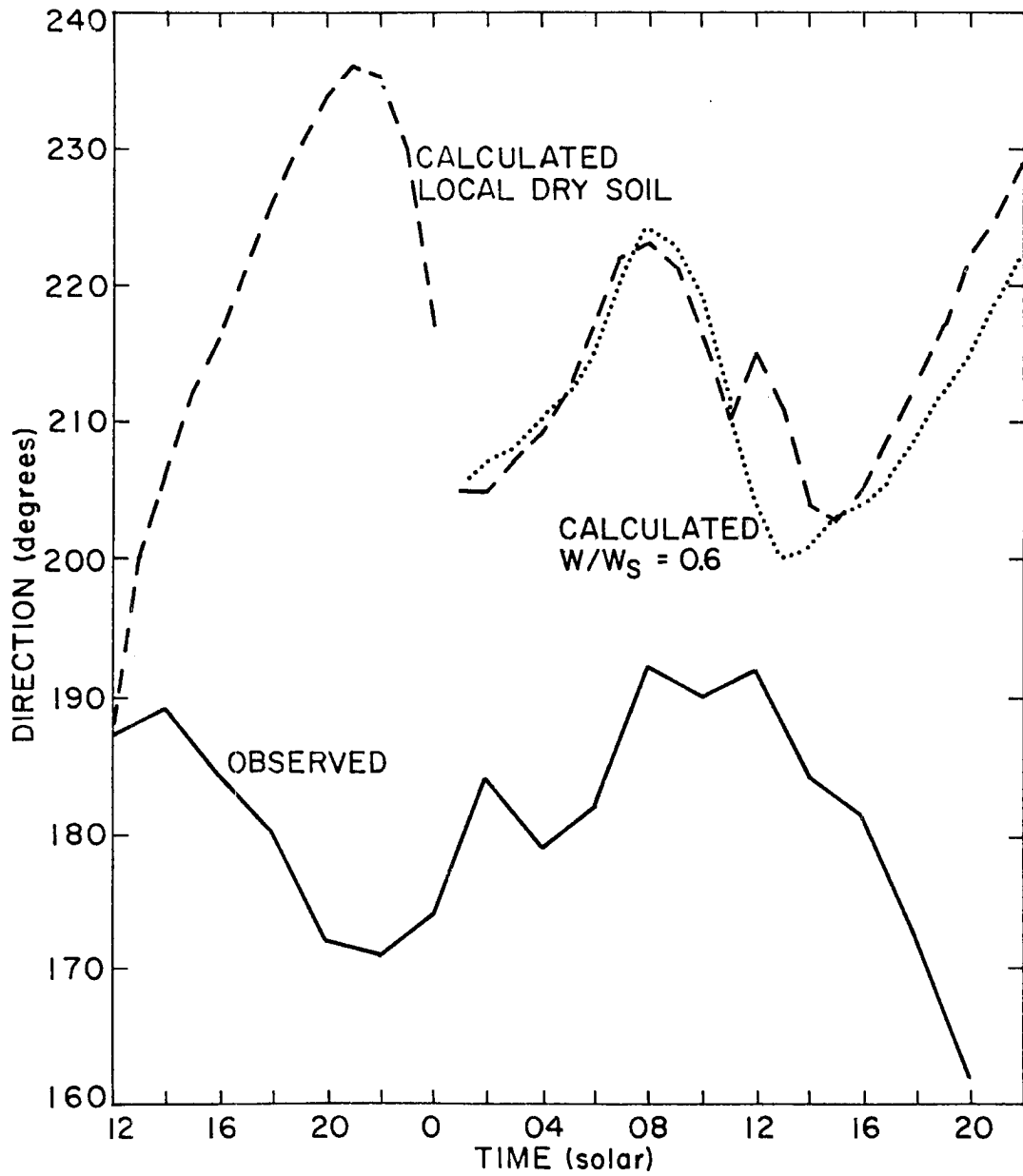


Figure 21b.) Surface layer wind direction-
O'Neill general observation period 5.

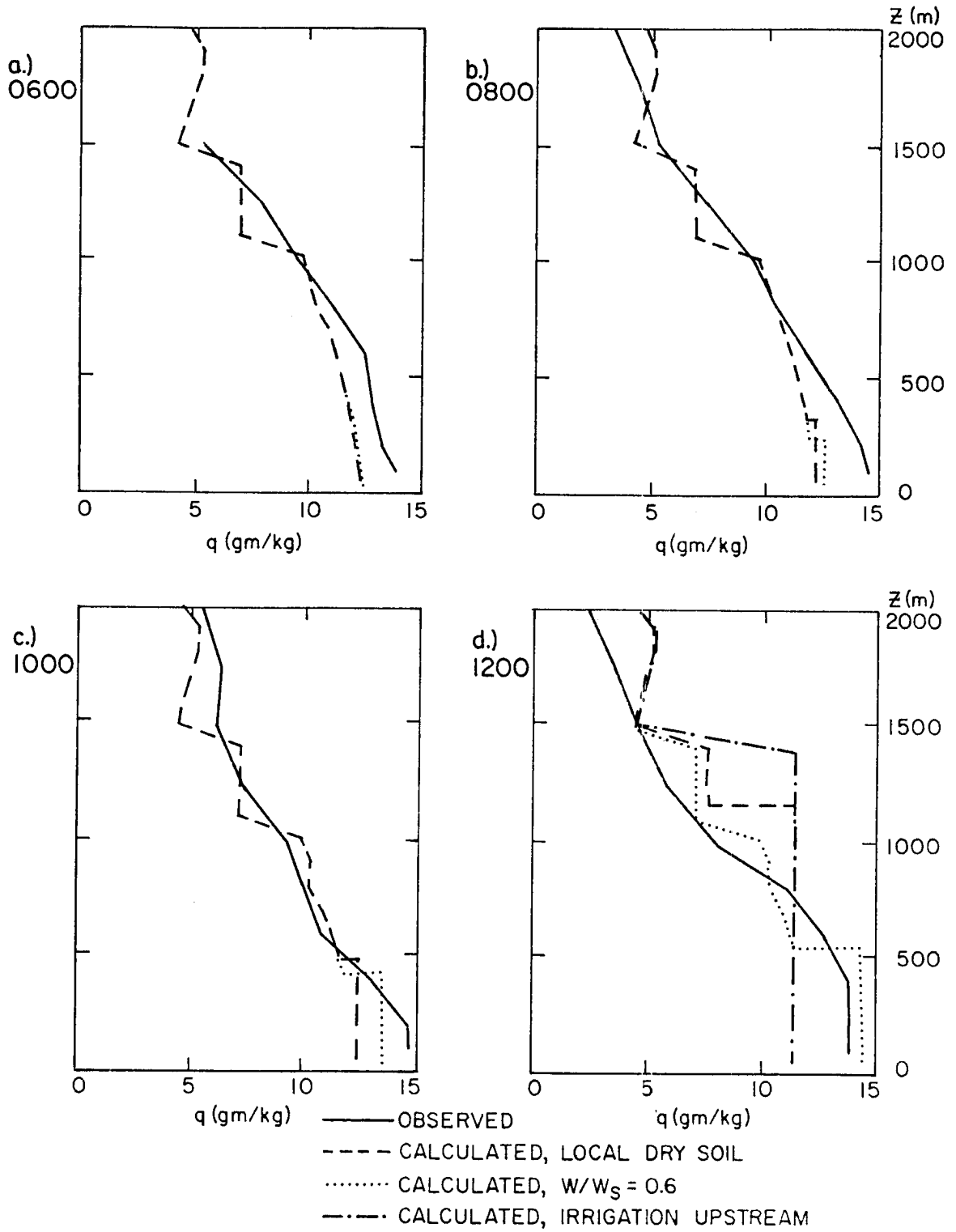


Figure 22.) Moisture profiles-
O'Neill general observation period 5 (second day).

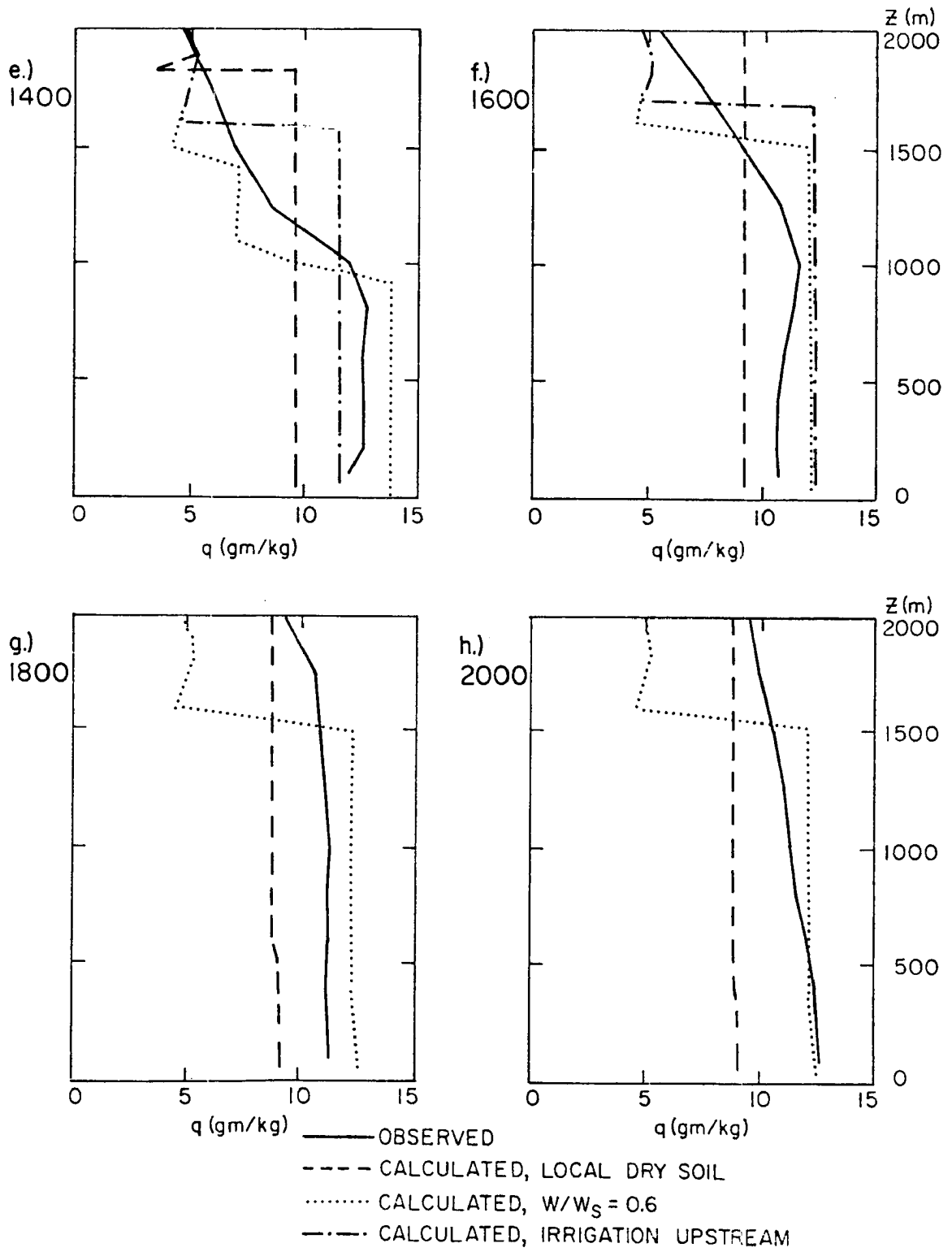


Figure 22.) (Continued)

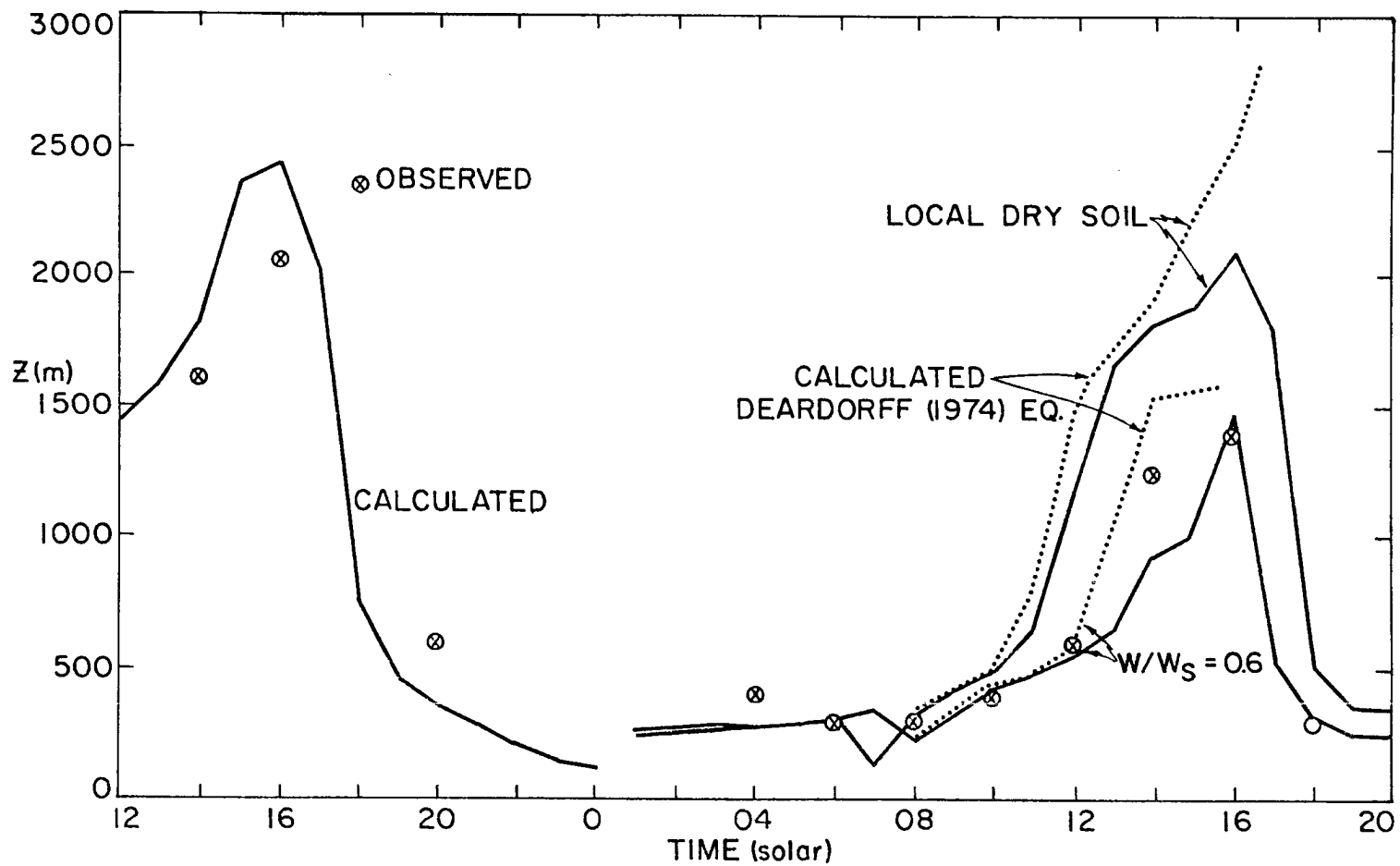


Figure 23.) Boundary layer height-
O'Neill general observation period 5.

4. Wangara, Day 16.

Day 16 of the Wangara experiment was chosen because it was a day in which a strato-cumulus topped PBL developed after a morning of solar heating. Low level advection appears to be minimal on this day and the geostrophic wind components varied in a nearly linear fashion with time from southwesterly at midnight when the model was initialized, through west to northwesterly by late in the evening. Figure 24 displays the energy budget and compares the cloud cover as observed with that modelled by eq. (59). The energy budget components are modelled quite well including the effect of the cloud cover. After sunset the soil heat release is somewhat overestimated, as is the net radiation loss. The latter may be explained by the lack of cloud cover in the model after sunset. When z_i falls as the surface heating stops, the crude cloud parameterization assumes that the cloud instantly dissipates because its base is now above the nocturnal z_i . The cloud cover prediction is quite good for such a simple parameterization. The model cloud forms when the observed sky is about 75% cloudy and dissipates at the time that the observed cloud cover decreases to about 2/3 of the full sky. It should be noted that because the effects of latent heat are neglected in the cloud parameterization, the model results after the onset of cloud cover should not be considered to be of the same quality as those under clear sky. The primary intent of this experiment is to show that the model can predict the onset of clouds in the PBL, and that it can handle the abrupt changes in the energy balance that occur when the cloud forms.

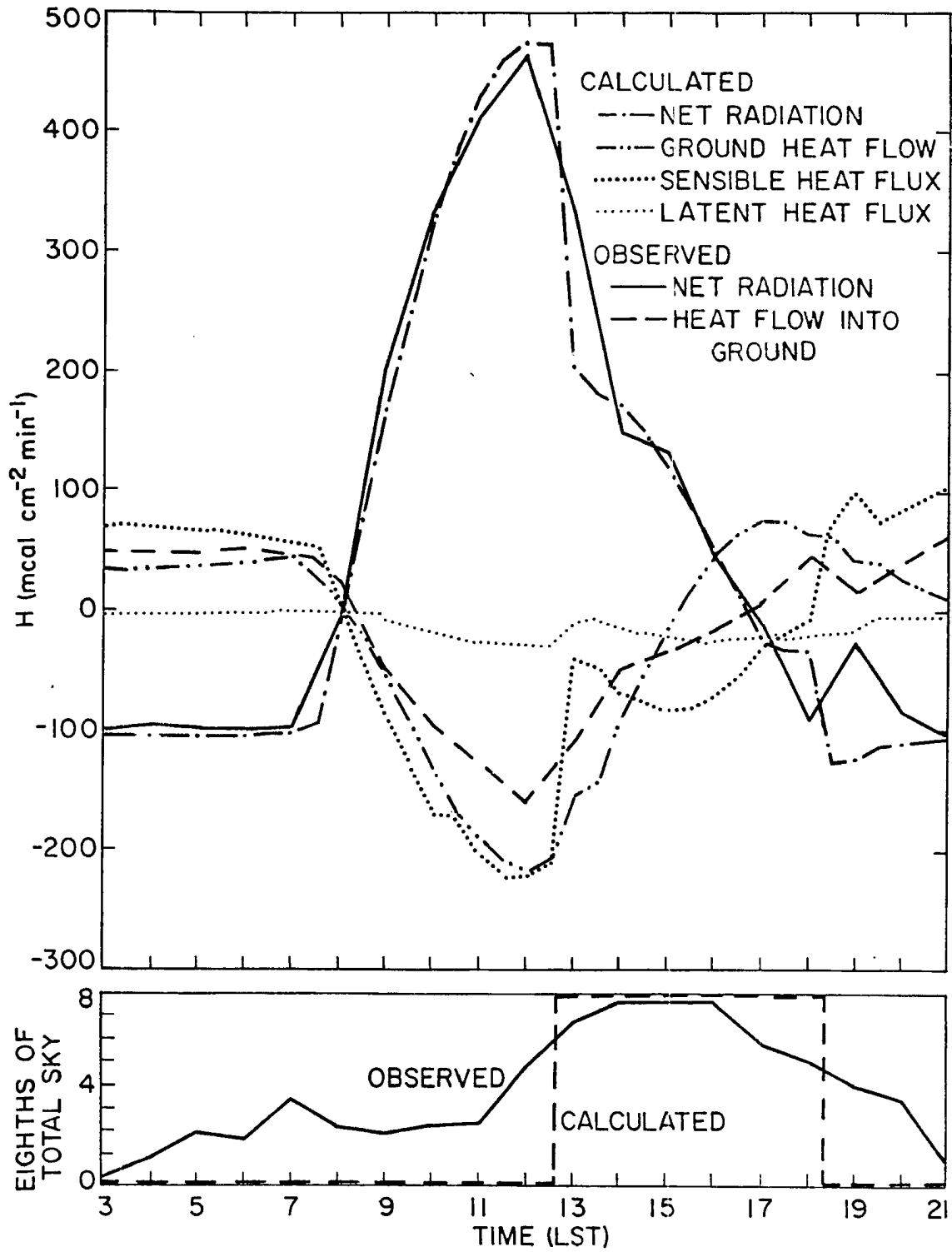


Figure 24.) Surface energy budget and cloud cover—Wangara 16.

Figures 25 compare the potential temperature profiles, which agree very well in the PBL. Above 1 km. some advective effect apparently occurred which brought a warm layer over the area. This layer apparently moved in around 0300 in the morning (after the model is initialized) and remained until sometime immediately after noon. The near surface temperatures are shown in Figure 26. The agreement is very good except for early morning temperatures about 1°C too warm.

Finally, the height of the boundary layer is quite well modelled, as shown in Figure 27, however the calculated cloud base is a bit too high. This is probably due to the requirement that the horizontally averaged relative humidity be 90% at cloud base.

B. Further considerations and experiments on model sensitivity.

As we have seen from the cases presented above, the entire PBL responds measurably to changes of surface conditions. For example the soil moisture amount and distribution are seen to have a remarkable influence on the thermal structure of the PBL in the O'Neill period 5 experiments. The PBL wind structure seems to be heavily influenced by non-homogeneous and advective effects. This section examines some other influences on the boundary layer and explores their ramifications with regard to modelling of the PBL.

1. The wind structure.

A number of considerations endemic to the nature of air motion conspire to make the modelling of low level winds difficult, and to make comparison with observational data nearly impossible. First, the frictional influence of the earth's surface is one or two orders of

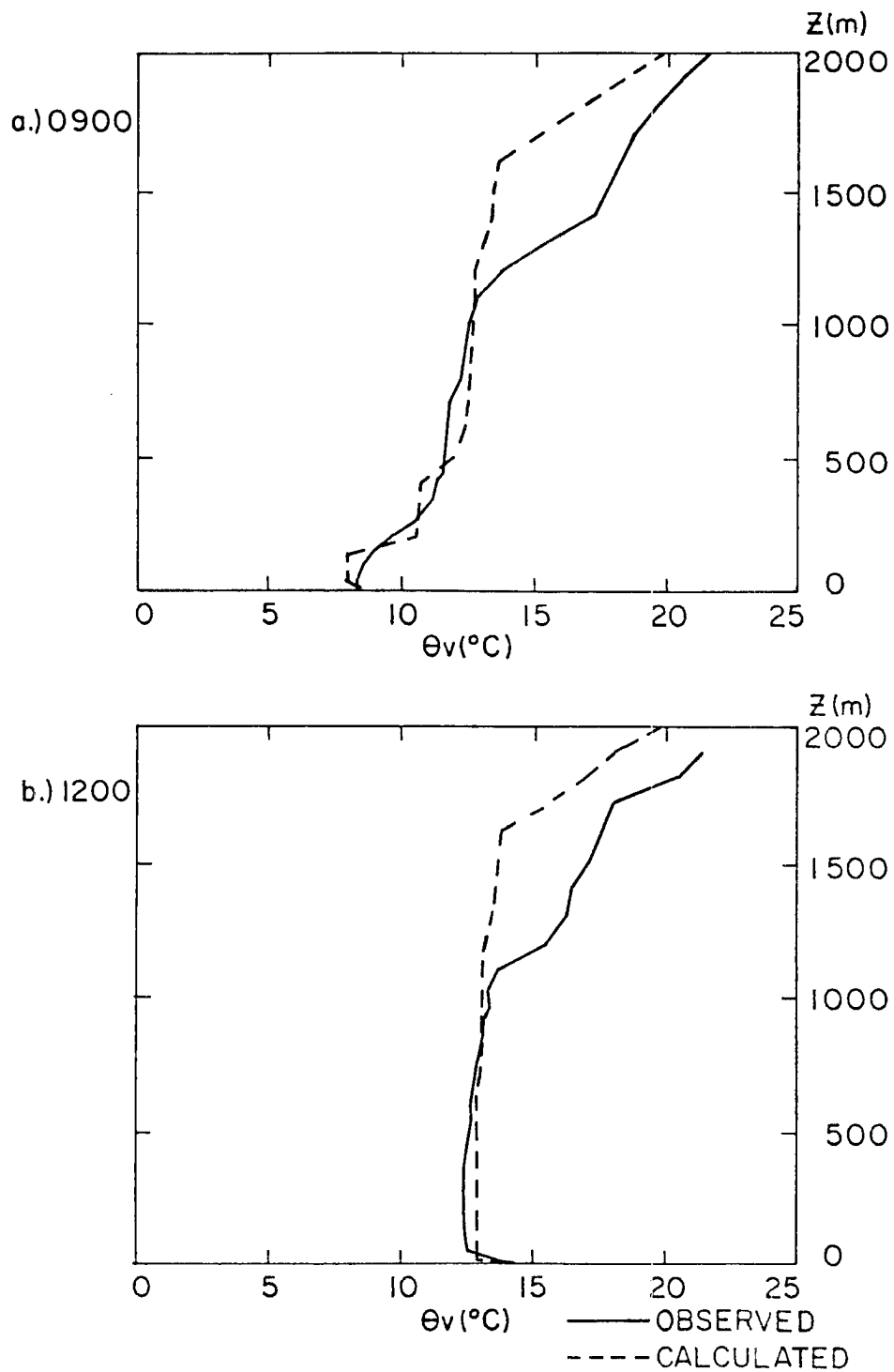


Figure 25.) Virtual potential temperature profiles-
Wangara 16.

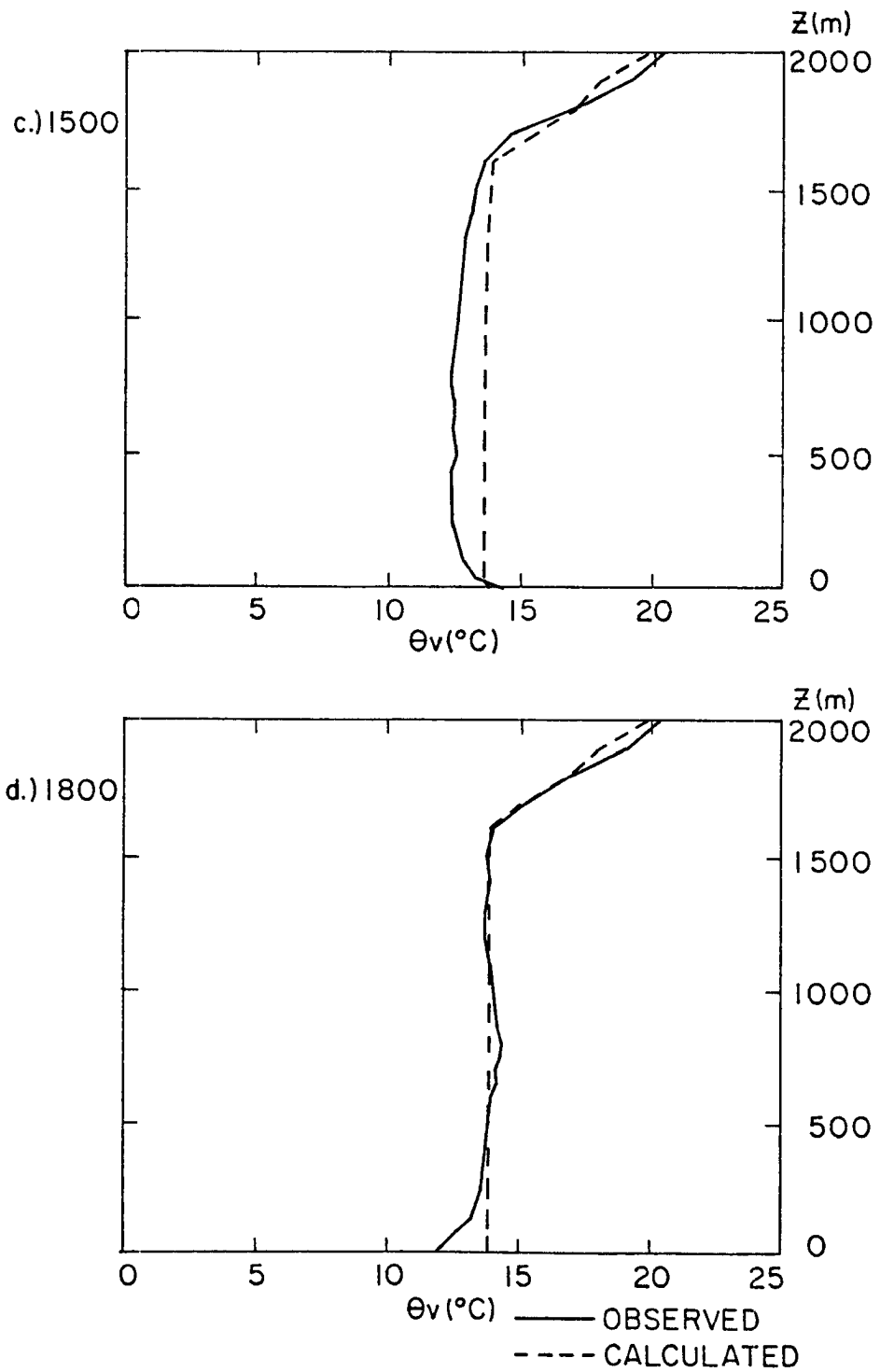


Figure 25.) (Continued)

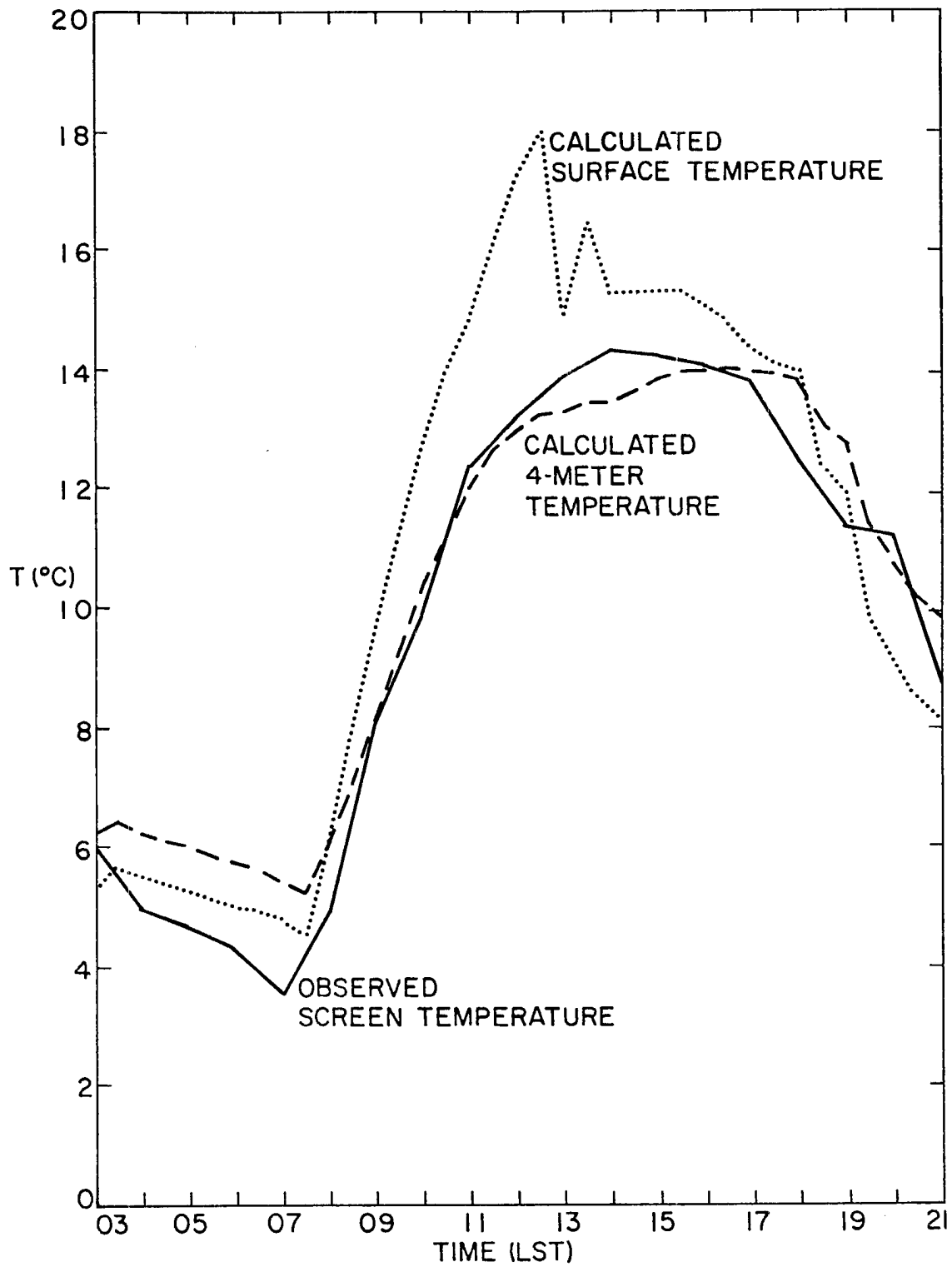


Figure 26.) Ground level temperature-
Wangara 16.

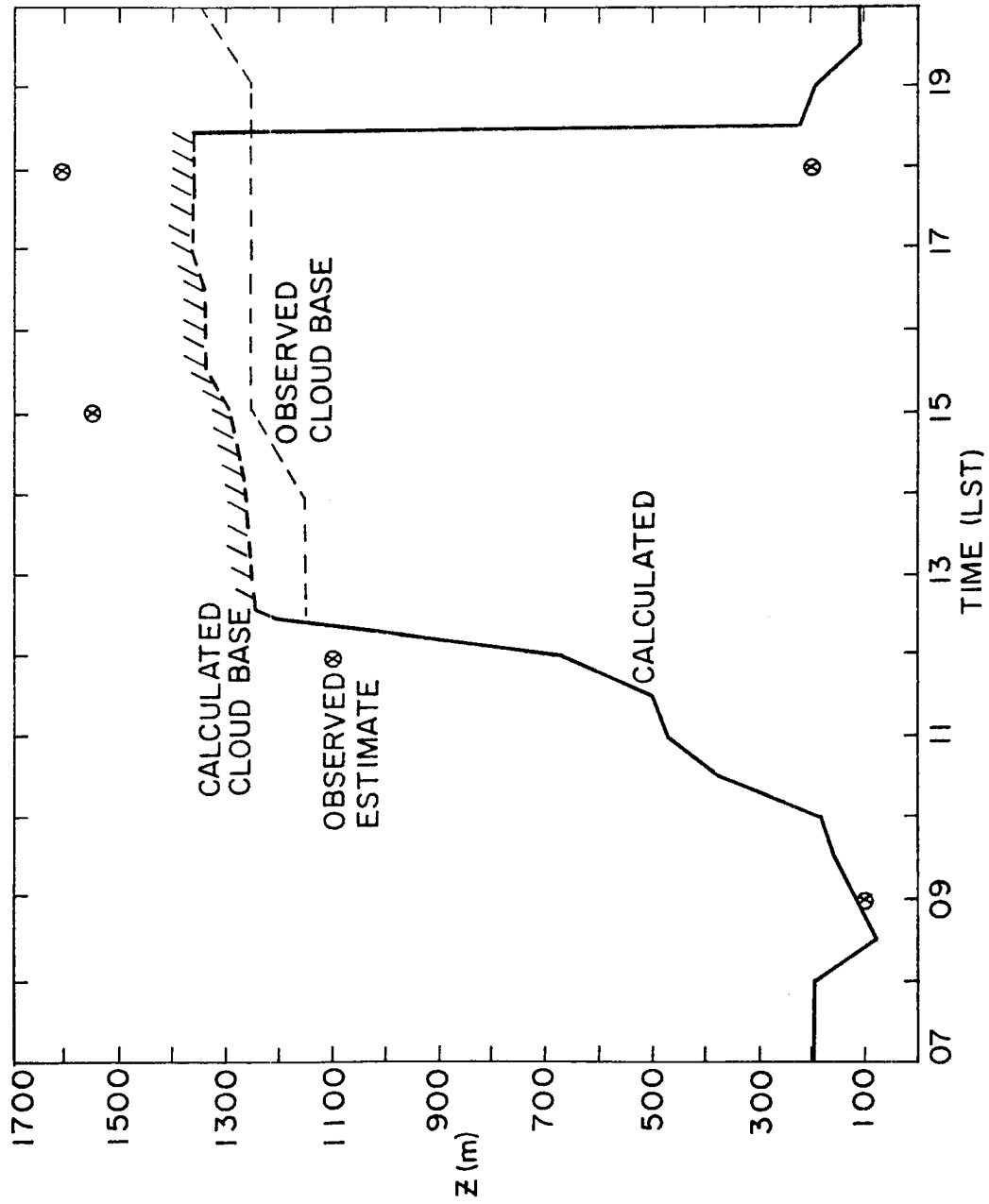


Figure 27.) Boundary layer and cloud base height-Wangara 16.

magnitude weaker than the geostrophic forcing which maintains air motion in the PBL. However mechanical friction is a major contributor to the turbulence in the boundary layer, particularly under stable stratification. As a result, a wind field moving over a heterogeneous surface is able to carry with it for long distances the irregular turbulent field caused by some large obstacle. A second problem is the difficulty in accurately determining the true geostrophic wind in the PBL. This is made difficult by the diabatic effects on slightly sloping surfaces, the need for precise standardized pressure measurements at several locations, and the influence of cross-isobar flow on the pressure field itself. Finally, in the unstable convective boundary layer a unique measurement problem has been pointed out by Wyngaard, et al. (1974). The turbulent motions in the convective PBL are primarily thermally driven. The mechanical influence of the surface gives rise to turbulent motions with magnitudes of the order u_* while the buoyant motions have a magnitude proportional to w_* , which is generally a much larger quantity. As a result, in order to accurately determine the stress profiles, measurements in a highly variable wind field must be averaged for many hours (during which large scale conditions may change). Any shorter-time average wind profile is likely to be extremely non-representative of the true long term average profile.

With all these considerations, it is clearly difficult to initialize a model with truly representative winds or their geostrophic forcing; and it is equally as difficult to compare

a calculated wind profile with an observed profile--even if it is averaged in time or space.

2. Thermodynamic influences.

Further numerical experiments. The O'Neill period 5 case study above shows that even a change of one of the smaller components of the surface energy balance can have a profound effect on the height and temperature of the PBL. In addition to that experiment, in which the soil moisture was varied, several sensitivity tests were run using the Wangara day 33 case. Some of the results are presented in Figures 28-31. Figure 28 displays the effects of varying z_0 and the interface layer biomass on the growth of the boundary layer. As is expected, the increased heat storage of a large biomass significantly delays and damps the boundary layer growth. The effect, if any, of increasing z_0 on the growth of z_i is unclear. Also shown on Figure 28 is an experiment in which a large amount of dew was initialized into the model and the soil moisture was set at its wilting point value. The values were set so that the total evaporation through the day would be about equal to that for the standard case. As expected the morning dew evaporation delayed the sensible warming, and thus the growth of the boundary layer, although the same ultimate height is reached. The dew evaporation was complete at a few minutes after noon at which time the predicted mixing ratio in the PBL was much higher than observed. This experiment tends to refute the hypothesis mentioned earlier in this chapter that there was a heavy deposit of dew or frost on the morning of this day.

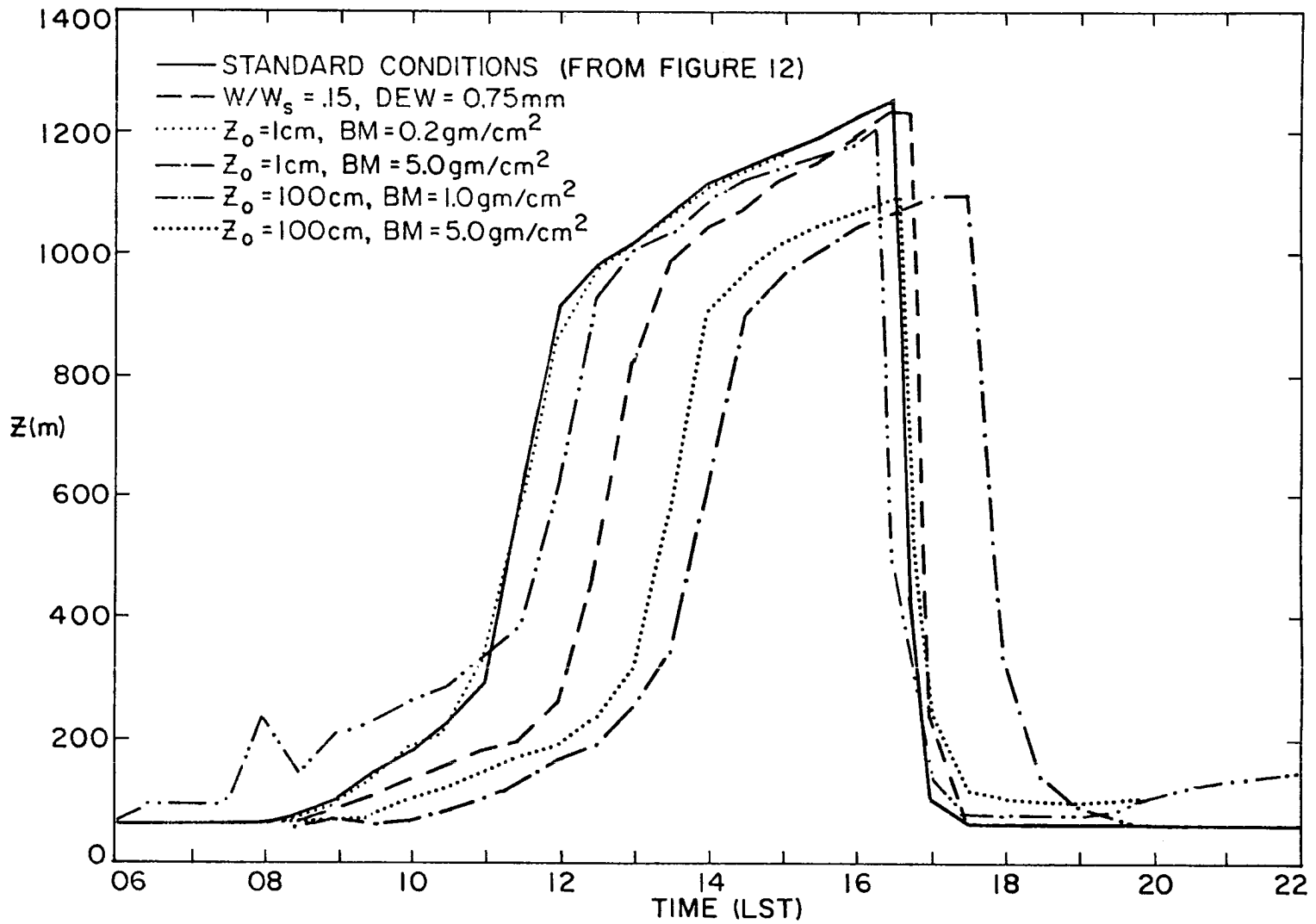


Figure 28.) Boundary layer height-Wangara 33. sensitivity tests for dew, z_0 , and biomass.

In Figure 29 the effects of z_o and biomass (BM) on the interface layer temperature are shown. Here increasing z_o reduces the extremes of temperature without introducing any phase delay, and increasing biomass both damps and delays the diurnal temperature changes at the surface.

The influence of varying the characteristic interface heights for temperature and moisture, z_θ and z_q , is explored in Figures 30 and 31. In Figure 30 the effect on the interface layer temperature is about what one would expect. When the characteristic heights are large (corresponding to a dense heat absorbing and transpiring layer high in the vegetation canopy) the temperature gradients between z_θ and $z_h = 10z_o$ are large and thus strong heat flux develops removing heat from the interface layer rapidly--it does not become as warm. On the other hand, with z_θ very small (sparse, scattered vegetation) the temperature gradient is kept smaller until the interface warms up substantially more. The effect of z_q on interface temperature can be seen in the other three cases which are clustered together (the standard case and the two cases where $z_\theta \neq z_q$). Here an increased loss of sensible heat when z_θ is large ($3.9z_o$) is compensated by the decreased evaporation. The heat not spent on evaporation warms the interface layer. Exactly the opposite occurs when $z_q > z_\theta$.

Figure 31 shows the effect that these parameters have on the evaporation rate. An important result of these tests is that the net latent heat flux into the PBL is strongly affected by these parameters (especially z_q) but the sensible heat flux is only weakly

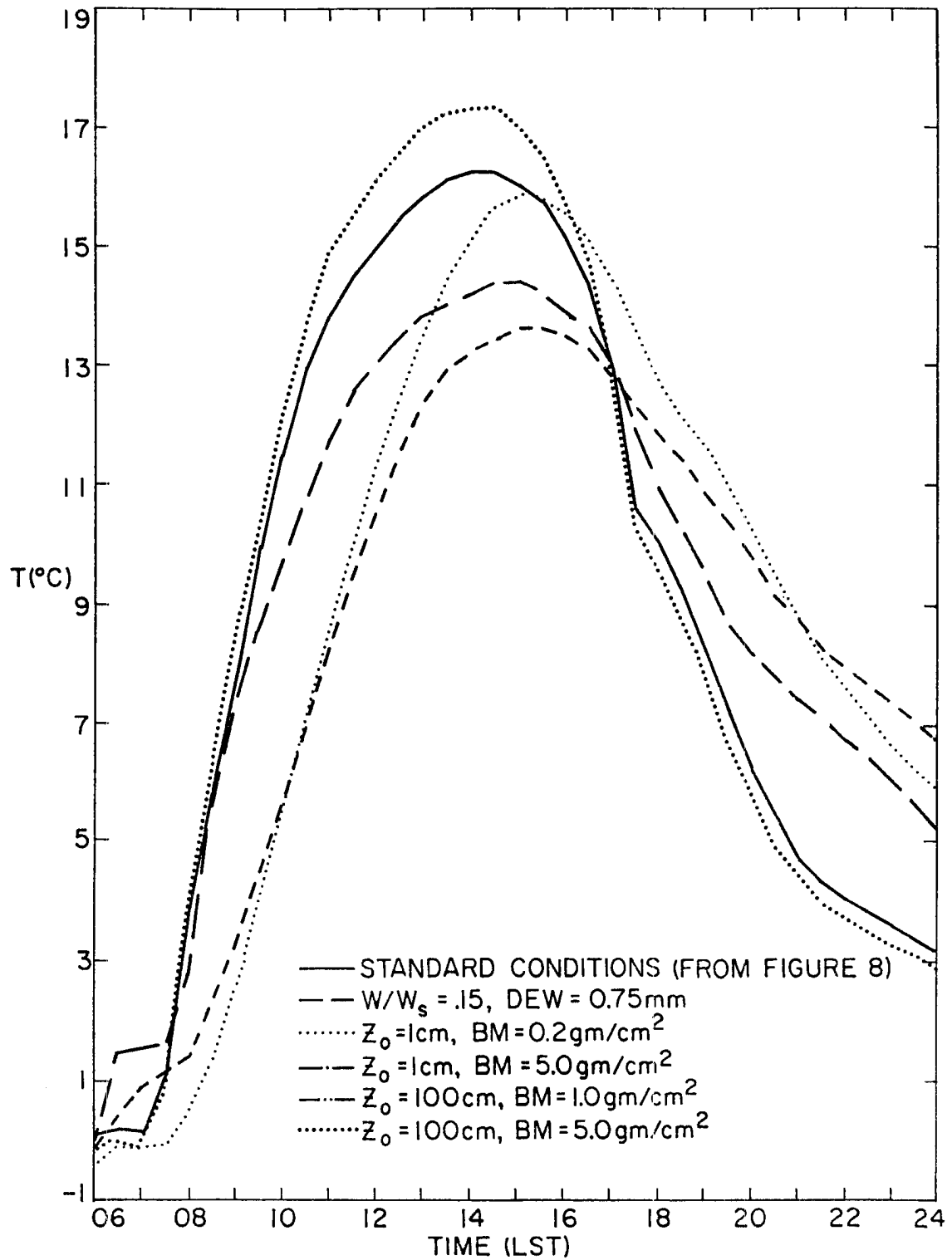


Figure 29.) Interface layer temperature-
Wangara 33. sensitivity tests for dew, z_0 , and biomass.

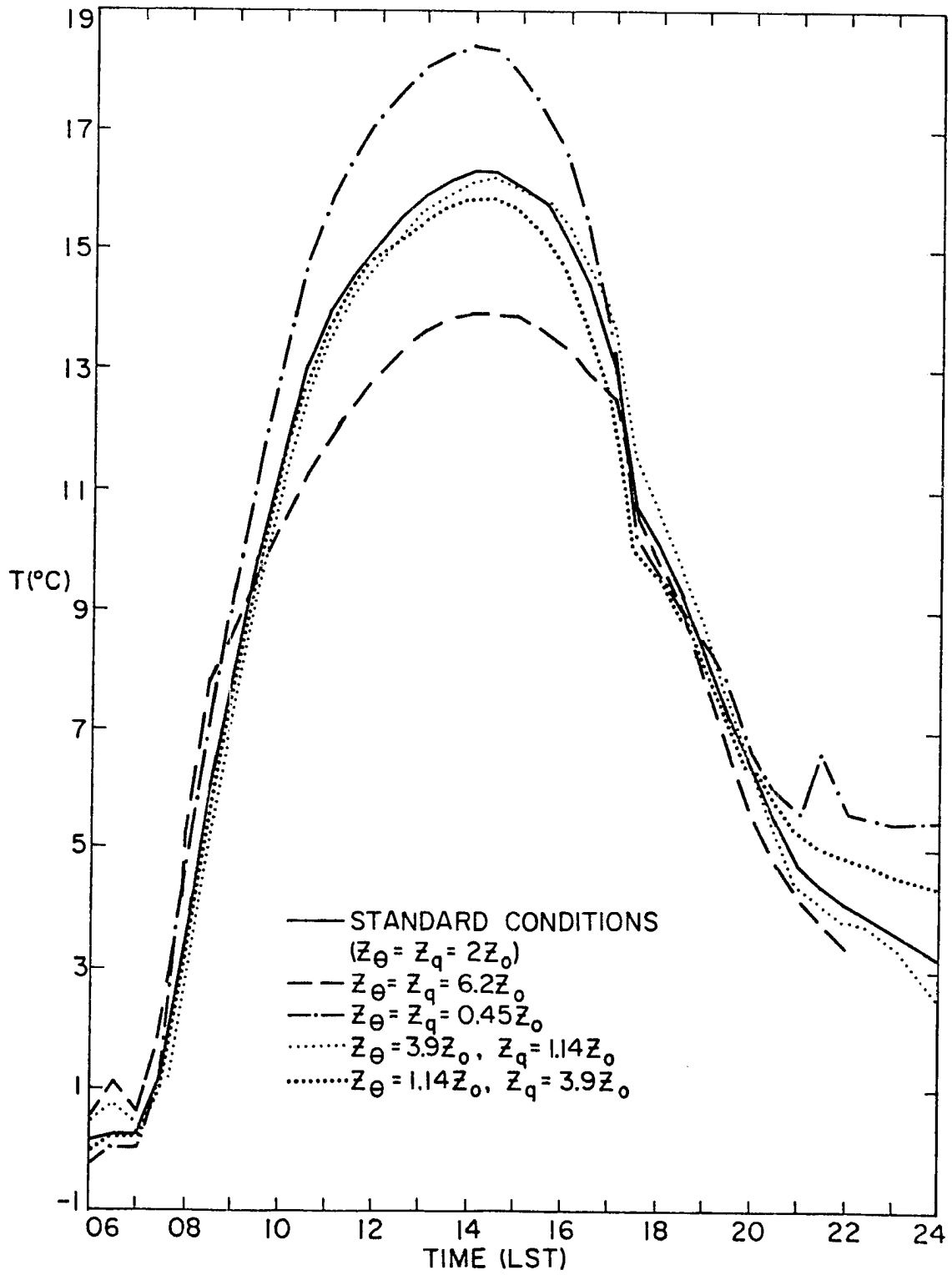


Figure 30.) Interface layer temperature-
Wangare 33. sensitivity tests for characteristic heights z_{θ} and z_q .

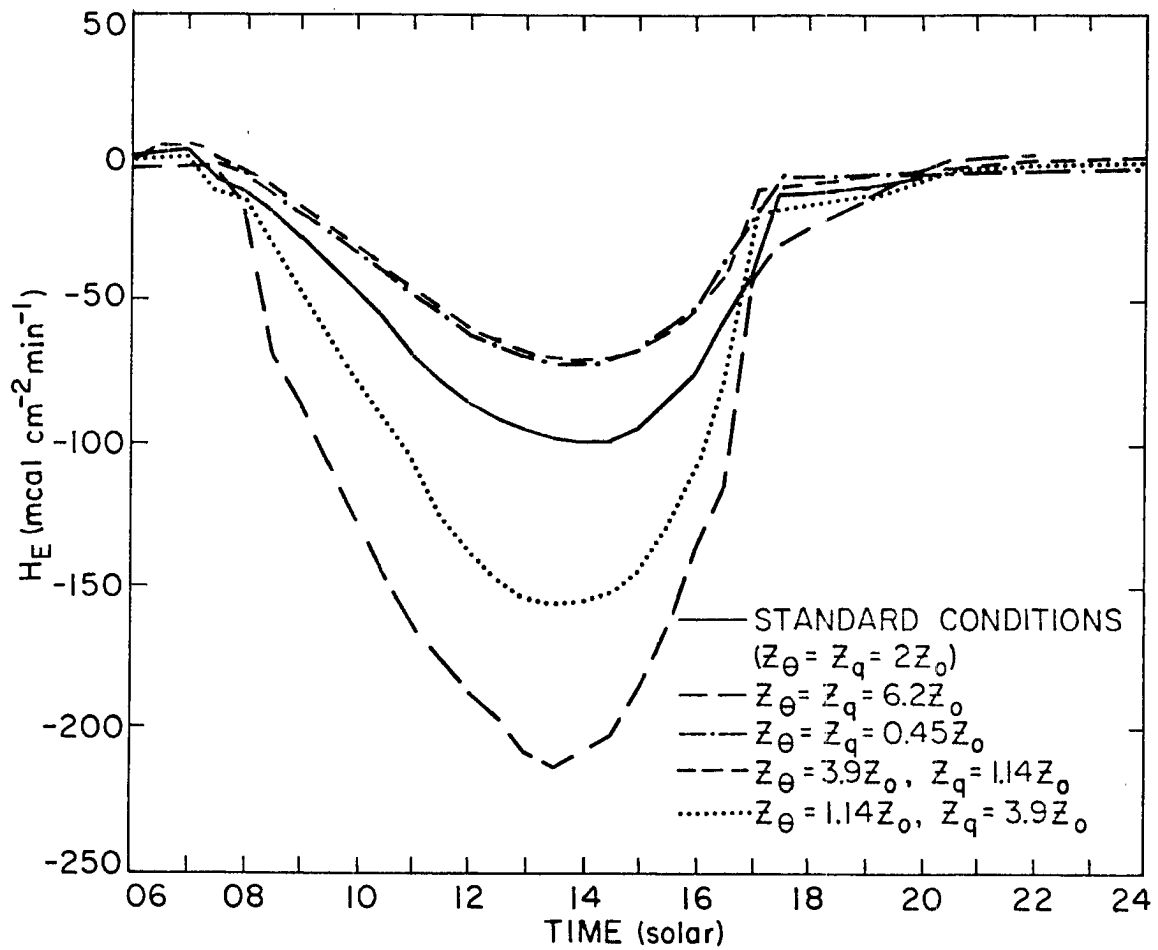


Figure 31.) Latent heat flux-
Wangara 33. sensitivity tests for characteristic heights z_θ and z_q .

modified (again mostly by z_q). The model was found to compensate readily to changes in z_θ by adjusting the heat flux at the top of the surface layer and the temperature profile in the surface layer so that the net flow of heat into the PBL remained quite constant from case to case. On the other hand the effect of z_q on the latent heat flux is large and direct as shown in Figure 31. The effect of z_θ is present but secondary.

The results of the experiments displayed by Figures 30 and 31 point to some important considerations for future work in surface parameterizations. First of all it would appear to be expedient to discriminate between actively transpiring vegetation and dead or inert roughness elements. In the latter case it is likely that z_q is much smaller than z_θ , and improper modelling could produce quite erroneous results based on the evidence of Figure 31. Secondly the stomatal activity of living vegetation takes on deeper significance in view of these experiments. During the cooler damper morning hours stomata are open and plants are generally transpiring freely. Presumably at this time z_q is larger than z_θ as the upper, better ventilated parts of the plant are kept cool by the transpiration. As the day progresses and the air becomes warmer and drier the stomata close, canopy temperatures rise, and transpiration is curtailed. Under these conditions (and depending of course on the type of vegetation) the value of z_q should drop markedly and z_θ may rise somewhat. The development of a comprehensive simple parameterization of these effects based on the concept of the characteristic heights z_θ and z_q should be a challenging but promising future endeavor.

Qualitative considerations. As an attempt to assess the influence of other aspects of the model, Table 5 has been constructed. Listed there are all the major factors which could conceivably affect the thermodynamic behavior of the PBL. On the right is listed the location from which each factor exerts its influence (e.g. the incoming shortwave radiation is primarily absorbed and becomes heat at the surface of the earth). The factors are listed in their approximate order of importance to the behavior of the unstable PBL. An approximate percentage figure is given for each factor, which represents the fraction of the available energy from the number one factor that may be diverted by or into each of the other factors during a maximum probable event (i.e. with each factor exerting its probable strongest influence).

The interesting overview to be drawn from Table 5 is the remarkable lack of self-determination that the PBL displays. The only structures within the PBL which affect its own behavior are any clouds developed beneath z_i as a result of vertical mixing of moisture, the rate of entrainment of heat into the PBL, which is influenced by the turbulence in the PBL itself, and the rate at which the fluxes of heat, moisture and momentum remove heat from the earth's surface-- also somewhat influenced by the PBL turbulence intensity. Otherwise most of the dominant influences on the PBL originate outside the layer, either in the free air above or, most importantly, in the interface layer below. Thus one begins to understand why a detailed high order model of the turbulent structure of the PBL may be quite inadequate in describing the quantitative structure of the PBL unless

Table 5. Factors affecting PBL temperature structure and behavior.

INFLUENCING FACTOR	ESTIMATED RANKING OF IMPORTANCE		WEIGHT (Approx. max. expected amt. of energy used, produced, or contained--as % of no. 1 factor)		SOURCE (location from which each factor influences the energy budget of the PBL)
	DAY	NIGHT	DAY	NIGHT	
incoming short-wave	1.		100		surface
cloud cover	2.	2.	80	90	external and/or PBL
sounding (airmass)	3.		70		external (PBL--some modifying effect)
latent heat flux from soil and vegetation, etc.	4.	4.	60	70	surface (PBL turbulence strong secondary effect)
interface biomass, sensible heat flux	5.		60		surface (PBL turbulence strong secondary effect)
horizontal advection and topography	6.	3.	50	80	external
atmospheric transmission of short-wave (pollutants, dust, haze, etc.)	7.		40		external (PBL--secondary modifying effect)
surface radiation properties--albedo, emissivity	8.		40		surface
net longwave flux	9.	1.	30	100	surface, PBL, external
ground heat flow	10.	5.	30	70	surface
entrainment through PBL top	11.		20		PBL (external--secondary effect)
momentum flux (through its effect on heat flux)	12.	6.	20	50	PBL and external

a good surface energy balance is employed. This point cannot be overemphasized. The PBL is not in control of its own destiny. Thus effective modelling of this layer is far more dependent on the modelling of external inputs and surface properties than on detailing the precise dynamics of the layer itself.

Future modelling tests are planned in which the estimates of Table 5 will be further quantified where possible. As a result of these tests it should become more clear which areas of modelling and parameterization can benefit from future efforts. The approach of Table 5 can thereby provide guidelines for further work so as to reap the greatest improvements in model accuracy from future parameterization and modelling work.

V. CONCLUSIONS

In this thesis a one dimensional parameterized model of the planetary boundary layer has been developed and tested. The model predicts the layer averaged values of virtual potential temperature, wind, and mixing ratio in the PBL by assuming boundary layer profile shapes. The unstable profile is assumed to be represented by the "jump" model where a zero-order discontinuity of all variables exists at the PBL top (z_i). The profiles in the stable PBL are assumed to be linear with height, and a first order discontinuity is assumed at z_i . As indicated both the stable and unstable PBL structure and depth are modelled here, whereas in past layer-averaged boundary layer models only the unstable case has been studied. Two newly developed formulas for describing the heights of the PBL top have been developed and tested: one predicts the heights of the unstable PBL, and the other diagnoses the stable z_i using a bulk Richardson number formulation. Transition between stable and unstable regimes is accomplished by the model without difficulty.

The model incorporates a detailed surface energy budget which leads to a predictive equation for surface temperature. All components of the energy balance at the surface are carefully formulated. The surface is assumed to be a layer of finite thickness containing the mass of all vegetation, organic debris and loose surface material (collectively called biomass). This representation of the surface is shown to be more physically realistic than the usual representation of an infinitesimally thin flat surface. Tests show that the biomass parameter affects the quantitative behavior of the entire PBL in that large values

of biomass store heat, slow and damp the daytime warming of the PBL and also delay and damp the nocturnal cooling. A new evaporation equation is developed and tested in the model. It is shown to work well for a wide range of soil moisture and atmospheric conditions. Also a new soil heat flux parameterization is formulated which does not require knowledge of the soil temperature profile or past history. This is also tested and shown to closely simulate both observational data and the full non-linear heat flow equation. The fluxes of heat and moisture leaving the surface are calculated based on their own characteristic heights, shown to be different, in general, from the characteristic height for momentum z_0 . This allows a degree of freedom which permits one to account for variation in the plant canopy structure. Tests show that the PBL is sensitive to the specification of these characteristic heights--especially the one for moisture which can grossly affect the evaporation rate.

The model was tested against data from O'Neill, Nebraska and from the Wangara experiment, and it was compared with other models of the PBL. Results show that the model simulates the observations well, including a case in which afternoon cloud cover develops at the PBL top both in the model and in the observations. The model was also found to be equal or superior to the other models examined.

A few exploratory tests were conducted in which it is seen that this model is useful as a tool in testing the effects of various surface characteristics and land-use patterns on the PBL. One such test showed that a surface which is covered by 20% irrigated land and 80% dry land evaporated considerably more than a uniformly damp surface with the same mean soil moisture. This test, supported by observations at O'Neill,

also shows that such irrigation has a very large effect of the quantitative structure of the unstable PBL and thus has implications toward inadvertent weather modification.

Finally, it is concluded that the planetary boundary layer is not very self-deterministic, but rather is strongly dependent on surface characteristics and on inputs from the larger scale external factors. As a result a good, carefully formulated surface energy budget and good representation of the large scale are vital to the proper quantitative description of the planetary boundary layer.

VI. SUGGESTIONS FOR FUTURE RESEARCH

There are unlimited possibilities for further study with the model developed here, both in exploratory use of the model to further our knowledge of the boundary layer and surface influences, and in improvement of the model itself. In the latter category there is considerable room for improvement of the evaporation and soil heat flux parameterizations, and of the representation of the nocturnal boundary layer. As more observations become available and the stable boundary layer becomes better understood it may be found that the linear profile assumed here is inappropriate. Other improvements may be possible in the area of kinetic energy equation such as that given by Zeman and Tennekes (1977) may prove useful. Also more exploration of the effects of the residual turbulence in the inertial layer above the nocturnal z_i could be fruitful.

An entire field of future research which is just beginning to be developed is the improved and more detailed representation of the earth's surface. As has been shown by the work reported here, the boundary layer is highly sensitive to surface characteristics. Toward the ultimate accurate parameterization of the surface a four layer model is proposed. The uppermost layer, the canopy layer, is a layer of living vegetation either open or closed to radiative penetration which has mass and transpires water vapor. Beneath the canopy is the stem layer which may be approximated by zero mass, zero transpiration, and relatively unrestricted air motion. Nearer the surface is the third layer, the undergrowth layer which again transpires and has mass and is assumed to consist of living vegetation either open or closed to

radiative penetration depending on the density of vegetation. Finally next to the surface is the thatch layer--a layer containing dead organic matter, loose soil, and any snow cover. This layer is assumed closed to radiative processes and to air motion and instead possesses a specified conductivity--usually considerably less than that of the soil below. Such a surface representation should be able to describe nearly every sort of surface cover using only a handful of parameters related to leaf density, mass characteristic heights, etc.

One further area in which improvement of the model is needed is the representation of cloud cover and/or fog in the PBL. Work has been done in this field by Schubert (1976), Deardorff (1976), and Benoit (1976). Some of their results could be applied to this model with a resulting great improvement in the generality of the model.

Uses of the model for exploratory research include testing the effects on the PBL of such things as timber harvesting techniques, urbanization, various combinations of agricultural land use, swamp drainage, etc.

In the near future tests are planned to eliminate the surface layer averaged parameters θ_{MA} , u_{MA} , v_{MA} and q_{MA} from the model, to assume a constant flux surface layer, and determine what effects these simplifications have on the overall model accuracy. Finally, work is currently underway to employ this model in a three dimensional mesoscale model with the purpose of describing the development and motion of mesoscale weather systems. Within this framework, then, it is hoped that numerous experiments will be performed to describe the effects of various types of ground cover, land usage, and topographic features on the boundary layer structure, the mesoscale flow field and the initiation of convection.

BIBLIOGRAPHY

- Albrecht, B.A., 1977: A time dependent model of the tradewind boundary layer. Atmospheric Science Paper No. 267, Dept. of Atmos. Sci., Colo. State Univ., 174 pp.
- Allen, C. W., 1963: Astrophysical Quantities, Univ. of London, 291 pp.
- Arya, S. P. S., 1975: Geostrophic drag and heat transfer relations for the atmospheric boundary layer. Quart. J. Roy. Meteor. Soc., V. 101, pp. 147-161.
- Arya, S. P. S., 1977: Suggested revision to certain boundary layer parameterization schemes used in atmospheric circulation models. Mon. Wea. Rev., V. 105, pp. 215-227.
- Arya, S. P. S., and J. C. Wyngaard, 1975: Effect of baroclinicity on wind profiles and the geostrophic drag law for the convective planetary boundary layer. J. Atmos. Sci., V. 32, pp. 767-778.
- Atwater, M. A., 1972: Thermal effects of urbanization and industrialization in the boundary layer: A numerical study. Boundary-Layer Meteor., V. 3, pp. 229-245.
- Baier, W., 1969: Concepts of soil moisture availability and their effect on soil moisture estimates from a meteorological budget. Agr. Meteor., V. 6, pp. 165-178.
- Benoit, R., 1976: A comprehensive parameterization of the atmospheric boundary layer for general circulation models, NCAR Cooperative thesis No. 39, McGill University and the National Center for Atmospheric Research, 278 pp.
- Betts, A. K., 1973: Non-precipitating cumulus convection and its parameterization. Quart. J. Roy. Meteor. Soc. V. 99, pp. 178-196.

- Blackadar, A. K., 1976: Modelling the nocturnal boundary layer. Preprints Third Symp. Atmospheric Turbulence, Diffusion and Air Quality Raleigh, Amer. Meteor. Soc., pp. 46-49.
- Brown, R. A., 1974: Matching classical boundary-layer solutions toward a geostrophic drag coefficient relation. *Boundary-Layer Meteor.*, V. 7, pp. 489-500.
- Brutsaert, W., 1965: Equations for vapor flux as a fully turbulent diffusion process under diabatic conditions. *Bull. I.A.S.H.*, V. 10, pp. 11-21.
- Budyko, M. I., 1948: Evaporation Under Natural Conditions. Israel Program for Scientific Transtations, 1963, 130 pp.
- Budyko, M. I., 1956: The Heat Balance of the Earth's Surface. English Trans. by U. S. Dept. of Commerce, Weather Bureau, 259 pp.
- Busch, N. E., S. W. Chang, and R. A. Anthes, 1976: A multi-level model of the planetary boundary layer suitable for use with mesoscale dynamic models. *J. Appl. Meteor.* V. 15 pp. 909-919.
- Businger, J. A., and S. P. S. Arya, 1974: Height of the mixed layer in the stably stratified planetary boundary layer. *Advances in Geophysics*, V. 18A, pp. 73-92.
- Businger, J. A., J. C. Wyngaard, Y. Izumi, and E. F. Bradley, 1971: Flux-profile relationships in the atmospheric surface layer. *J. Atmos. Sci.*, V. 28, pp. 181-189.
- Calder, K. L., 1939: A note on the constancy of horizontal turbulent sheering stress in the lower layers of the atmosphere. *Quart. J. Roy. Meteor. Soc.*, V. 65, pp. 537-541.
- Carslaw, H. S. and J. C. Jaeger, 1959: Conduction of Heat in Solids. 2nd ed., Oxford, Clarendon Press, 510 pp.

- Carson, D. J., 1973: The development of a dry inversion-capped convectively unstable boundary layer. *Quart. J. Roy. Meteor. Soc.*, V. 99, pp. 450-467.
- Cattle, H. and K. I. Weston, 1975: Budget studies of heat flux profiles in the convective boundary layer over land. *Quart. J. Roy. Meteor. Soc.*, V. 101, pp. 353-363.
- Clarke, R. H., 1970a: Observational studies in the atmospheric boundary layer, *Quart. J. Roy. Meteor. Soc.*, V. 96, pp. 91-114.
- Clarke, R. H., 1970b: Recommended methods for the treatment of the boundary layer in numerical models. *Australian Meteorological Magazine*, V. 18, pp. 51-71.
- Clarke, R. H., A. J. Dyer, R. R. Brook, D. G. Reid, and A. J. Troup, 1971: The Wangara experiment: boundary layer data. *Div. Meteor. Phys. Tech. Paper No. 19*, CSIRO, 362 pp.
- Clarke, R. H., and G. D. Hess, 1973: On the appropriate scaling for velocity and temperature in the planetary boundary layer. *J. Atmos. Sci.*, V. 30, pp. 1346-1353.
- Clarke, R. H., and G. D. Hess, 1974: Geostrophic departure and the functions A and B of Rossby-Number similarity theory. *Boundary-Layer Meteor.*, V. 7, pp. 267-287.
- Csanady, G. T., 1967: On the "resistance law" of a turbulent Ekman layer. *J. Atmos. Sci.*, V. 24, pp. 467-471.
- Csanady, G. T., 1972: Geostrophic drag, heat and mass transfer coefficients for the diabatic Ekman layer. *J. Atmos. Sci.*, V. 29, pp. 488-496.
- Deacon, E. L., 1973: Geostrophic drag coefficients. *Boundary-Layer Meteor.* V. 5, pp. 321-340.

- Deardorff, J. W., 1972a: Numerical investigation of neutral and unstable planetary boundary layers. *J. Atmos. Sci.*, V. 29, pp. 91-115.
- Deardorff, J. W., 1972b: Parameterization of the planetary boundary layer for use in general circulation models. *Mon. Wea. Rev.*, V. 100, pp. 93-106.
- Deardorff, J. W., 1973: An explanation of anomalously large Reynolds stresses within the convective planetary boundary layer. *J. Atmos. Sci.*, V. 30, pp. 1070-1076.
- Deardorff, J. W., 1974a: Three dimensional numerical study of the height and mean structure of a heated planetary boundary layer. *Boundary-Layer Meteor.*, V. 7, pp. 81-106.
- Deardorff, J. W., 1974b: Three dimensional numerical study of turbulence in an entraining mixed layer. *Boundary-Layer Meteor.* V. 7, pp. 199-226.
- Deardorff, J. W., 1976: On the entrainment rate of a stratocumulus-topped mixed layer. *Quart. J. Roy. Meteor. Soc.* V. 102, pp. 563-582.
- Deardorff, J. W., 1978: Efficient prediction of ground surface temperature and moisture, with inclusion of a layer of vegetation. *J. Geophys. Res.*, V. 83, 1889-1903.
- Delsol, F., K. Miyakoda, and R. Clarke, 1971: Parameterized processes in the surface boundary layer of an atmospheric circulation model. *Quart. J. Roy. Meteor. Soc.*, V. 97, 181-208.
- Denmead, O. T., and R. H. Shaw, 1962: Availability of soil water to plants as affected by soil moisture content and meteorological conditions. *Agron. J.*, V. 54, pp. 385-390.
- Dirks, R. A., 1969: A theoretical investigation of convective patterns in the lee of the Colorado Rockies. *Atmospheric Science Paper No. 145*,

- Colo. State Univ., 122 pp.
- Donaldson, C. duP., 1973: Construction of a dynamic model of atmospheric turbulence and the dispersal of atmospheric pollutants. Workshop on Micrometeorology, Boston, Amer. Meteor. Soc., pp. 313-390.
- Dyer, A. J., 1967: The turbulent transport of heat and water vapor in an unstable atmosphere. Quart. J. Roy. Meteor. Soc., V. 93, pp. 501-508.
- Dyer, A. J., 1974: A review of flux-profile relationships. Boundary-Layer Meteor. V. 7, pp. 363-372.
- Dyer, A. J., and B. B. Hicks, 1970: Flux-gradient relationships in the constant flux layer. Quart. J. Roy. Meteor. Soc., V. 96, pp. 715-721.
- Ellison, T. H., 1957: Turbulent transport of heat and momentum from an infinite rough plane. J. Fl. Mech. V. 2, pp. 463-466.
- Estoque, M. A., 1963: A numerical model of the atmospheric boundary layer. J. Geophys. Res., 68, 1103-1113.
- Gadd, A. J., and J. F. Keers, 1970: Surface exchanges of sensible and latent heat in a 10-level model atmosphere. Quart. J. Roy. Meteor. Soc., V. 96, pp. 297-308.
- Gannon, P. T. Sr., 1976: On the influence of the surface thermal properties and clouds on the south Florida sea breeze. Ph.D. Dissertation, the University of Miami, Coral Gables.
- Garratt, J. R., 1978: Transfer characteristics of a heterogeneous surface of large aerodynamic roughness. Quart. J. Roy. Meteor. Soc., V. 104, pp. 491-502.
- Geiger, R., 1959: The Climate Near The Ground. Harvard University Press, Cambridge, Mass., 494 pp.

- Gill, A. E., 1968: Similarity theory and geostrophic adjustment. *Quart. J. Roy. Meteor. Soc.*, V. 94, pp. 586-588.
- Hadeen, K. D., and A. L. Friend, 1972: The Air Force Global Weather Central operational boundary-layer model. *Boundary-Layer Meteor.* V. 3, 98-112.
- Hess, G. D., 1973: On Rossby number similarity theory for a baroclinic planetary boundary layer. *J. Atmos. Sci.*, V. 30, pp. 1722-1723.
- Hicks, B. B., 1976: Wind profile relationships from the Wangara experiment. *Quart. J. Roy. Meteor. Soc.*, V. 102, pp. 535-551.
- Hoxit, L. R., 1973: Variability of planetary boundary layer winds. Atmospheric Science Paper No. 199, Dept. of Atmos. Sci., Colo. State Univ.
- Hoxit, L. R., 1974: Planetary boundary layer winds in baroclinic conditions. *J. Atmos. Sci.*, V. 31, pp. 1003-1020.
- Hsu, S. A., 1969: Mesoscale structure of the Texas Coast sea breeze. Report No 16, Atmospheric Science Group, College of Engineering, Univ. of Texas of Austin, 237 pp.
- Kaimal, J. C., J. C. Wyngaard, D. A. Haugen, O. R. Coté, Y. Izumi, J. C. Caughey, and C. J. Readings, 1976: Turbulence structure in the convective boundary layer. *J. Atmos. Sci.*, V. 33, pp. 2152-2169.
- Kazansky, A. B., and A. S. Monin, 1956: Turbulence in the inversion layer near the surface, *Izv. Akad. Nauk. USSR, Ser. Geofiz.*, V. 1, pp. 79-86.
- Kazansky, A. B. and Monin, A. S., 1960. A turbulent regime above the ground atmospheric layer. *Izv. Acad. Sci. USSR. Geophys. Ser.*, V. 1, pp. 110-112.

- Kondo, J., O. Kanechika, and N. Yasuda, 1978: Heat and momentum transfers under strong stability in the atmospheric surface layer, *J. Atmos. Sci.*, V. 35, pp. 1012-1021.
- Kraus, E. B., and J. S. Turner, 1967: A one-dimensional model of the seasonal thermocline, II. The general theory and its consequences. *Tellus*, V. 19, pp. 98-105.
- Krishna, K., 1968: A numerical study of the diurnal variation of meteorological parameters in the planetary boundary layer, I. Diurnal variation of winds. *Mon. Wea. Rev.*, V. 96, pp. 269-276.
- Lavoie, R. L., 1971: A mesoscale numerical model of lake-effect storms. *J. Atmos. Sci.*, V. 29, pp. 1025-1040.
- Lenschow, D. H., 1970: Airplane measurements of planetary boundary layer structure. *J. Appl. Meteor.* V. 9, pp. 874-884.
- Lettau, H. H. and B. Davidson, 1957: Exploring the Atmosphere's First Mile, Pergamon Press, New York, N. Y., Vs. I and II.
- Lilly, D. K., 1968: Models of cloud-topped mixed layers under a strong inversion. *Quart. J. Roy. Meteor. Soc.*, V. 94, pp. 292-309.
- Lo, A. K., 1977: Boundary layer flow over gentle curvilinear topography with a sudden change in surface roughness. *Quart. J. Roy. Meteor. Soc.*, V. 103, pp. 199-209.
- Long, P. E., Jr., and W. A. Shaffer, 1975: Some physical and numerical aspects of boundary layer modelling. NOAA Technical Memorandum NWS TDL-56. Techniques Development Laboratory, Silver Spring, Maryland, 37 pp.
- Lumley, J. L., and B. Khajeh-Nouri, 1974: Computational modelling of turbulent transport. *Adv. in Geophys.* V. 18A, pp. 169-192.

- Mahrer, Y., and R. A. Pielke, 1975: A numerical study of the air flow over mountains using the two-dimensional version of the University of Virginia mesoscale model. *J. Atmos. Sci.*, V. 32, pp. 2144-2155.
- Mahrt, L. and D. H. Lenschow, 1976: Growth dynamics of the convectively mixed layer. *J. Atmos. Sci.*, V. 33, pp. 41-51.
- Manabe, S., 1969: Climate and the ocean circulation, I. the atmospheric circulation and the hydrology of the earth's surface. *Mon. Wea. Rev.*, V. 97, pp. 739-774.
- Manton, M. J. and W. R. Cotton, 1977: Formulation of approximate equations for modelling moist deep convection on the mesoscale. Atmospheric Science Paper No. 266., Dept. of Atmos. Sci., Colo. State Univ., 62 pp.
- Melgarejo, J. W. and J. W. Deardorff, 1974: Stability functions for the boundary layer resistance laws based upon observed boundary layer heights. *J. Atmos. Sci.*, V. 31, pp. 1324-1333.
- Mellor, G. L. and T. Yamada, 1974: A hierarchy of turbulence closure models for planetary boundary layers. *J. Atmos. Sci.*, V. 31, pp. 1791-1806.
- Monin, A. S., and A. M. Obukhov, 1954: Basic laws of turbulent mixing in the ground layer of the atmosphere. *Akad. Nauk. SSSR, Geofiz. Inst. Trudy*, V. 151, pp. 163-187.
- Monteith, J. L., ed. 1975: Vegetation and the Atmosphere, Academic Press, New York V. 1, 278 pp.
- Munn, R. E., 1966: Descriptive Micrometeorology, Academic Press, New York, 245 pp.
- Nappo, C. J., Jr., 1975: Parameterization of surface moisture and evaporation rate in a planetary boundary layer model. *J. Appl.*

- Meteor. V. 14, pp. 289-296.
- Nickerson E. C., and V. E. Smiley, 1975: Surface layer and energy budget parameterizations for mesoscale models. J. Appl. Meteor., V. 14, pp. 297-300.
- O'Brien, J., 1970: On the vertical structure of the eddy exchange coefficient in the planetary boundary layer. J. Atmos. Sci., V. 27, pp. 1213-1215.
- Obukhov, A. M., 1946: Turbulence in the atmosphere with non-uniform temperature. Reprinted in English (1971), Boundary-Layer Meteor. V. 2, pp. 7-29.
- Orlanski, I., B. B. Ross, and L. J. Polinski, 1974: Diurnal variation of the planetary boundary layer in a mesoscale model. J. Atmos. Sci., V. 31, pp. 965-999.
- Pandolfo, J. P., 1969: Motions with inertial and diurnal period in a numerical model of the navifacial boundary layer. J. Mar. Res. V. 27, pp. 301-317.
- Pandolfo, J. P., 1971: Numerical experiments with alternative boundary layer formulations using BOMEX data. Boundary-Layer Meteor., V. 1, pp. 277-289.
- Panofsky, H. A., 1961: An alternative derivation of the diabatic wind profile. Quart. J. Roy. Meteor. Soc., V. 87, pp. 109-110.
- Paulson, C. A., 1970: The mathematical representation of wind speed and temperature profiles in the unstable atmospheric surface layer. J. Appl. Meteor. V. 9, pp. 857-861.
- Peterson, E. W., 1971: Predictions of the momentum exchange coefficient for flow over heterogeneous terrain. J. Appl. Meteor. V. 10, pp. 958-961.

- Phillip, J. R., 1957: Evaporation, and moisture and heat fields in the soil. *J. Meteor.*, V. 14, pp. 354-366.
- Pielke, R. A., 1973: A three-dimensional numerical model of the sea breezes over south Florida. NOAA Tech. Memorandum ERL WMPO-2, U. S. Dept. of Commerce, NOAA, Env. Res. Labs. Wea. Mod. Program Office, Boulder, CO., 136 pp.
- Pielke, R. A. and Y. Mahrer, 1975: Representation of the heated planetary boundary layer in mesoscale models with a coarse vertical resolution. *J. Atmos. Sci.*, V. 32, pp. 2288-2308.
- Pierson, F. W., and A. P. Jackman, 1975: An investigation of the predictive ability of several evaporation equations, *J. Appl. Meteor.* V. 14, pp. 477-487.
- Prandtl, L., 1932: Meteorologische anwendungen der Strömungslehre *Beitr. Phys. frei. Atmos.*, V. 19, pp. 188-202.
- Pruitt, W. O., D. L. Morgan, and F. J. Lourence, 1973: Momentum and mass transfers in the surface boundary layer. *Quart. J. Ro . Meteor. Soc.*, V. 99, pp. 370-386.
- Rao, K. S., J. C. Wyngaard, and O. R. Coté, 1974: The structure of the two-dimensional internal boundary layer over a sudden change of surface roughness. *J. Atmos. Sci.*, V. 31, pp. 738-746.
- Ross, J., 1975: Radiative transfer in plant communities, Vegetation and the Atmosphere, V. 1, J. L. Monteith, ed., Academic Press, New York, pp. 13-55.
- Rowland, J. R., 1973: Intensive probing of a clear air convective field by radar and instrumented drone aircraft. *J. Appl. Meteor.*, V. 12, pp. 149-155.

- Rutter, A. J., 1975: The hydrological cycle in vegetation, Vegetation and the Atmosphere, V. 1. J.L. Monteith, ed., Academic Press, New York, pp. 111-154.
- Sasamori, T., 1968: The radiative cooling calculation for application to the general circulation experiments. *J. Appl. Meteor.*, V. 7, pp. 721-729.
- Sasamori, T., 1970: A numerical study of the atmospheric and soil boundary layers. *J. Atmos. Sci.*, V. 27, pp.1122-1137.
- Schickedanz, P. T., 1976: The effect of irrigation on precipitation in the Great Plains. Final Report, NSF grant GI-43871, Illinois State Water Survey at the University of Illinois, Urbana, 105 pp.
- Schubert, W. H., 1976: Experiments with Lilly's cloud-topped mixed layer model. *J. Atmos. Sci.*, V. 33, pp. 435-446.
- Sellers, W. D., 1962: A simplified derivation of the diabatic wind profile. *J. Atmos. Sci.*, V. 19, pp. 180-181.
- Sellers, W. D., 1965: Physical Climatology. Univ. of Chicago Press, p. 41.
- Shaffer, W. A. and P. E. Long, Jr., 1975: A predictive boundary layer model, NOAA Technical Memorandum NWS TDL-57, Techniques Development Laboratory, Silver Spring, Maryland, 44pp.
- Slatyer, R. O., 1956: Evapotranspiration in relation to soil moisture. *Neth. J. Agric. Sci.*, V. 4, pp. 73-76.
- Stull, R. B., 1973: Inversion rise model based on penetrative convection, *J. Atmos. Sci.*, V. 30, pp. 1092-1099.
- Stull, R. B., 1976a: The energetics of entrainment across a density interface. *J. Atmos. Sci.*, V. 33, pp.1260-1267.

- Stull, R. B., 1976b: Mixed-layer depth model based on turbulent energetics. *J. Atmos. Sci.*, V. 33, pp. 1268-1278.
- Stull, R. B., 1976c: Internal gravity waves generated by penetrative convection. *J. Atmos. Sci.*, V. 33, pp. 1279-1286.
- Taylor, P. A., 1970: A model of airflow above changes in surface heat flux, temperature and roughness for neutral and unstable conditions. *Boundary-Layer Meteor.*, V. 1, pp. 18-39.
- Tennekes, H., 1970: Free convection in the turbulent Ekman layer of the atmosphere. *J. Atmos. Sci.*, V. 27, pp. 1027-1034.
- Tennekes, H., 1973: A model for the dynamics of the inversion above a convective boundary layer. *J. Atmos. Sci.*, V. 30, pp. 558-567.
- Tennekes, H., 1975: Reply. *J. Atmos. Sci.*, V. 32, pp. 992-995.
- Thompson, R. S., 1978: Note on the aerodynamic roughness length for complex terrain. *J. Appl. Meteor.*, V. 17, pp. 1402-1403.
- Thorntwaite, C. W., and J. R. Mather, 1955: The water budget and its use in irrigation. U. S. Dept. Agri., Yearbook of Agriculture 1955 pp. 346-358.
- Webb, E. K., 1970: Profile relationships: the log-linear range, and extension to strong stability. *Quart. J. Roy. Meteor. Soc.*, V. 96, pp. 67-90.
- Wetzel, P. J., 1973: Moisture sources and flow patterns during the northeast Colorado hail season. Unpublished M. S. thesis, Dept. of Atmos. Sci., Colo. State Univ., 91pp.
- Willis, G. E., and J. W. Deardorff, 1974: A laboratory model of the unstable planetary boundary layer. *J. Atmos. Sci.*, V. 31, pp. 1297-1307.

- Woods, J. D., 1969: On Richardson's number as a criterion for laminar-turbulent-laminar transition in the ocean and atmosphere. *Radio Science*, V. 4, pp. 1289-1298.
- Wyngaard, J. C., 1975: Modelling the planetary boundary layer--extension to the stable case. *Boundary-Layer Meteorol.*, V. 9, pp. 441-460.
- Wyngaard, J. C., S. P. S. Arya, and O. R. Coté, 1974: Some aspects of the structure of convective planetary boundary layers. *J. Atmos. Sci.*, V. 31, pp. 747-754.
- Wyngaard, J. C., and O. R. Coté, 1974: The evolution of a convective planetary boundary layer--a higher-order-closure model study. *Boundary-Layer Meteorol.*, V. 7, pp. 289-308.
- Yamada, T., 1976: On the similarity functions A, B, and C of the planetary boundary layer. *J. Atmos. Sci.*, V. 33, pp. 781-793.
- Yamada, T., and G. Mellor, 1975: A simulation of the Wangara atmospheric boundary layer data. *J. Atmos. Sci.*, V. 32, pp. 2309-2329.
- Yamamoto, G., 1952: On a radiation chart. *Sci. Rept. Tohoku Univ.*, Ser. 5, Geophys., V. 4, pp. 9-23.
- Yamamoto, G. 1959: Theory of turbulent transfer in non-neutral conditions. *J. Meteorol. Soc. Japan*, V. 37, pp. 60-69.
- Yamamoto, G., 1962: Direct absorption of solar radiation by atmospheric water vapor, carbon dioxide, and molecular oxygen. *J. Atmos. Sci.*, V. 19, pp. 182-188.
- Yamamoto, G., and J. Kondo, 1959: Effect of surface reflectivity for long wave radiation on temperature profiles near the bare soil surface. *Sci. Rept. Tohoku Univ.*, Ser. 5, Geophys., V. 11, pp. 1-9.

- Yu, T.-w., 1978: Determining height of the nocturnal boundary layer. *J. Appl. Meteor.*, V. 17, pp. 28-33.
- Zahner, R., 1967: Refinement in empirical functions for realistic soil-moisture regimes under forest cover, *Forest Hydrology*, W. E. Soper and M. W. Lull, eds., Pergamon Press, Oxford, pp. 261-274.
- Zeman, O., and J. L. Lumley, 1976: Modelling buoyancy driven mixed layers. *J. Atmos. Sci.*, V. 33, pp. 1974-1988.
- Zeman, O., and H. Tennekes, 1977: Parameterization of the turbulent energy budget at the top of the daytime atmospheric boundary layer. *J. Atmos. Sci.*, V. 34, pp. 111-123.
- Zilitinkevitch, S. S., 1972: On the determination of the height of the Ekman boundary layer. *Boundary-Layer Meteor.*, V. 3, pp. 141-145.
- Zilitinkevitch, S. S., 1975a: Resistance laws and prediction equations for the depth of the planetary boundary layer. *J. Atmos. Sci.*, V. 32, pp. 741-752.
- Zilitinkevitch, S. S., 1975b: Comments on "A model for the dynamics of the inversion above a convective boundary layer". *J. Atmos. Sci.*, V. 32, pp. 991-992.
- Zilitinkevitch, S. S., and D. V. Chaliknov, 1968: The laws of resistance and of heat and moisture exchange in the interaction between the atmosphere and an underlying surface. *Izv. Atmos. and Ocean. Phys.*, V. 4, No. 7, pp. 765-772, trans. by J. Findlay.
- Zilitinkevitch, S. S., and J. W. Deardorff, 1974: Similarity theory for the planetary boundary layer of time dependent height. *J. Atmos. Sci.*, V. 31, pp. 1449-1452.

APPENDIX. Initial Conditions used in testing the model.(all units CGS)

A. O'NEILL period 2

θ	= 303.1	u_M	= 1100.0	D	= 0.0	ϕ	= 0.74177
θ_{vM}	= 300.3	v_M	= 1400.0	q_s	= 0.0105	d	= 225.0
θ_{vMA}	= 0.0099	z_M	= 27500.0	z_s	= 5000.0	mc_s	= 0.3
q_M	= 0.0094	L_i	= 15000.0	$\Delta\theta_v$	= 0.0	$\bar{\alpha}^s$	= 0.18
q_{MA}	= 292.1	z	= 1.0	time	= 14400.0	T_{15cm}	= 296.45
T^s	= 292.1	$\partial z_i^0 / \partial t$	= 0.7	δt	= 180.0	k	= 0.0012
u^s_{MA}	= 600.0	W_i	= 4.8	c	= 1.0		
v^s_{MA}	= 1100.0						

P(mb)	T($^{\circ}$ K)	q(g/kg)	u(cm/s)	v(cm/s)	$1/\rho \times \partial p / \partial x$	$1/\rho \times \partial p / \partial y$
945	292.2	10.1	200	800	0.005	-0.13
916	296.8	9.8	1550	1550	0.005	-0.13
906	299.5	9.8	2000	1600	0.005	-0.13
862	298.9	7.3	2000	500	0.005	-0.13
826	296.8	6.6	1500	110	0.005	-0.13
700	284.6	5.8	850	0	0.005	-0.13
678	282.6	2.2	850	0	0	-0.085
646	279.9	1.5	850	0	0	-0.085
610	276.0	1.0	850	0	0	-0.085
572	274.0	0.8	850	0	0	-0.085
542	271.0	0.6	850	0	0	-0.085
400	250.2	0.27	850	0	0	-0.085
300	235.2	0.1	850	0	0	-0.085
150	210.6	0.01	850	0	0	-0.085
0.01	213.0	0.003	0	0	0	-0.085

B. O'NEILL period 5, Day 1

θ_{vM}	= 310.4	u_M	= 350.0	D	= 0.0	ϕ	= 0.74177
θ_{vMA}	= 312.3	v_M	= 1300.0	q_s	= 0.0121	d	= 236.0
q_M	= 0.0121	z_i	= 135000.0	z_s	= 3000.0	mc_s	= 0.3
q_{MA}	= 0.0121	L_i	= 3000.0	$\Delta\theta_v$	= 1.2	π_s	= 0.025
T^s	= 308.05	z	= 1.0	time	= 43200/0	T_{15cm}	= 296.4
u_{MA}^s	= 150.0	$\partial z_i / \partial t$	= 10.0	δt	= 180.0	k^{15cm}	= 0.0009
v_{MA}	= 1100.0	W_i	= 3.3	c	= 1.0		

P(mb)	T($^{\circ}$ K)	q(g/kg)	u(cm/s)	v(cm/s)	$1/\rho \times \partial p / \partial x$	$1/\rho \times \partial p / \partial y$
941	285.4	12.5	100	1000	0.106	-0.095
895	297.3	11.5	320	1300	0.072	-0.096
885	295.9	11.3	350	1305	0.070	-0.096
828	291.2	10.1	540	1315	0.077	-0.105
800	290.6	9.1	580	1280	0.090	-0.117
760	298.5	7.7	610	910	0.115	-0.115
718	283.0	6.9	350	350	0.035	-0.035
675	282.1	5.78	350	350	0.035	-0.035
622	277.7	4.99	350	350	0.035	-0.035
610	277.3	4.47	350	350	0.035	-0.035
586	274.6	4.02	350	350	0.035	-0.035
528	269.4	1.51	350	350	0.035	-0.035
400	254.0	0.36	1000	0	0.0	-0.1
300	235.5	0.1	1000	0	0.0	-0.1
150	208.0	0.01	1000	0	0.0	-0.1
0.01	213.0	0.003	0	0	0.0	0.0

C. O'NEILL period 5, Day 2

θ_{VM}	= 305.2	u_M	= 541.3	D	= 0.0	ϕ	= 0.74177
θ_{VMA}	= 304.2	v_M	= 1035.7	q_s	= 0.0121	d	= 237.0
q_M	= 0.0121	z_i	= 24260.7	z_b	= 5000.0	mc_s	= 0.3
q_{MA}	= 0.0121	L _i	= 5686.6	$\Delta\theta_v$	= 0.0	\bar{x}_s	= 0.205
T_s	= 293.95	z_o	= 1.0	time	= 180.0	T_{15cm}	= 296.4
u_{MA}	= 478.3	$\partial z_i / \partial t$	= 1.25	δt	= 180.0	k	= 0.0009
v_{MA}	= 923.5	W _i	= 2.8667	c	= 1.0		

P(mb)	T(°K)	q(g/kg)	u(cm/s)	v(cm/s)	$1/\rho \times \partial p / \partial x$	$1/\rho \times \partial p / \partial y$
941	285.4	12.5	100.0	1000.0	0.106	-0.095
895	297.8	11.5	840.0	1066.0	0.072	-0.096
885	300.8	11.3	847.3	1062.5	0.070	-0.096
828	296.4	9.2	884.5	1324.9	0.077	-0.105
800	294.4	4.0	936.4	1521.6	0.090	-0.117
718	288.5	3.8	898.2	-148.1	0.035	-0.035
675	283.9	3.2	350.0	350.0	0.035	-0.035
622	281.5	2.4	350.0	350.0	0.035	-0.035
610	281.1	2.3	350.0	350.0	0.035	-0.035
586	278.4	1.2	350.0	350.0	0.035	-0.035
528	273.2	1.2	350.0	350.0	0.035	-0.035
400	254.0	0.36	1000.0	0.0	0.0	-0.1
300	235.5	0.1	1000.0	0.0	0.0	-0.1
150	208.0	0.01	1000.0	0.0	0.0	-0.1
0.01	213.0	0.003	0.0	0.0	0.0	0.0

D. WANGARA, Day 33

θ	= 276.0	u_M	= -300.0	D	= 0.0	ϕ	= -0.60214
θ_{vM}	= 273.0	v_M	= 75.0	q_s	= 0.0036	d	= 228.0
θ_{vMA}	= 0.0036	z_i^M	= 8000.0	z_b	= 800.0	mc	= 0.2
q_M	= 0.0036	L^i	= 800.0	$\Delta\theta_v$	= 0.0	$\bar{\alpha}^s$	= 0.28
q_{MA}	= 0.0036	z	= 4.0	time	= 20700.0	T	= 280.0
T_M	= 273.0	$\partial z_i^O / \partial t$	= 0.0	δt	= 180.0	k^{15cm}	= 0.0015
u_M^s	= -150.0	W_i	= 4.2	c	= 1.0		
u_{MA}^s	= 200.0						
v_{MA}^s							

P(mb)	T($^{\circ}$ K)	q(g/kg)	u(cm/s)	v(cm/s)	$1/\rho \times \partial p / \partial x$	$1/\rho \times \partial p / \partial y$
1021	272.7	3.4	-150	200	0	-0.045
1008	277.9	4.2	-340	100	0	-0.043
996	280.1	3.9	-340	80	0	-0.041
984	281.0	3.7	-308	95	0	-0.038
950	278.0	3.2	-300	100	0	-0.031
911	275.8	2.1	-230	-130	0	-0.022
851	275.4	0.8	-170	0	0	-0.016
799	273.2	0.6	50	0	0	0.01
700	265.0	0.4	500	0	0	0.05
500	248.0	0.2	1000	0	0	0.1
300	225.0	0.1	1000	0	0	0.1
150	220.0	0.01	1000	0	0	0.1
0	213.0	0.003	1000	0	0	0.1

E. WANGARA, Day 16

θ	= 282.7	u_M	= 985.0	D	= 0.0	ϕ	= -0.60214
θ^{vM}	= 279.7	v_M	= 280.0	q_s	= 0.0048	d	= 211.0
θ^{vMA}	= 0.0048	z_M	= 20000.0	z_s	= 5000.0	mc_s	= 0.2
q_M	= 0.0052	L^i	= 5000.0	$\Delta\theta^b$	= 0.0	\bar{a}^s	= 0.25
q^{MA}	= 278.4	z	= 4.0	time	= 9900.0	T^{15cm}	= 282.0
T^s	= 600.0	$\partial z^o / \partial t$	= 1.0	δt	= 180.0	k	= 0.0015
u^{MA}	= 0.0	W^i	= 2.5	c	= 1.0		
v^{MA}							

P(mb)	T($^{\circ}$ K)	q(g/kg)	u(cm/s)	v(cm/s)	$1/\rho \times \partial p / \partial x^*$	$1/\rho \times \partial p / \partial y^*$
1008	276.4	5.2	200	-100	-0.033	0.074
983	282.3	5.1	1040	500	-0.033	0.074
936	279.5	4.5	960	600	-0.033	0.074
870	274.3	3.9	800	80	-0.033	0.074
828	271.6	3.6	600	300	-0.033	0.074
787	274.2	1.8	640	520	-0.033	0.074
700	267.0	0.4	900	400	-0.033	0.074
500	248.0	0.2	900	400	-0.033	0.074
300	225.0	0.1	900	400	-0.033	0.074
150	220.0	0.01	900	400	-0.033	0.074
0.01	213.0	0.003	0	0	0	0

*through the course of the run these values are modified as follows

$$\frac{1}{\rho} \partial p / \partial x = \frac{1}{\rho} \partial p / \partial x + 1.472222 \times 10^{-6} \delta t$$

$$\frac{1}{\rho} \partial p / \partial y = \frac{1}{\rho} \partial p / \partial y - 7.648148 \times 10^{-7} \delta t$$

1. TITLE A Detailed Parameterization of the Atmospheric Boundary Layer		2. Report No. CSU-ATSP - 302	3. Recipient's Order No.
4. AUTHOR Peter J. Wetzel		5. Report Date December, 1978	6.
9. Performing Organization Name and Address Department of Atmospheric Science Colorado State University Foothills Campus Fort Collins, Colorado		8. Performing Organization Report No. CSU-ATSP- 302	10. Project/Task/Work Unit
11. NCAR-24-73;NSG 5105 04-5-022-8;NSG1023Sub#1		11. Contract Grant No. NRC-04-75-197;GA 31588 ATM 77-09770	
12. Sponsoring Organization Name and Address National Science Foundation 1951 Constitution Avenue, N.W. Washington, D.C. 20550		13. Type of Report & Period Covered Ph.D. Dissertation Nov. Dec. 1973 - 1978	

14. Supplementary Notes

A one-dimensional parameterized model of the planetary boundary layer (PBL) is developed and tested. The model predicts layer averaged values of wind, temperature and moisture under both stable and unstable conditions by assuming standard profile shapes. A predictive equation is developed for the unstable PBL height z_i , and a new diagnostic equation is used for the stable z_i . Transition between stable and unstable regimes is accomplished by the model without difficulty. The model incorporates a detailed surface energy budget-- shown to be of vital importance to an accurate quantitative description of the PBL. New parameterizations for evaporation and soil heat flux are constructed and shown to work well under a wide range of conditions.

The model is tested against data from O'Neill, Nebraska and from the Wangara experiment, and it is compared with other models of the PBL. Results show that the model simulates the observations well, and that it is equal or superior to the other models examined. Sensitivity tests and exploratory tests of the model were performed. In these it is shown that the PBL is very sensitive to changes in parameters such as the mass of the layer at the surface, the difference between the characteristic heights for moisture (z_q) and momentum (z_0), the amount of dew present at dawn, and the soil moisture content. Such tests are useful in studying man's inadvertent modification of the weather through land use patterns.

17. Key words and phrases
- (1) Atmospheric Boundary Layer
 - (2) Mesoscale Modelling
 - (3) Parameterization of Boundary Layer
 - (4) Surface energy budget
 - (5) Micrometeorology
 - (6) Numerical modelling

18. COSATI Field/Group	19. Report	20. Report
19. Availability	20. Report	21. Report